FACULTY
OF MATHEMATICS
AND PHYSICS
Charles University

DOCTORAL THESIS

Artem Kovalenko

LABORATORY STUDIES OF REACTIONS OF O^+ AND N^+ IONS WITH MOLECULAR HYDROGEN AND ITS ISOTOPOLOGUES, HD AND D_2, AT LOW TEMPERATURES

Department of Surface and Plasma Science

Supervisor of the doctoral thesis: Prof. RNDr. Juraj Glosík, DrSc.

Study programme: Physics

Specialisation: Physics of Plasma and Ionized Media

Prague 2021

I declare that I carried out this doctoral thesis independently, and only with the cited sources, literature and other professional sources. It has not been used to obtain another or the same degree.

I understand that my work relates to the rights and obligations under the Act No. 121/2000 Sb., the Copyright Act, as amended, in particular the fact that the Charles University has the right to conclude a license agreement on the use of this work as a school work pursuant to Section 60 subsection 1 of the Copyright Act.

In…..... date..... Author's signature

Acknowledgements

Study at Charles University is an important step in my life and obtained experience is significant for a further scientific career. All this happened due to the influence of the people surrounding and guiding me through these years. In this acknowledgement, I would like to express my gratitude to these people.

Firstly, I thank my supervisor Prof. RNDr. Juraj Glosík, DrSc., who played a significant role during my Ph.D. study. I sincerely appreciate his pieces of advice, knowledge and life experience that were given to me. Then, I would like to thank doc. RNDr. Radek Plašil, Ph.D. and RNDr. Štěpán Roučka, Ph.D. for their guiding and developing my working skills. And finally, I thank all my colleagues and co-workers, especially my wife RNDr. Thuy Dung Tran, Ph.D. for supporting and productive discussions.

I also thank the Czech Science Foundation and The Charles University Grant Agency (especially projects GAUK 1144616) for financial support.

Я хочу подякувати своїй родині та друзям за їх підтримку та нескінченне натхнення. Ви завжди були та будете поряд всюди, де б я не був.

Název práce: Laboratorní studia reakcí iontů O^+ a N^+ s molekulárním vodíkem a jeho izotopology HD a D_2 při nízkých teplotách

Autor: Artem Kovalenko

Katedra: Katedra fyziky povrchů a plazmatu

Vedoucí disertační práce: Prof. RNDr. Juraj Glosík, DrSc., Katedra fyziky povrchů a plazmatu

Abstrakt: Tato práce je zaměřena na laboratorní studium reakcí iontů O^+ a N^+ s molekulárním vodíkem a jeho izotopology HD (deuterid vodíku) a D_2. Experimentální studia byla provedena pomocí 22-polové radiofrekvenční iontové pasti při teplotách od 15 K do 300 K. Teplotní závislosti měřených reakčních koeficientů jsou prezentovány pro všechny reakce. Studované reakce jsou důležité pro astrochemii. Reakce O^+ s H_2 zahajuje sekvenci reakcí produkujících vodu v mezihvězdném prostředí a rychlostní koeficient této reakce se dramaticky nemění s teplotou v daném rozsahu. Získané hodnoty rychlostních koeficientů reakcí O^+ s H_2, HD a D_2 jsou blízké hodnotám odpovídajících Langevinových rychlostních koeficientů. Reakce O^+ s HD má dva kanály produkující OH^+ nebo OD^+. Poměr rychlostního koeficientu kanálu produkujícího OH^+ vůči celkovému rychlostnímu koeficientu je blízký hodnotě 0,5 pro celý teplotní rozsah, pro který byla reakce studována. Reakce N^+ s H_2 zahajuje sekvenci reakcí produkující amoniak v mezihvězdném prostředí. Tato reakce má aktivační energii v řádu několika meV, která hraje výraznou roli při podmínkách panujících v mezihvězdném prostředí. Aktivační energie reakcí N^+ s H_2 a jeho izotopology byly určeny z měřených teplotních závislostí.

Klíčová slova: astrochemie, iontová past, iont-molekulové reakce, aktivační energie, izotopický efekt.

Title: Laboratory studies of reactions of O^+ and N^+ ions with molecular hydrogen and its isotopologues, HD and D_2, at low temperatures

Author: Artem Kovalenko

Department: Department of Surface and Plasma Science

Supervisor of the doctoral thesis: Prof. RNDr. Juraj Glosík, DrSc., Department of Surface and Plasma Science

Abstract: This work is focused on the laboratory studies of reactions of O^+ and N^+ ions with molecular hydrogen and its isotopologues, HD (hydrogen deuteride) and D_2. The experimental studies were performed using a 22-pole radiofrequency ion trap in the temperature range from 15 K to 300 K. The temperature dependencies of measured reaction rate coefficients are presented for all reactions. Studied reactions are important for astrochemistry. The reaction of O^+ with H_2 initiates a water production sequence in the interstellar medium, and the rate coefficient does not change dramatically with temperatures in the covered range. The measured rate coefficients for reactions of O^+ with H_2, HD, and D_2 are close to the corresponding Langevin rate coefficients. The reaction of O^+ with HD has two reaction channels with products, OH^+ and OD^+. The ratio of rate coefficient of the OH^+ production channel to the total reaction rate coefficient is close to 0.5 in the studied temperature range. The reaction of N^+ with H_2 initiates the ammonia production sequence in the interstellar medium. This reaction has activation energy on the order of a few meV, which is significant in the conditions of the interstellar medium. For reactions of N^+ with H_2 and its isotopologues, activation energies were determined from measured temperature dependencies.

Keywords: astrochemistry, ion trap, ion-molecule reactions, activation energy, isotope effect.

Contents

1. Thesis overview

The presented doctoral thesis includes the results of the experimental study of chosen reactions of ions with molecules. These fundamental processes are relevant to astrochemistry and atmospheric chemistry.

Obtained crucial information about studied reactions can illuminate the fundamental knowledge about the Universe, formation of polyatomic inorganic and organic molecules in space and processes occurring in the atmospheres of the planets. Our experimental study is an essential source of information for further modelling chemical kinetics and evolution scenarios of matter in space.

In the present work, the most attention is paid to the laboratory studies of reactions of O^+ or N^+, with molecular hydrogen or its isotopologues: HD (hydrogen deuteride) or D_2.

The thesis consists of six chapters, bibliography, a list of studied reactions, figures, tables, used acronyms and lists of publications with attached publications.

Chapter 2: Introduction, gives information about the presence of studied molecules and ions in various space environments and the current knowledge about deuterated species in some regions of the Universe. This chapter also contains a short historical overview of measuring techniques with further development into the idea of our apparatus.

Chapter 3: Goals of the thesis outlines the main aims based on the information given in the introduction.

In *Chapter 4: Experimental facility,* the detailed explanations of our experimental technique from a clear description of the vacuum and gas inlet system to production, guiding and confinement of the ions, are given. This chapter also defines the determination of two main measured parameters, such as the temperature of the ions and the number density of the reactant gas inside the trap. The measuring methodology of the reaction rate using our equipment is also described in this chapter.

Chapter 5: Experimental study of ion-molecule reaction in the RF 22-pole ion trap gives the fundamental results of our studies for the reactions $O^+ + H_2$, $O^+ + HD$, $O^+ + D_2$, $N^+ + HD$, and $N^+ + D_2$. For the last two reactions, the activation energies are determined from obtained Arrhenius fits and compared with previously obtained results. The temperature dependencies of the reaction rate coefficients are presented together with discussions of their behaviour. Our measured data are compared with data obtained in other experiments.

All studied reactions which relate to this work are collected in a *List of studied reactions.* There can be found the respective reference to the chapter in the text along with a link to our published article.

The relevant publications are given in *the list of publications,* and some selected articles are given in a corresponding attachment.

In the presented experiments, I worked in a group with other students and co-workers. We investigated the ion-molecule reactions and prepared all experiments. My responsibilities included: conducting and organisation of experimental procedures, preparing of the experimental equipment, and processing of the results that had been later published or will be published.

Studies have been carried out during my PhD studies at the Department of Surface and Plasma Science, Faculty of Mathematics and Physics, Charles University.

2. Introduction

Since 1937, over 200 molecules and molecular ions have been detected in the interstellar medium or circumstellar shells. All of them play their role in the cosmic chemistry and also participate in the evolution of the mater in the Universe. Molecular hydrides are among the first molecules detected outside the solar system, and studying their chemistry is a key to understand the production of the essential polyatomic inorganic and organic molecules in the Universe.

2.1 Molecular ions and conditions in the interstellar medium

There are regions in the interstellar medium (ISM) that have a significant influence on the evolution of the molecular hydrides in the Universe. The number density of the particles in the regions that are called molecular clouds varies from 10^2 cm^{-3} to 10^6 cm^{-3}. These regions are denser-than cold atomic (number density of the particles 50 – 100 cm^{-3}) or hot atomic regions of the interstellar medium (number density of the particles 0.2 – 0.5 cm^{-3}), (Ferrière, 2001). These molecular clouds consist of matter in the gaseous form and the form of dust particles, or grains, ranging in a wide range with radius from more than ≈ 1μm to less than ≈ 10 nm (Li & Draine, 2001). The dust particles contain 1 % of the mass in molecular clouds. The gaseous matter can be studied via high-resolution spectroscopic observations, whereas the dust particles are more difficult to characterise (Herbst, 1995).

The main two categories of the interstellar cloud are diffuse and dense/molecular clouds. The diffuse interstellar clouds are not dense enough to absorb most of the light coming from stars. Such regions have typical temperatures 50 – 100 K, and the total gas number densities can be 10^2 cm^{-3}. The gaseous phase in the diffuse clouds is primarily neutral, and the ratio of

electron number density (n_e) to the number density of hydrogen atoms (n_H) or fractional ionisation is $n_e/n_H = 2\times10^{-4}$ (Draine, 2011).

The chemistry of dense clouds is more complex than the chemistry of diffuse clouds. The dense clouds usually associate with giant molecular clouds. These clouds are a large heterogeneous region of dust and gas, ranging in mass up to $\approx 10^5 M_\odot$ (Herbst, 2005). The densest regions of the dense clouds are virtually black in the visible range of observations, and known as "cores". The typical temperatures of such regions are only 10 K and number densities can reach $\approx 10^4$ cm^{-3}. The dense clouds consist overwhelmingly of molecular rather than atomic hydrogen (Pratap et al., 1997). A common, estimated fractional ionisation in dense cores is 10^{-7} (Caselli et al., 1998). The hot cores in the dark clouds have temperatures in range 100 – 300 K and can contain some organic molecules such as methyl, ethyl alcohol, dimethyl ether, methyl formate, and more others (Herbst, 2005).

Table 2.1 displays known positive molecular ions found in the different regions of the interstellar medium and circumstellar envelopes (adapted from (Roueff, 2015) with some data from The Cologne Database for Molecular Spectroscopy (Endres et al., 2016)).

Table 2.1: Molecular ions found in the different regions of the interstellar medium and circumstellar envelopes (Roueff, 2015; Endres et al., 2016).

Diatomic	Triatomic	Polyatomic
CH^+	H_3^+	H_3O^+
OH^+	H_2D^+	NH_3^+
SH^+	H_2O^+	NH_4^+
CO^+	HCO^+	C_3H^+
SO^+	HOC^+	$HCNH^+$
HCl^+	DCO^+	$HOCO^+$
SF^+	HCS^+	H_2COH^+
	N_2H^+	NH_3D^+
	N_2D^+	

The table also includes several deuterated ions as they are the indicators of the physical conditions in star formation regions, especially pre-stellar cores.

2.1.1 Ammonia formation in the interstellar medium

Ammonia is one of the most commonly observed interstellar molecule. This molecule was firstly detected towards Sgr B2 from its emission spectrum in the microwave region (Cheung et al., 1968). Later, there were detected other nitrogen hydrides such as NH (Meyer & Roth, 1991), NH_2 (van Dishoeck et al., 1993), and NH_3D^+ (Cernicharo et al., 2013). Spectra of deuterated types of ammonia were obtained by CSO (Caltech Submillimeter Observatory), IRAM (Institute for Radio Astronomy in the Millimeter range) 30m telescope and Arecibo telescopes with derived ND_3/NH_3 ratio between 2×10^{-4} and 2×10^{-3} in various pre-stellar cores (Roueff et al., 2018). Chemistry of the nitrogen hydrides in the ISM was discussed in many works, e.g., (Rist et al., 2013; Harju et al., 2017) and reviews (Le Gal et al., 2014; Acharyyea & Herbst, 2015; Gerin et al., 2016).

It is commonly accepted that the main path to the gas-phase formation of ammonia in the interstellar medium is a chain of hydrogen abstraction reactions followed by the recombination of NH_3^+ or dissociative recombination of NH_4^+ ions with the electron (Herbst & Klemperer, 1973; Le Gal et al., 2014; Gerin et al., 2016). The proposed by Le Gal et al. (2014) pathway of the gas-phase formation of the NH_3^+ and NH_4^+ in interstellar medium starting from N^+ is:

$$N^+ \xrightarrow{+H_2} NH^+ \xrightarrow{+H_2} NH_2^+ \xrightarrow{+H_2} NH_3^+ \xrightarrow{+H_2} NH_4^+. \qquad (2.1)$$

Production of N^+ ions can be a result of dissociative ionisation of N_2 in reaction with He^+ ions in the low-temperature regions (10 K) of dark clouds (Hily-Blant et al., 2013; Le Gal et al., 2014). Although, the reaction $H_3^+ + N \rightarrow NH_2^+ + H$ has high activation energy, and it is another possible

way to initiate the chain of reactions (2.1) (Herbst et al., 1987; Scott et al., 1997; Le Gal et al., 2014).

All main reactions from the chain (2.1) and their 0 K enthalpy changes are listed below:

$$N^+ + H_2 \rightarrow NH^+ + H \qquad E_a = 16.5 \text{ meV} \qquad (2.2)$$

$$\rightarrow NH_2^+ + H \qquad \Delta H^0 = -1.9 \text{ eV} \qquad (2.3a)$$

$$NH^+ + H_2$$

$$\rightarrow H_3^+ + N \qquad \Delta H^0 = -0.8 \text{ eV} \qquad (2.3b)$$

$$NH_2^+ + H_2 \rightarrow NH_3^+ + H \qquad \Delta H^0 = -1.1 \text{ eV} \qquad (2.4)$$

$$NH_3^+ + H_2 \rightarrow NH_4^+ + H \qquad \Delta H^0 = -1.0 \text{ eV} \qquad (2.5)$$

The precise value of energy difference between the ground states of reactants and products or enthalpy changes at 0 K ΔH^0 of the first binary reaction (2.2) has been not yet known. Thus, we provide the activation energy E_a obtained by Zymak et al. (2013).

Previous studies of the reaction of N^+ with $H_2(j)$ did not show whether the activation energy is caused by an endoergicity or an energy barrier as well. The isotopic variant can provide us with the new information concerning the origin of the activation energy of the reaction of N^+ with $H_2(j)$.

For the other hydrogen abstraction reactions, the enthalpy changes were calculated by Rist et al. (2013). The enthalpy changes of the proton transfer channel (2.3b) was calculated from the proton affinities given by Hunter & Lias, (1998).

Experimental studies of these reactions were mainly provided at room temperatures (≈ 300 K) by Fehsenfeld et al. (1967), Kim et al. (1975), and Adams et al. (1980). New experimental data has been obtained by Rednyk et al. (2019) at temperatures down to 15 K and can be used for modelling of production and destruction of nitrogen species in some regions of the interstellar medium.

2.1.2 Formation of water in the interstellar medium

Oxygen is the third most abundant element in the Universe, and it plays an essential role in the chemistry of many astronomical environments. In the ISM, the production of OH^+ ions in reactions of O^+ ions with molecular hydrogen is a crucial process in the synthesis of water molecules (Gerin et al., 2016). The key importance of H_2O molecules in the ISM has been reviewed by Hollenbach et al. (2012).

In our galaxy, OH^+ ions have been found toward regions with high electron density: the Orion Bar (van der Tak et al., 2013), the supernova remnant in the Crab Nebula (Barlow et al., 2013) and planetary nebula hosting hot central stars with $T_{\rm eff} > 100{,}000$ K (Aleman et al., 2014). The H_2O^+ and H_3O^+ emissions have not been detected in these regions, and it shows that OH^+ lines arise in gas layers. The OH^+ ions are mainly formed in the exothermic reaction $O^+ + H_2 \rightarrow OH^+ + H$ (Gerin et al., 2016).

Significant advancement in the astronomical studies of the oxygen hydrides has been recently made by the Atacama Pathfinder Experiment, the Atacama Large Millimeter/submillimeter Array, the Herschel space observatory, and other observatories. The detection of OH, OH^+, H_2O, H_2O^+, and H_3O^+ in diffuse and dense Galactic interstellar mediums is of particular interest (Gerin et al., 2010; Ossenkopf et al., 2010; Pilbratt et al., 2010; Wyrowski et al., 2010; Hollenbach et al., 2012; Gómez-Carrasco et al., 2014; Muller et al., 2016; Neufeld & Wolfire, 2016).

New space- and ground-based observations (Hollenbach et al., 2008, 2012; Gerin et al., 2016) that aimed at the study of the role of the oxygen hydrides in the ISM show that in diffuse clouds, there are two main pathways to produce OH^+ ions. These main routes are shown in Figure 2.1. Approaching closer to the centre of the diffuse cloud, it becomes denser, and most of the hydrogen exists in the molecular form. Therefore, the formation of OH^+ proceeds through the first pathway where cosmic rays (CR) ionise molecular hydrogen, and the H_2^+ ion reacts with molecular hydrogen forming the H_3^+

ion, which transfers a proton to O (de Ruette et al., 2016). At the border of the diffuse clouds where most hydrogen is in the atomic form, production of OH^+ proceeds through the second pathway. Hydrogen cations are formed by CR ionisation, and in the next step, O^+ ions are produced from oxygen atoms in the slightly endothermic electron transfer to H^+. Subsequent reaction of OH^+ with H_2 leads to H_2O^+ and H_3O^+ formation. Produced H_2O^+ and H_3O^+ ions can be followed by recombination or dissociative recombination with electrons and form the molecule of H_2O (Jensen et al., 2000; Neau et al., 2000).

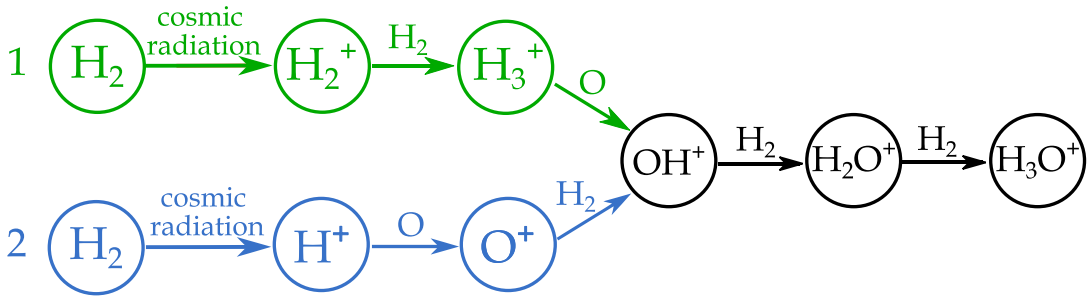

Figure 2.1: Water formation pathways in the interstellar medium.

In the present work, the attention is paid to the second pathway. All main reactions from the chain and their enthalpy changes at 0 K are listed below:

$$O^+ + H_2 \rightarrow OH^+ + H \qquad \Delta H^0 = -0.54 \text{ eV}, \qquad (2.6)$$

$$OH^+ + H_2 \rightarrow H_2O^+ + H \qquad \Delta H^0 = -1.02 \text{ eV}, \qquad (2.7)$$

$$H_2O^+ + H_2 \rightarrow H_3O^+ + H \qquad \Delta H^0 = -1.7 \text{ eV}. \qquad (2.8)$$

For reactions (2.6 − 2.8), the enthalpy changes ΔH^0 at 0 K were calculated using tabulated enthalpies of formation (Haney & Franklin, 1969), dissociation energies (Liu et al., 2009), and ionisation energies (Lauzin et al., 2015).

Another possible way of H_2O formation in the interstellar medium is a reaction:

$$O^- + H_2 \rightarrow H_2O + e^- \qquad \Delta H^0 = -3.58 \text{ eV}, \qquad (2.9)$$

which was experimentally studied by Jusko et al. (2015).

Hydrogen isotopologues HD or D_2 could also be involved in reactions with O^+ or with produced OH^+, H_2O^+, then partly deuterated H_3O^+ and H_2O can be formed. To understand astronomical observations of these deuterated molecules, more experimental and theoretical studies of reactions with HD and D_2 and more astronomical observations are needed. The latter studies may reveal the role of deuterium products in the ISM.

2.1.3 Deuterated molecular species and their importance for astrochemistry

The role and chemistry of deuterium species in the ISM have been reviewed and discussed in many works by Roberts et al. (2003), Neil et al. (2013), Ceccarelli et al. (2014), Award & Shalabiea (2017), Caselli et al. (2019), etc. The estimated local interstellar medium atomic deuterium-to-hydrogen ratio (D/H ratio) is ~ 10^{-5} (Oliveira et al., 2003; Weinberg, 2017). However, some observations show that molecular deuterium-to-hydrogen ratio can be higher in several astrophysical regions by few orders of magnitude (Ceccarelli et al., 2001; Crapsi et al., 2005; Vastel et al., 2016). For this phenomenon, i.e., super-deuteration, D to H ratio can reach > 10% (Ceccarelli et al., 2007). Till now, more than 30 deuterated molecules and ions have been discovered in various regions of the interstellar medium, and in some regions, the abundance is comparable to their normal hydrogen counterparts (also known as the protium isotope). These deuterated species are classified into two categories: singly-deuterated (e.g. HD, H_2D^+, DCO^+, NH_2D, HDO) and multi-deuterated (e.g. D_2H^+, CD_3OH, D_2CO, NHD_2, D_2O, ND_3). A list of the most observed deuterated species in cores of massive and low-mass forming regions with the corresponding reference is given by Avad et al. (2014, Table 1) or The Cologne Database for Molecular Spectroscopy (Endres et al., 2016). Summary of the molecular D/H ratio in various interstellar environments is given by Albertsson et al. (2013, Table 19).

In cold regions (< 30 K), the formation of deuterated molecules or ions starts from one of the most important molecular ion H_3^+ (Glosík et al., 2015).

Further subsequent replacement of H atom by D atom in reaction with HD finally forms the D_3^+ ion. Intermediate products from this reaction chain (H_2D^+, HD_2^+) can further react with other molecules to form D-bearing molecules (DCO^+, NH_2D, N_2D^+, etc.). These general steps are summarised in Figure 2.2.

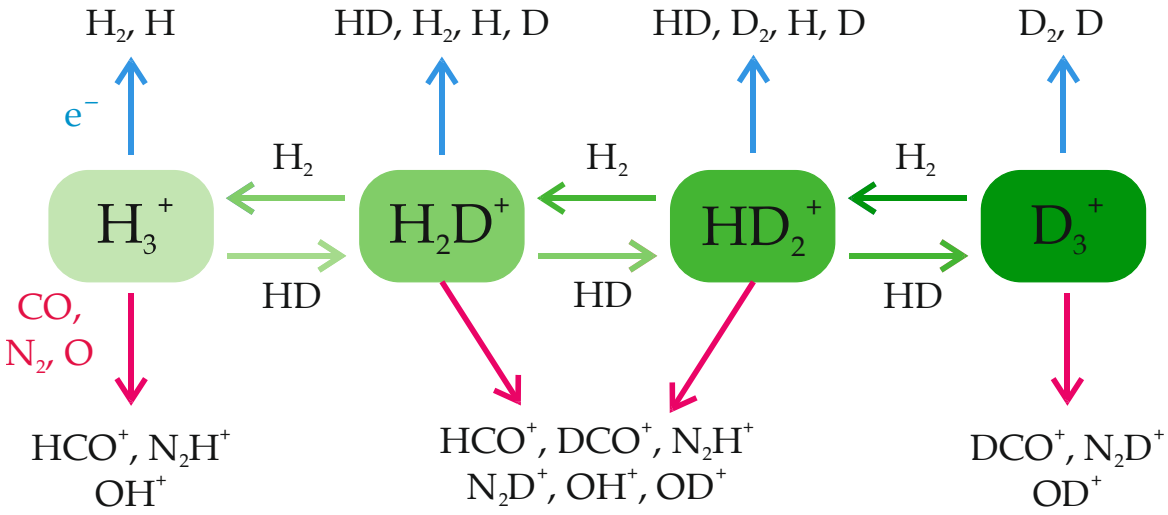

Figure 2.2: Schematic diagram of the formation of the deuterated fraction and some related ions in ISM starting from H_3^+ and reacting with HD, CO, N_2, and O.

Although hydrogen deuteride (HD) in the interstellar clouds has been investigated by Ceccarelli (2002), there are no experimental proofs of the finding of the molecular deuterium in the ISM. As deuterium molecule does not have a dipole moment and at the same time, the number density of D_2 is lower in comparison to number densities of hydrogen deuteride it imposes limitations on detection of molecular deuterium in the ISM.

The reported observation and calculated fractional abundances of D_2O/H_2O and D_2O/HDO in the protostellar binary system IRAS 16293 − 2422 are 5×10^{-5} and 1.7×10^{-3}, respectively (Butner et al., 2007). Three major processes that cause the water deuteration are formation on the surface of the cold grains, hydrogen-deuterium exchange in the gas-phase and isotopic exchange between solid H_2O and HDO with other solid species (Ceccarelli et al., 2014). In our situation, we just consider the possible reaction

of atomic oxygen ions with molecular hydrogen isotopologues in the gas-phase as we have a technique for studying such processes. We suggest that the reactions O^+ + HD could be one of the possible starters of deuterated water formation; thus, we decided that their temperature dependence must be experimentally studied.

The formation of isotopologues of ammonia can start from N^+ + HD, D_2 reactions with the further subsequent attachment of H or D atoms from HD or D_2 molecules. The spectroscopic study of the dense dark cloud LDN 134N has shown that the upper limit of ND_3/NH_3 ratio is 1.6×10^{-4}, while some theories predict this ratio between 2×10^{-4} and 2×10^{-3} in various pre-stellar cores (Roueff et al., 2005).

Obtaining the rate coefficients of theses reactions helps many astrophysicists to better define and predict its ratio in the ISM. The chemistry of these species can be used as a powerful modelling tool for the planet`s atmospheres and star-forming regions. This knowledge can also unveil the history of origin and further evolution of the matter in the Universe.

2.2 Definitions of the rate coefficient of the reaction of an ion with a molecule

The simple binary ion-molecule reaction is

$$A^+ + B \rightarrow C^+ + D, \tag{2.10}$$

where A^+ and B are reactants, C^+ and D are products. The reaction rate coefficient k is one of the most useful concepts in general chemical kinetics, and it defines as an integral factor, which includes information on energy distribution functions and depends on temperature or mean energy of the colliding particles:

$$k(T) = \int_0^\infty \sigma(v) v f(v) \mathrm{d}v = \langle \sigma v \rangle, \tag{2.11}$$

where σ is a cross-section and v designates the velocity averaging for the Maxwell-Boltzmann distribution in the thermal equilibrium. The reaction rate coefficient is a parameter of the rate equation of the ion-molecular system.

For the simple binary ion-molecule reaction (2.11) the decay of the ion reactant number density in time is:

$$\frac{\mathrm{d}[\mathrm{A}^+]}{\mathrm{d}t} = -\, k[\mathrm{A}^+][\mathrm{B}] = -\, r_{\mathrm{reaction}}[\mathrm{B}], \tag{2.12}$$

where k is the reaction rate coefficient, r_{reaction} is a reaction rate, $[\mathrm{A}^+]$ and $[\mathrm{B}]$ are number densities of the ions and the reactant gas, respectively. When we add into the reaction volume far more reactant B than A^+, $[\mathrm{B}] >> [\mathrm{A}^+]$, thus assuming that the number density $[\mathrm{B}]$ is constant, the respective solution of the equation (2.12) is:

$$[\mathrm{A}^+] = [\mathrm{A}_0^+] e^{-k[\mathrm{B}]t}, \tag{2.13}$$

where $[\mathrm{A}_0^+]$ is the number density of the reactant ions at time $t = 0$. With increasing the gas number density $[\mathrm{B}]$, the rate of reaction increases due to the growth of the number of collisions.

Some reactions have two or more channels:

$$\mathrm{A}^+ + \mathrm{B} \xrightarrow{k_{\mathrm{C}^+}} \mathrm{C}^+ + \mathrm{D} \tag{2.14a}$$

$$\mathrm{A}^+ + \mathrm{B} \xrightarrow{k_{\mathrm{E}^+}} \mathrm{E}^+ + \mathrm{F}, \tag{2.14b}$$

where k_{C^+} and k_{E^+} are rate coefficients for a particular channel of the reaction.

Overall rate coefficient of the reaction can be defined as a sum of rate coefficients of single channels (2.14a) and (2.14b):

$$k = k_{\mathrm{C}^+} + k_{\mathrm{E}^+}. \tag{2.15}$$

The system of differential equations for reactions (2.14) is:

$$\begin{cases} \dfrac{\mathrm{d}[\mathrm{A}^+]}{\mathrm{d}t} = -\,k_{\mathrm{C}^+}[\mathrm{A}^+][\mathrm{B}] - k_{\mathrm{E}^+}[\mathrm{A}^+][\mathrm{B}] = -\,k[\mathrm{A}^+][\mathrm{B}] \\ \dfrac{\mathrm{d}[\mathrm{C}^+]}{\mathrm{d}t} = k_{\mathrm{C}^+}[\mathrm{A}^+][\mathrm{B}] \\ \dfrac{\mathrm{d}[\mathrm{E}^+]}{\mathrm{d}t} = k_{\mathrm{E}^+}[\mathrm{A}^+][\mathrm{B}]. \end{cases} \tag{2.16}$$

The respective solution to this system in this simple case is:

$$\begin{cases} [\mathrm{A}^+] = [\mathrm{A}_0^+]e^{-(k_{\mathrm{C}^+} + k_{\mathrm{E}^+})\cdot[\mathrm{B}]t} \\ [\mathrm{C}^+] = \dfrac{k_{\mathrm{C}^+}}{k}\left[\mathrm{A}_0^+\right]\left(1 - e^{-(k_{\mathrm{C}^+} + k_{\mathrm{E}^+})\cdot[\mathrm{B}]t}\right) + [\mathrm{C}_0^+] \\ [\mathrm{E}^+] = \dfrac{k_{\mathrm{E}^+}}{k}\left[\mathrm{A}_0^+\right]\left(1 - e^{-(k_{\mathrm{C}^+} + k_{\mathrm{E}^+})\cdot[\mathrm{B}]t}\right) + [\mathrm{E}_0^+], \end{cases} \tag{2.17}$$

where $[\mathrm{A}_0^+]$, $[\mathrm{C}_0^+]$, and $[\mathrm{E}_0^+]$ are number densities of reactants at time t = 0. Solving this system of equations, for known number densities and time, we can obtain rate coefficients for separate reaction channel and the total value k.

In this work, such reactions were experimentally studied. Some calculation of the rate coefficient was performed according to this system of equations.

2.2.1 Langevin collisional rate coefficient

In 1905, Langevin proposed the most straightforward collision theory that can characterise the ion-molecule reaction (Langevin, 1905). The Langevin collision theory is applied for reactions of ions with molecules that do not have a permanent dipole moment. This theory found wide applications in many theoretical studies of the interaction of an ion with a molecule (Turulski & Niedzielski, 1994; Benitez et al., 2016; T. Li, 2020).

According to this theory long-range interaction in attractive potential between a point charge and a point-polarisable neutral lead to the capture of the collision partners, so-called Langevin collision of the charged particle. In case when the neutral molecule does not have a permanent dipole moment, the charge-dipole interaction is caused by induction of dipole moment of the

neutral molecule by the electric field of the ion. The potential of charge-induced dipole interaction can be written as:

$$V_{\text{pot}} = -\frac{\alpha q^2}{2r^4}, \tag{2.18}$$

where r is the distance of molecule from the ion, q is a charge of the ion and α is polarizability of a neutral molecule (Tielens, 2005, page 92).

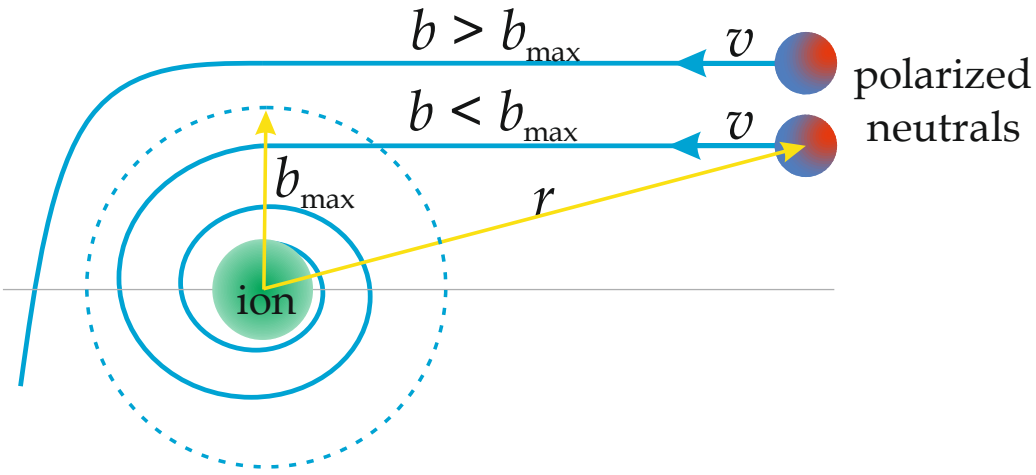

Figure 2.3: Langevin scattering in polarisation potential.

Figure 2.3 shows a case when the neutral molecule approaches from an infinity distance with a relative velocity v and impact parameter b to the ion. The angular momentum of this system is conserved during the collision. For large b, the system has more considerable angular momentum. The centrifugal potential of this system is:

$$V_{\text{cent}} = \frac{b^2}{r^2}\frac{\mu v^2}{2}, \tag{2.19}$$

where μ is a reduced mass of the ion-neutral system, which can be defined as:

$$\mu = \frac{m_{\text{Ion}} \cdot m_{\text{N}}}{m_{\text{Ion}} + m_{\text{N}}}, \tag{2.20}$$

where m_{Ion} is mass of the ion and m_{N} is mass of the neutral molecule. The interaction potential is given by a sum of (2.18) and (2.19) relations and can be

written as:

$$V(r) = -\frac{\alpha q^2}{2r^4} + \frac{b^2}{r^2}\frac{\mu v^2}{2}, \tag{2.21}$$

with the maximum value:

$$V_{\max} = \frac{b^4 \mu^2 v^4}{8\alpha q^2}. \tag{2.22}$$

A collision occurs when the initial energy is higher than the potential maximum (2.22). The maximum value of b for initial kinetic energy ($\mu v^2/2$) is:

$$b_{\max}^2 = \sqrt{\frac{4\alpha q^2}{\mu v^2}}. \tag{2.23}$$

When b is larger than the critical value, $b_{\max}$, then the collision between neutral species and the ion does not happen.

The collisional cross-section follows:

$$\sigma_0 = \pi b_{\max}^2 = \frac{2\pi q}{v}\sqrt{\frac{\alpha}{\mu}}, \tag{2.24}$$

and the collisional reaction rate coefficient $k_{L,}$ according to (2.11) is:

$$k_L = \langle \sigma_0 v \rangle = 2\pi q \sqrt{\frac{\alpha}{\mu}}, \tag{2.25}$$

where, q is an elementary charge of the ion (1.6×10^{-19} C = 4.8×10^{-10} statC or $cm^{3/2}g^{1/2}s^{-1}$), α is polarizability (1 Å^3 = 10^{-24} cm^3), and μ is reduced mass (1 Da = 1.66×10^{-24} g).

In the case of molecules with a permanent dipole moment, the capture rate coefficient needs to consider the dipole moment of the neutral molecule and temperature of the neutral gas (Chesnavich et al., 1980). For HD molecule the estimated correction is less than 0.2% at 10 K.

Substituting in the equation (2.25) CGS units indicated above, we can estimate the value of reaction rate coefficient k_L in typical form, used for chemical applications as:

$$k_L = 2\pi \cdot 4.8 \cdot 10^{-10} \mathrm{cm}^{\frac{3}{2}}\, \mathrm{g}^{\frac{1}{2}} \mathrm{s}^{-1} \sqrt{\frac{10^{-24}\,\frac{\mathrm{cm}^3}{\mathrm{\AA}^3} \cdot \alpha(\mathrm{\AA}^3)}{1.66 \times 10^{-24}\,\frac{\mathrm{g}}{\mathrm{Da}} \cdot \mu(\mathrm{Da})}}. \qquad (2.26)$$

This value gives a necessary approximation for study ion-molecule reactions, and from the (2.26) the estimated value is ~ 2.3×10^{-9} cm^3s^{-1}. This value is about 200 times higher than gas kinetic value for a neutral-neutral reaction: $k_{neutral} \approx 10^{-11}$ cm^3s^{-1} (Smith et al., 2004). The Langevin rate coefficient k_L is not dependent on temperature, and it is an upper estimation of the reaction rate coefficient of the ion-molecule reaction.

2.3 Overview of measurement techniques

A variety of different experimental techniques helps many scientists to study ion-molecule reactions. Over the years, these experiments have been upgraded, and significant efforts have been devoted to study ion-molecule reactions at low temperatures. Each technique has its advantages and disadvantages and respectively solves the specific tasks.

Two main categories of experimental techniques exist for studying ion-molecule processes. One of them is swarm experiments, and the second one is based on direct trapping of ions in an RF electromagnetic field.

Pioneer in swarm experiments may be considered flowing afterglow (FA) method (Ferguson et al., 1969). Further developments of the FA experiment led to the construction of selected ion flow tubes technique (SIFT) by Adams & Smith, (1976).

The SIFT technique removes many sources of noises in the ion-molecule reaction experiments such as the energetic photons, presence of electrons, neutral fragments and exciting species. It is achieved by using a mass filter to select ions from a separate ion source and injecting them, at low energy, into a

flow of neutral gas. After thermalisation of the ions in the flow tube, they react with gases, which are added downstream of the injection point. A mass spectrometer analyses ions. A scheme of the SIFT experiment is shown in Figure 2.4.

Early SIFT experiments have been provided in the temperature range down to ≈ 80 K by cooling the flow tube with liquid nitrogen (Adams et al., 1979; Henchman et al., 1989). Also, the temperature of 18 K has been achieved in the SIFT technique by using liquid He as a coolant (Böhringer et al., 1986).

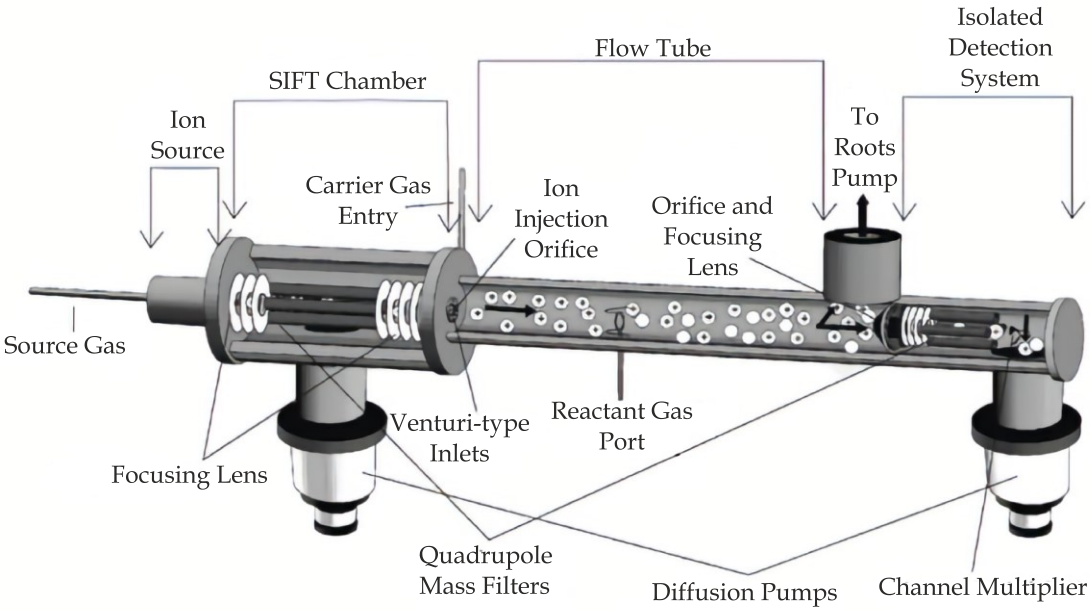

Figure 2.4: A schematic diagram of the University of Georgia SIFT apparatus. The figure is reproduced from the paper by Jackson et al. (2005).

Another type of flow-beam experiment is the Cinétique de Réaction en Ecoulement Supersonique Uniforme (CRESU) technique, which is described in detail by Rowe et al. (1984). The CRESU experiment is based on the theoretic concept of the isentropic expansion of gas from a reservoir through a Laval nozzle into a vacuum chamber, where reactants are injected.

This method is employed to study the kinetics of different ion-molecule reactions at temperatures down to ≈ 8 K (Rowe et al., 1985). Temperature 8 K is achieved by pre-cooling the gas prior to its expansion.

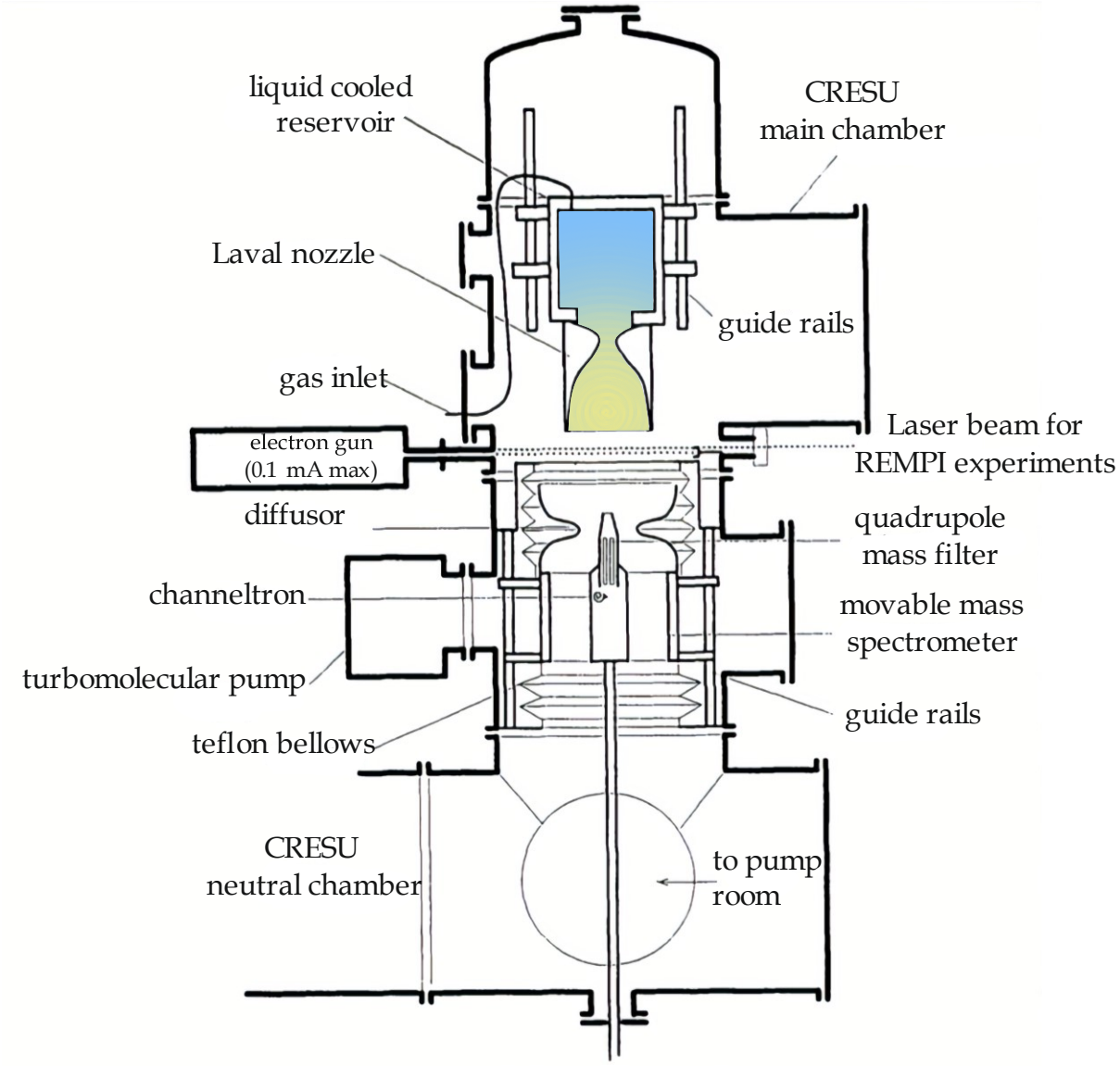

Figure 2.5: The sketch of CRESU (Cinétique de Réaction en Ecoulement Supersonique Uniforme) apparatus constructed to study the ion-molecule reactions, reproduced from paper by Rowe et al. (1995).

A scheme of the CRESU experiment is shown in Figure 2.5. First CRESU experiments were performed in a similar configuration that was used in the SIFT experiments: ions were produced by irradiation of the gas outside the Laval nozzle using an electron beam. A mass spectrometer was used to analyse any ion products. Rate coefficients were determined by observing the change in the ion signals by considering the composition of the flowing gas and the distance of the sampling point from the nozzle. Some upgrades of the

CRESU allow selecting the ion species (Rebrion et al., 1989) and producing ions by resonance-enhanced multiphoton ionisation (Schlappi et al., 2015).

2.4 Trapping of ions in the radiofrequency field

An alternative instrument to study ion-molecule reactions is the ion-trap technique. Despite achieving the low number of charged particles, these experiments have significant advantages. Among the main benefits, there are: reaching lower temperatures, longer observation times, and providing additional tools for controlling ions (Gerlich et al., 1995). Radiofrequency (RF) traps (Major et al., 2005; March et al., 2005) have been used as the primary tool for trapping and storage ions at low temperatures. Here I consider only the main principles, the detailed explanation can be found in the book by Gerlich, (1992a).

In the ion-trap technique, ions are confined in the inhomogeneous electric field $\vec{E}$:

$$\vec{E}(\vec{r},t)=\vec{E}_0(\vec{r})\cos(\Omega t), \tag{2.27}$$

with angular frequency $\Omega = 2\pi f$. Here, $\vec{E}_0$ is the field amplitude vector and t is time. The inhomogeneity of the RF field causes the additional slow drift of the charged particle toward the weaker field region. Created inhomogeneous RF field stores ions in the trap in a radial direction. The ions can be confined in an axial direction by applying a DC voltage to the exit and entrance of the trap. This combination of electrostatic and RF filed characterised by the stability parameter η, defined as:

$$\eta = \frac{2q|\nabla\vec{E}_0|}{m\Omega^2}, \tag{2.28}$$

where m is the mass of the ion and q is its charge. The stability parameter η defines the condition that over the full distance of the oscillation, which is $r = 2q/m\Omega^2$, change of the field must be much smaller than the field itself. According to numerical calculations and empirical results, the stability

parameter η should be less than ≈ 0.3 (Gerlich, 1992a). For quadrupole fields, this limit can also be acceptable for $\eta < 0.4$. In this operating mode, the motion of the ions in the RF trap can be characterised by a slow thermal motion imposed on a fast motion (micromotion) induced by the fast oscillation of the RF field. The time-averaged kinetic energy accumulated in the micromotion equals to a pseudopotential and can be expressed as

$$V^*(\vec{r}) = \frac{q^2 \vec{E}_0(\vec{r})}{4m\Omega^2}, \tag{2.29}$$

which defines the secular motion of the ions in the trap. Some examples of calculations and simulations of the stability parameter and energies of charged particles in an octupole are shown in Figure 2.6.

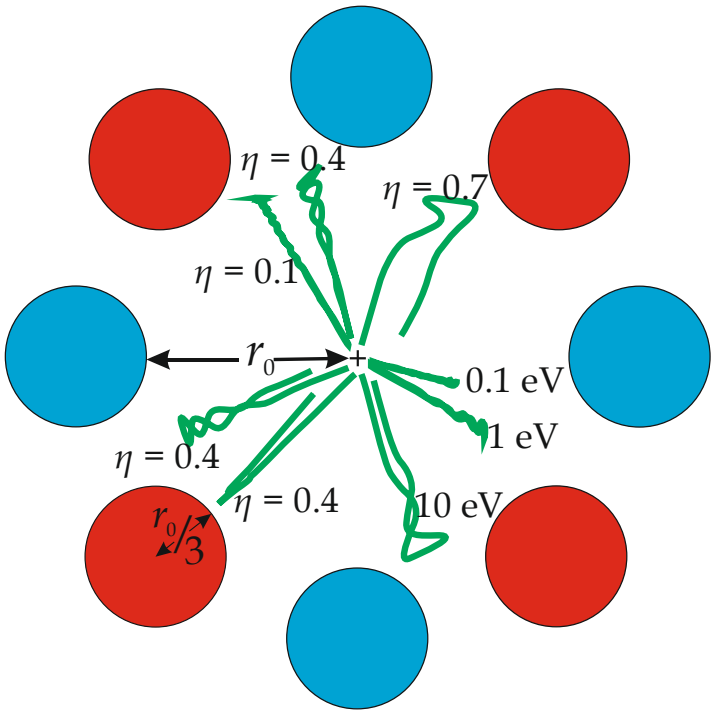

Figure 2.6: Examples of simulated ion trajectories in the octupole. All ion trajectories start in the centre of the octupole. r_0 is a radius of the circle inscribed in the trap electrodes. The examples for stability parameter η = 0.1, 0.4, and 0.7 show that with increasing η the amplitude of the oscillating motion increases and the number of oscillations after one reflection from the RF wall decreases. With increasing energy, the stability of ions trajectory is also decreasing. In the last case for η = 0.4 only the initial angle is different. The figure was reproduced from the book by Gerlich (1992a).

A set of Mathieu equation can express the motion of a single charged particle in the Paul trap:

$$\frac{\mathrm{d}^2u}{\mathrm{d}t^2}+\left[a_{\mathrm{u}} - 2q_{\mathrm{u}}\cos(2\tau)\right]u = 0, \qquad (2.30)$$

where u is one of the cartesian coordinates x, y or z and $\tau = (1/2)\Omega t$. Selection of parameters a_{u} and q_{u} determines proper conditions to confine the ion in the Paul trap. If the values of the Mathieu parameters a_{u} and q_{u} fall into a "region of stability" then ions remain stored in the RF trap.

Historically first RF ion trap was constructed and designed by Wolfgang Paul in 1954. The Paul trap has two main modifications − the 2D linear trap and the 3D ring trap. The simple 2D linear trap consists of four cylindrical electrodes arranged in a quadrupole configuration. The RF voltages $V_{\mathrm{RF}}=V_0\cos(\Omega t)$ with amplitude V_0 alternates between adjacent electrodes. In this configuration, the oscillating quadrupolar potential is created in the direction perpendicular to the longitudinal trap axis, which dynamically confines the ions.

The 3D ring trap is designed as a ring electrode which locates between two hyperbolic end-cap electrodes. Combination of static and oscillating electric fields is used to induce the 3D quadrupole electric potential. The particles are confined in all three directions; thus, they are not able to leave the trap. A scheme of the 3D ring trap is shown in Figure 2.7.

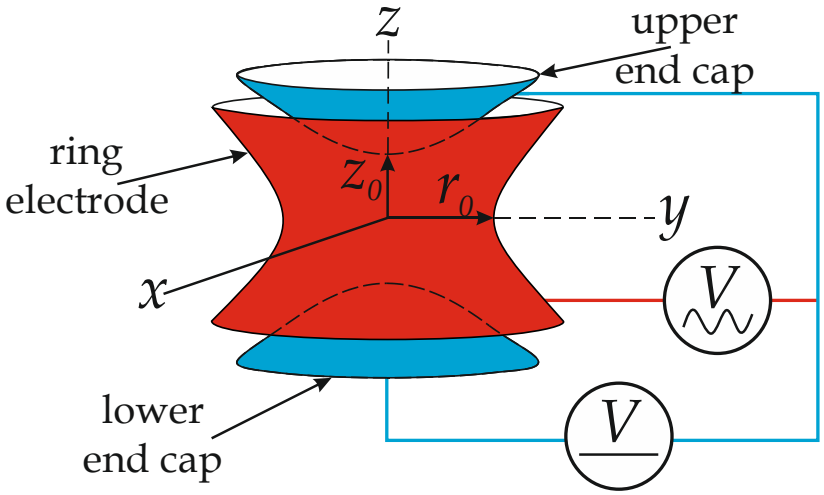

Figure 2.7: The 3D ring trap setup (Major et al., 2005).

2.5 Trapping in higher-order multipoles

The linear higher-order-multipole RF traps are the next step for trapping and studying charged particles. This type of traps consists of $2n$ electrodes, which are placed around a circle. In this multipole, each pair of adjacent rods has opposite polarity with applying oscillating voltages $V_{RF}=V_0\cos(\Omega t)$ and direct current (DC) voltage difference U_0. It creates electric potential φ on the adjacent rods:

$$\varphi = U_0 - V_0\cos(\Omega t). \tag{2.31}$$

The approximate value of the pseudopotential of a linear multipole with $2n$ number of rods is calculated as follows:

$$V^* = \frac{q^2 n^2 V_0^2}{4m\Omega^2 r_0^2}\left(\frac{r}{r_0}\right)^{2n-2} + qU_0\left(\frac{r}{r_0}\right)^n \cos(n\theta), \tag{2.32}$$

where θ is in cylindrical coordinate (Gerlich, 1992a). The equation is valid for higher-order multipoles with the identical rods. A solution of equation (2.32) for n = 2 represents the harmonic pseudopotential of a linear quadrupole trap. With increasing multipole order n, the pseudopotential becomes increasingly weaker to the centre (at the centre the pseudopotential is minimum for any n) of the trap and stronger towards the electrodes, i.e., it becomes a closed space for charged particles. Figure 2.8 represents the simulation where is shown a comparison of effective potentials of some types of multipoles. In this case, the function of distance from the centre of a trap was calculated when DC difference U_0 was 0. Different types of lines show calculated results for the most common types of n-poles. It may be noticed that the effective potential of the multipoles depends on the number of rods. Table 2.2 collects figures of the calculated potential of oscillating fields and pseudopotentials for most used n-poles.

In this work, the RF 22-pole ion trap has been used to study reactions of ions with molecules. The construction and application of this ion trap are discussed in the further section.

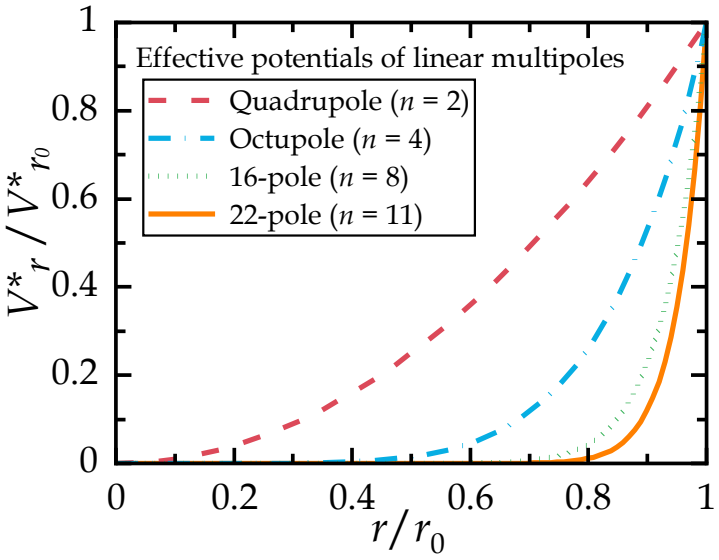

Figure 2.8: Dependence of effective potentials of the linear multipoles on a function of the distance from the centre of the trap in the case when DC difference U_0 is equalled to 0. The figure was reproduced from the book by Gerlich (1992a).

The different types of linear multipoles usually have different practical usage. Quadrupoles are generally used in ion mass-filtration, octupoles apply in guiding systems, and higher-ordered multipoles find application in the confinement of the charged particles.

Table 2.2: Oscillating fields potentials and pseudopotentials of the most used multipoles.

	Quadrupole (n = 2)	Octupole (n = 4)	16-pole (n = 8)	22-pole (n = 11)
Potentials of oscillating fields	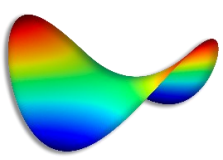	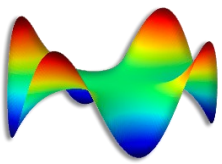	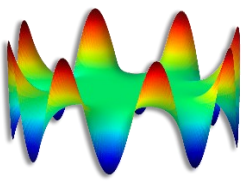	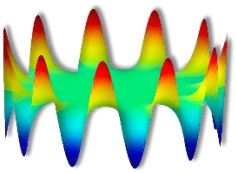
Pseudo-potentials	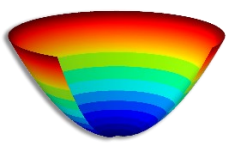	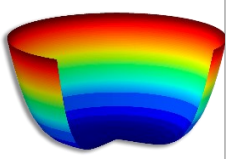	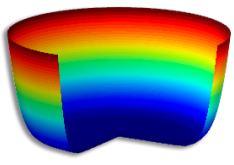	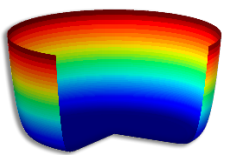

3. Goals of the thesis

The primary purpose of my work is to obtain the temperature-dependence of the rate coefficient of the exoergic ion molecular reaction of ground-state oxygen ion $O^+(^4S)$ with molecular hydrogen H_2. This reaction is vital for astrochemistry as it is a crucial process in the synthesis of water molecules in the interstellar medium.

The next goal is to study an isotope effect of reaction of $O^+(^4S)$ with hydrogen isotopologues (D_2, HD). It is also essential to determine the ratio of rate coefficient of the OH^+ production channel to the total reaction rate coefficient of the reaction of $O^+(^4S)$ with hydrogen deuteride.

Another task is the determination of activation energies and to study the isotope effect in reactions of N^+ ion with D_2 and HD molecules. Study of these reactions can be also helpful for solving the problem with the pathway of the reaction of $N^+(^3P_{ja})$ with $H_2(j)$.

Listed reactions were studied at temperatures down to 15 K, which corresponds to temperatures of many different regions in the interstellar medium.

4. Experimental facility

The RF 22-pole ion trap (22PT) instrument was designed and constructed by the group led by prof. Dieter Gerlich in Chemnitz University of Technology (Gerlich & Horning, 1992; Gerlich, 1995; Asvany, 2003; Borodi, 2008). This instrument is efficient and sensitive equipment to study ion-molecule reactions experimentally. In 2009 the apparatus was transferred to Prague.

Until today it has been used in more than 30 experimental studies of ion-molecule reactions. The basic principles of ion production, trapping and detection are discussed in detail in this chapter.

4.1 Radiofrequency 22-pole ion trap apparatus

The RF 22PT ion trap apparatus consists of different separate components to produce, filter, guide, trap, and analyse the ions. These components are mounted in series and placed in the vacuum chambers. To provide measurements with temperatures down to 10 K, the cryogenic system is used.

The apparatus (Figure 4.1) consists of the RF 22-pole ion trap, a Storage Ion Source (SIS), a Quadrupole Mass Filter (QMF), a cold head, a Quadrupole Mass Spectrometer (QMS) and a MicroChannel Plate Detector (MCPD).

Ions are produced in the SIS by electron impact ionisation of neutral gas. The quadrupole mass filter is configured to pass only ions with specific mass. After filtration, the ions are guided to the trap where they are confined. The kinetic energy of trapped ions is thermalised after collisions with helium atoms of the buffer gas, which is earlier pre-cooled by collisions with trap walls. In most experiments, one filling of the trap contains a few hundred reactant ions which come from the SIS. The temperature of the trap (T_{22PT}) can be changed in ranger from 300 K to 10 K.

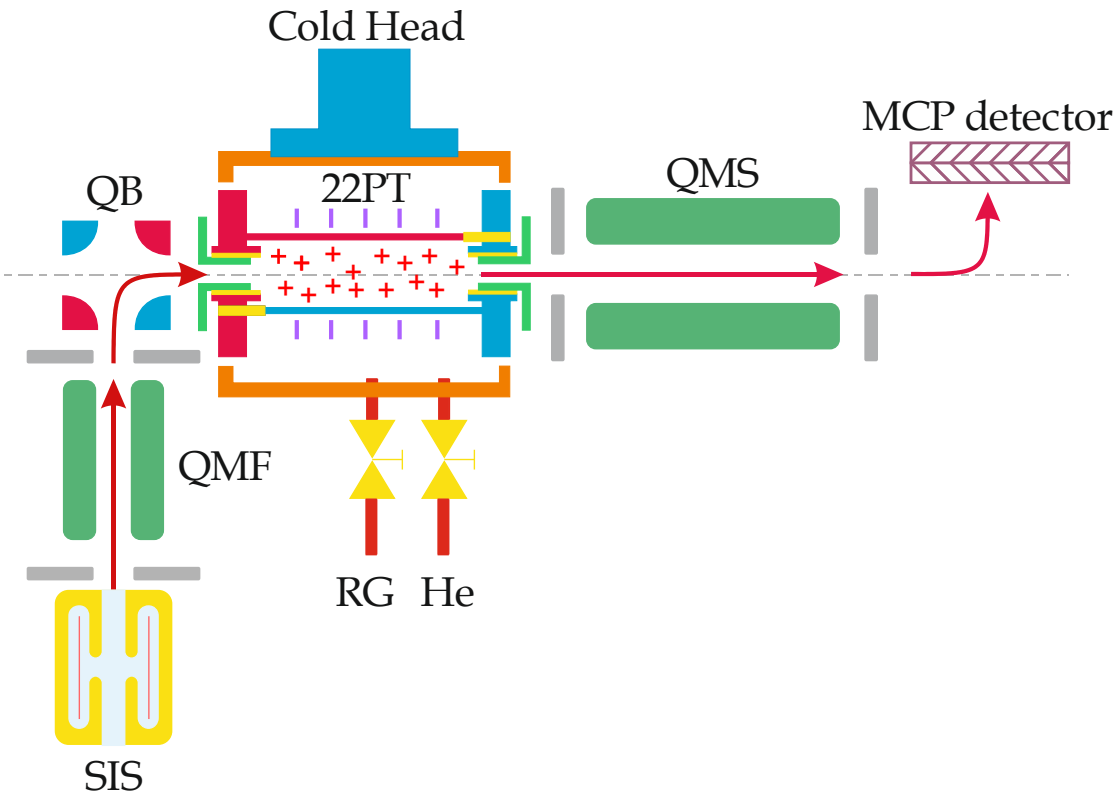

Figure 4.1: Schematic diagram of the cryogenic radiofrequency 22-pole ion trap (22PT). The main elements of our apparatus: Storage Ion Source (SIS or IS), Quadrupole Mass Filter (QMF), QB (Quadrupole Bender), Quadrupole Mass Spectrometer (QMS), MicroChannel Plate Detector (MCPD). The figure is adopted from the paper by Zymak et al. (2013).

The three-stages vacuum system consists of 8 pumps and supports the ultra-high vacuum (UHV) inside our technique. The detail description of the vacuum system is given in subchapter 4.1.1.

The number densities of buffer (helium) and reactant gases (RG) inside the trap are monitored using a spinning rotor gauge (SRG) connected directly the coper housing where the 22PT is located. Furthermore, an ion gauge (IG) is used to measure the pressure in the vacuum chamber, which contains the ion trap. It is calibrated by using the spinning rotor gauge.

The delay pulse generator is used to synchronise guiding, trapping, and detection of ions. The generator sends "opening" pulses to electrodes in a sequence from the ion source to the trap. Setting and managing of the apparatus are implemented from the computers with a set of specific

LabVIEW programmes. In addition, the realisation of the control scheme is implemented on the base of a Meilhaus Electronic RedLab 3105 USB digital-analogue converter (DAC) and a Novation Nocturn plug-in controller. The required voltage values are set up in the potentiometers of the plug-in controller which sends the intended signals to the computer via USB interface. At the same time, the USB signals from the computer are converted to an analogue voltage by DAC, which sends these analogue voltage values to the necessary electrodes.

4.1.1 Vacuum system

Maintaining the high vacuum conditions, inside the apparatus, is the crucial requirement for carrying out the astrophysical-relevant experiments. In our studies, the experiments have been performed at gas number densities from 10^{10} cm^{-3} to 10^{14} cm^{-3} inside the RF 22-pole ion trap, which is equivalent to the pressure of the gas inside the 22PT chamber $10^{-7} - 10^{-3}$ Pa at 11 K. The upper limit of the residual pressure in the chambers is 10^{-8} Pa and the fraction of impurities in the gas at 11 K is small enough to study rate constant around 10^{-16} cm^3s^{-1}.

For calculation of the rate coefficient, it is essential to know the precise value of number density or respectively pressure inside the chambers. As the main instruments to control the pressure inside the chambers, an ionisation gauge with electronic system AML AIG NGS2 and a spinning rotor gauge are used. The SRG consists of measuring head SRG–SH700, a ball/flange assembly SRG-BF and an electronic control unit MKS SRG 3. The IG is mounted on the top of the 22PT chamber and can measure over the ultra-high vacuum range 1×10^{-5} to 3×10^{-9} Pa. The SRG instrument is connected directly to the copper housing where the 22PT instrument is located. The SRG instrument is also used for direct pressure measurements inside the trap.

The scheme of the vacuum and the gas-inlet systems of the RF 22PT apparatus is shown in Figure 4.2.

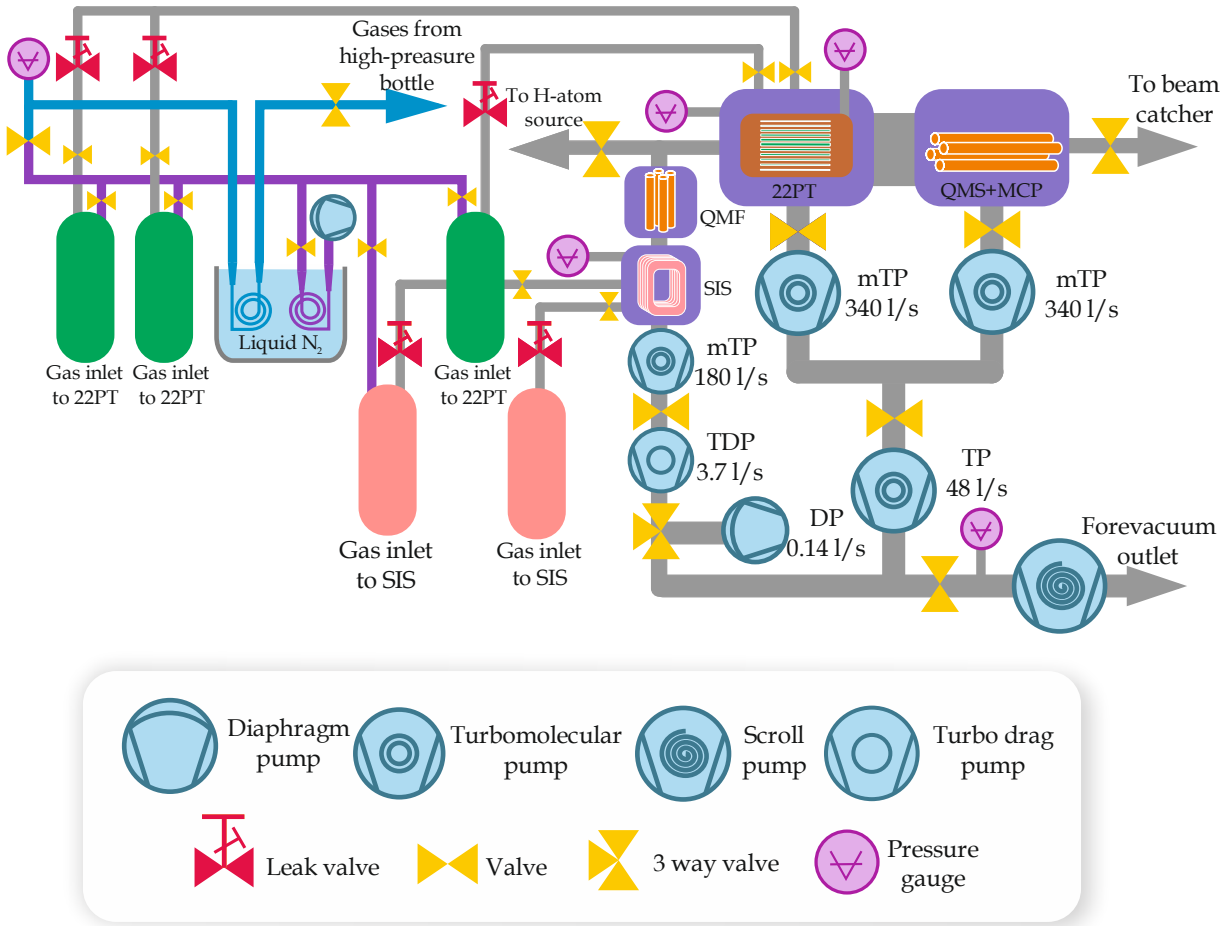

Figure 4.2: Combined diagram of the three-stage pumping system with the inlet system of the 22PT apparatus. The chambers are pumped by magnetic-levitation turbomolecular pumps (mTP). Forevacuum for all chambers is generated by a scroll pump (SP), and a supporting diaphragm pump (DP). The supporting turbomolecular pumps (TP) and turbo drag pumps (TDP) are used to increase pumps compression ratio for light gasses (H_2, He). The pumping speed values for hydrogen are shown in litres per second (l/s).

The 22PT instrument is pumped by Leybold Vacuum magnetic-levitation turbomolecular pumps Turbovac 340M (the 22PT and detector chambers), TMU 200M (the ion source chamber). Turbo drag pump Pfeiffer Vacuum HiPace® 10 is applied to increase the compression ratio of the turbomolecular pump. This pump is mounted in series with the TMU 200M. For the detector and the 22PT chambers, we use more efficient HiPace® 80.

The forevacuum condition is formed by Varian SH 110 scroll pump. We also apply a separate diaphragm Pfeiffer Vacuum MVP 015–4 pump to form forevacuum for the ion source to increase the compression ratio of the turbomolecular pump. Pfeiffer Vacuum TPR 280 Pirani gauges are used to measure and monitor forevacuum pressure.

The inlet system consists of a set of reservoirs, a cryogenic filter, a Pfeiffer Vacuum MVP 015–4 diaphragm pump and a capacitive pressure sensor. The reservoirs are filled up to $1\times10^5 - 3\times10^5$ Pa from high-pressure cylinders with required gases. Depending on the gas-filled from high-pressure bottles, the cryogenic filter is filled with liquid nitrogen or cooled ethanol 96%. The cooled ethanol 96% is used for gases with high boiling points (CO_2, CH_4) to reduce the impurities. The filter allows getting rid mainly of water in the gas which is sent to reservoirs. UHV variable leak valves Leybold 87395, Varian 951-5106, Balzers UVD – 040 are used to control the flow of the gases injected into the trap or the ion source volume. One of the reservoirs is connected to a piezoelectric valve (Piezo Valve) which is used in some cases to regulate flow and periods of injection of the buffer gas for trapping of ions.

4.1.2 Storage ion source and ions extraction

The RF storage ion source (SIS) is applied for the production of primary reactant ions. It is well described by Gerlich and Teloy (Gerlich, 1992a; Teloy & Gerlich, 1974). In this subchapter, the ion preparation routine starting from production and guiding of the ions directly into the 22PT is described.

Ions are produced using the focused electrons, emitted from a cathode. The ions accumulate inside the SIS until the trap filling process begins. Ions can be extracted from the ion source through the quadrupole filter of ions and additional electronic optic lenses components directly into the 22PT.

After adding neutral gas into the SIS chamber, production of ions starts from the emission of electrons from a cathode (filament), which is heated by an applied direct current between 3.6 A and 5.8 A. The cathode is a tensioned Rhenium wire with diameter 0.3 mm, purity 99.97% and 5.0 eV work function.

Rhenium is used as it has a high melting temperature of 3459 K, and it is more resistant to oxidation than tungsten. After a thermal electron emission, the electrons accelerated by a potential of a filament-repeller, after which the potential of the focus electrode distributes them. The emission current is monitored at the B_0 electrode, and the measured electron emission current is in order of 0.1 − 1 mA.

A simplified scheme of the storage ion source is shown in Figure 4.3. Before extraction, ions are stored in a cavity between the RF plates, which is shown in the upper part of Figure 4.3. Produced ions usually are highly excited, but inelastic collisions with the neutral gas thermalise their kinetic energy before the extraction.

Generally, the resonant frequency of the SIS is maintained as 19 MHz, and in some cases, we use a coil with a resonant frequency of 16 MHz. These frequencies allow the SIS to confine the ions with masses from 1 Da to 30 Da with high efficiency. For masses, over 30 Da we use a coil with resonant frequency 3.3 MHz. The MFG-269C, together with MFJ-259C RF impedance analyser devices are used for monitoring and analysing of the RF impedance of the ion source generator. This device is a 300–watt RF output power antenna tuner that matches any transmitter or transceiver to virtually any antenna.

A potential barrier is created along a horizontal axis of the SIS by B_{-1} electrode with the static potential of several volts. The end plate electrodes create the potential barrier in the perpendicular direction to the planar electrodes. An opening pulse B_0 allows extracting the ions into a quadrupole filter. The potential and the length of the pulse are regulated for obtaining a directed beam of ions, and depending on ion mass, the pulse can last from ~ 5 μs to 20 μs. The electric separation is provided by sapphire balls that are inserted between the RF electrodes.

The SIS has two identical cathode assemblies (focusing electrodes and cathodes) thus, we can easily switch from one to another in case one of them is out of order. The specific methodology of ion production is described in the experimental sections.

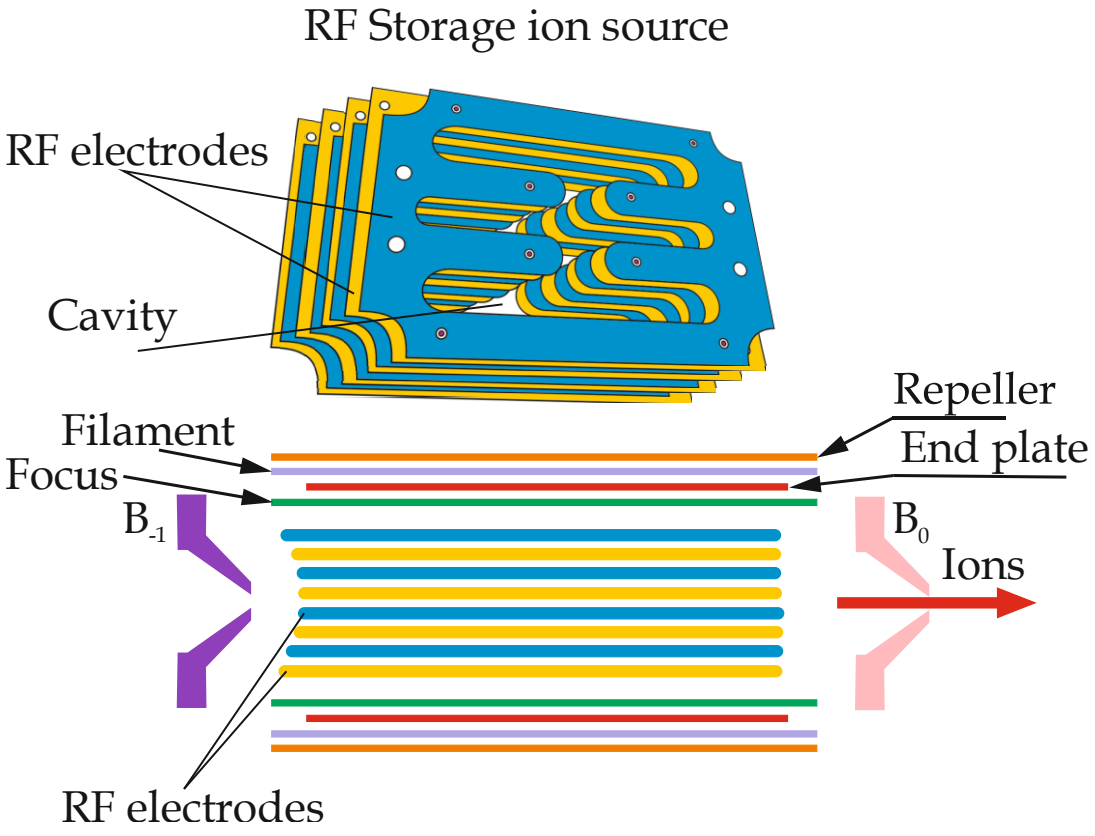

Figure 4.3: A simplified scheme of the RF storage ion source. Blue and yellow electrodes represent the opposite signal phases. Upper panel: Simplified 3D view of the RF electrodes shows the cavity regions. Lower panel: Position of the electrodes in the storage ion source. Electrodes B_{-1} and B_0 have DC potentials and perform trapping of the ions along the horizontal direction. The end plate electrodes are used to confine ions along the vertical direction.

After sending the opening pulse to the B_0 electrode, ions enter the quadrupole mass-filter (QMF). The QMF is located in a separate chamber which is connected to the ion source. Required type of ions can be filtered by the QMF from the mixture coming from the SIS, and then the mass-selected ions continue their movement to the trap. The detailed description of the QMF can be found in the book by Gerlich (1992a), and its operating principles are discussed in the next subchapter.

4.1.3 Quadrupole mass filter and ion guiding system

As it has already been mentioned in Chapter 2.4, the motion of the charged particle in the RF field of a multipole is described by Mathieu equation (2.30). The field in the QMF is generated by DC potential U_0 and AC voltage $V_0 \cos(\Omega t)$ on the quadrupole rods. Mathieu stability diagram (Figure 4.4) shows the region of the stable trajectories in the RF field of the quadrupole. The stability parameters q_1 and a_1 of quadrupole are defined as

$$q_1 = \frac{4qV_0}{m\Omega^2 r_1^2}, \tag{4.1}$$

$$a_1 = \frac{8qU_0}{m\Omega^2 r_1^2}, \tag{4.2}$$

where r_1 is quadrupole inscribed radius.

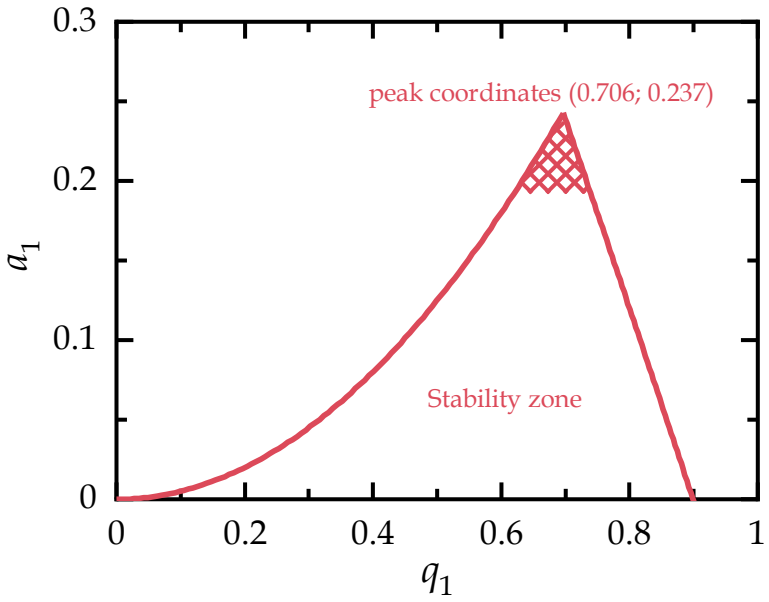

Figure 4.4: First stability zone of the Mathieu (a_1, q_1) diagram. On top of the Mathieu diagram, there is a region near the peak, which is the appropriate region of high-resolution mass-filter operation (Gerlich, 1992a).

As an RF signal source is used a generator with frequency f = 6.7 MHz. The primary purpose of mass filtration is the separation of undesirable ions. From the equations (4.1) and (4.2) the values U_0, V_0 can be calculated to obtain

the optimal parameters of a stable motion trajectory for a particular type of ions. An example of $U_0 - V_0$ diagram for several masses is presented in Figure 4.5. These masses correspond to the most used ions that are involved in experiments related to this work.

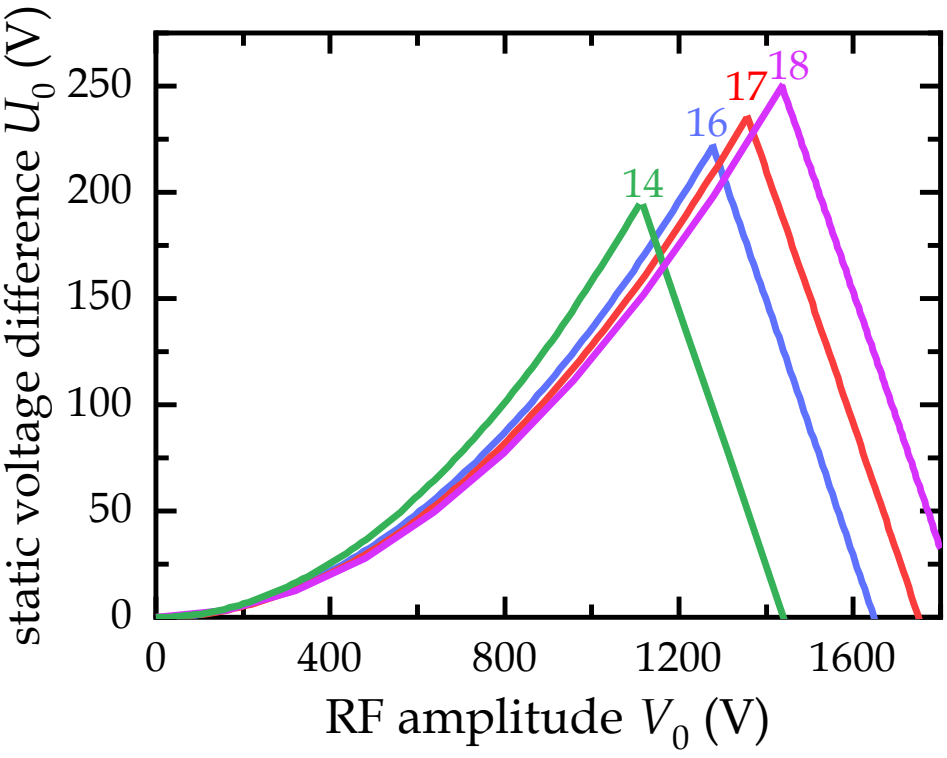

Figure 4.5: Regions of stability for several ion trajectories in the QMF. Masses of ions are given in Daltons (Da) or a.m.u and refer to N^+, (14 Da); O^+, NH_2^+, ND^+ (16 Da); OH^+, NH_3^+, (17 Da); H_2O^+, OD^+ (18 Da) ions. In the calculation, I used the RF frequency f = 6.7 MHz and the quadrupole inscribed radius r_1 = 5 mm.

The practical example of the QMF is shown in Figure 4.6. The integral spectrum of ions mixture produced from N_2O molecules in the SIS represented in Figure 4.6. The trapping or storage time t and trap temperature T_{22PT} of this measurement are 10 ms and 135 K, respectively.

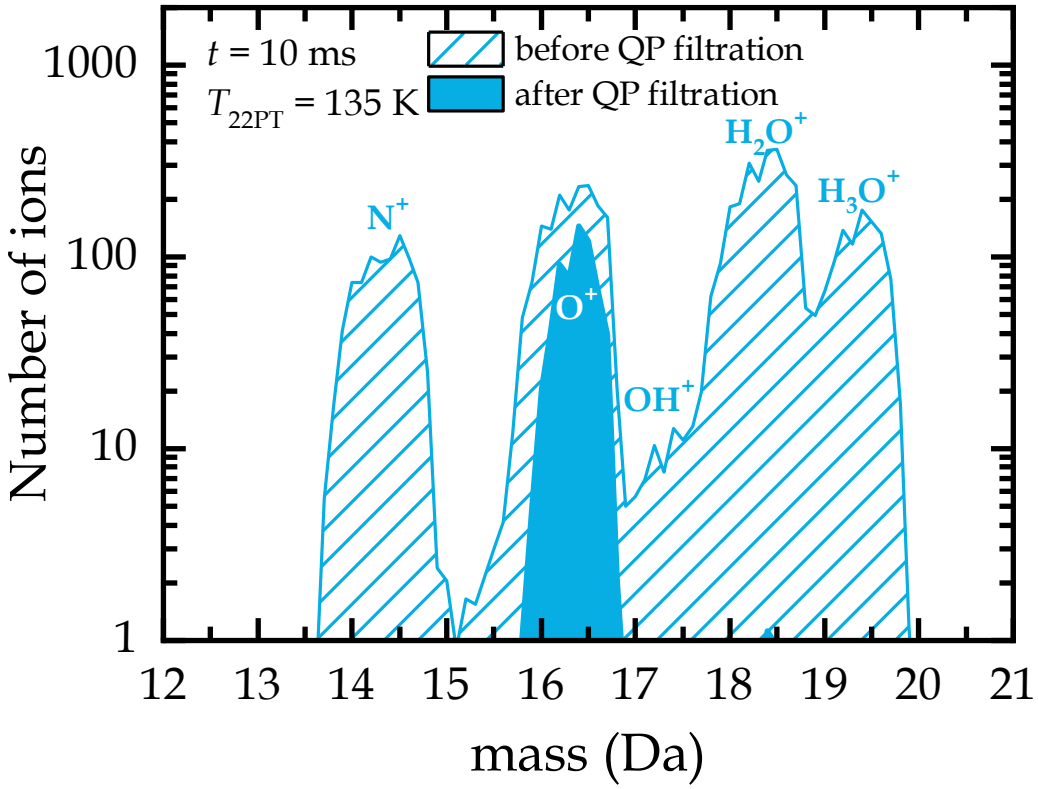

Figure 4.6: An integral spectrum of ions in the 22PT before filtration (cross-filling) and the integral spectrum after filtration (full-filling). The O^+ ions are in the mixture of ions which comes from the SIS.

After the QMF, the ion beam passes through an electro-optic guiding system. A pair of pulsed electrodes B_1 creates a potential barrier on the ion's pathway, keeping the trap from continuous filling. Extraction pulse B_0 is synchronised with the respective B_1 pulse. The pair of B_2/B_3 electrodes have DC potential, and they are used for additional control of the ion beam. The simplified scheme of the electro-optic guiding system is shown in Figure 4.7.

An electrostatic quadrupole beam deflector or quadrupole bender (QB) is used to bend a beam of charged particles by 90 degrees. The bending can be performed by setting the DC potentials $+V_{QB}$ and $-V_{QB}$ on opposite rods. The deflector plates are placed around the quadrupole rods to prevent the ion beam from bending in the vertical direction due to the fringe fields. After the QB, ions enter the 22PT ion trap.

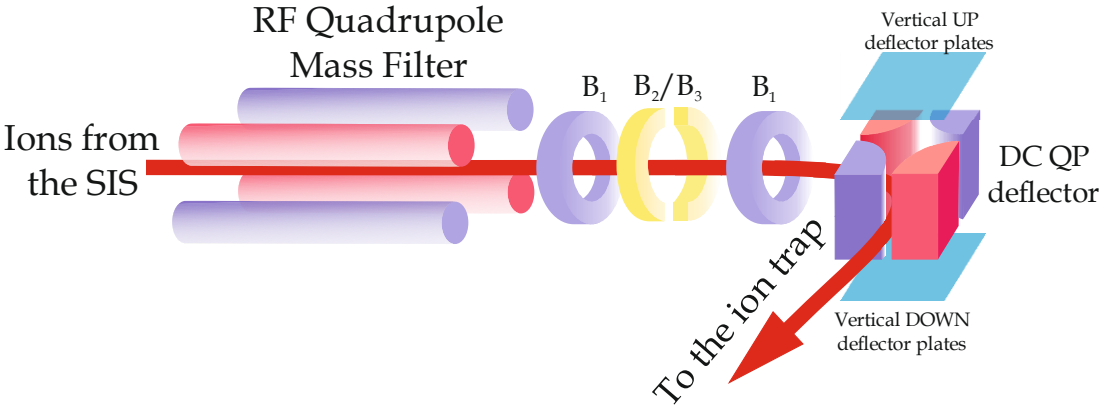

Figure 4.7: Simplified scheme of the guiding system of the 22PT instrument. Pulse electrode B_1 is used to avoid continuous filling of the trap. The electrodes B_2/B_3 are applied to improve the focusing of the ion beam. The quadrupole deflector bends the beam and aligns it with the axis of the ion trap.

4.1.4 The radiofrequency 22-pole ion trap

The temperature variable RF 22-pole ion trap is a central element of our experimental equipment. It was developed in 1992 (Gerlich & Horning, 1992), and its simplified scheme is shown in Figure 4.8. The trap consists of two sets of 11 stainless steel rods with diameter d = 1 mm, which are evenly distributed around the circle with inscribed radius r_0 = 5 mm. The adjacent rods have opposite polarity, and altogether they create a 22-pole-shape pseudopotential (see Table 2.2, n = 11). The combination of the RF field with electrostatic fields of cylindrical entrance and extraction electrodes in axial direction creates the condition for confining the ions in the radial and axial directions. A set of five ring electrodes can also generate a potential gradient in the axial direction. This modification allows compensating the stray fields, reaching better extraction from the trap, and it also provides movement of the ions close to the trap centre.

The 22-pole trap is located in a copper housing which is thermally connected to the cold head refrigerator system (a compressor RW 2/3 and Leybold RGD 210 cold head). The temperature of the copper housing can be changed from 312 K (or room temperature) down to 10 K. A silicon diode (Lakeshore DT-471-C4) is mounted to the trap copper housing and measures

its temperature. The temperature of the trap is controlled by a heater which represents a resistive wire mounted on the first stage of the cold head.

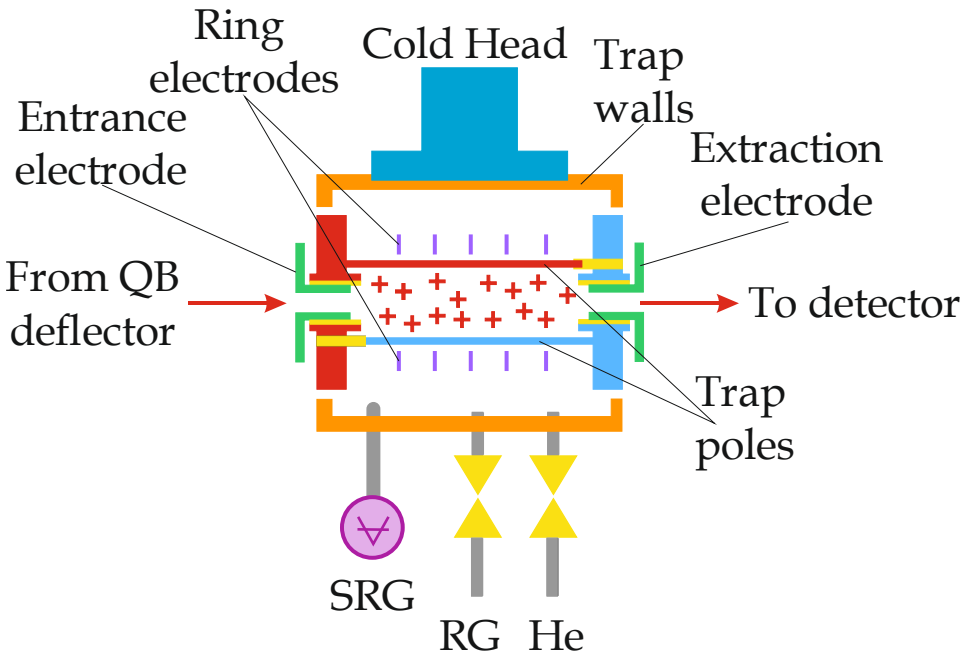

Figure 4.8: Scheme of RF 22-pole ion trap. All main parts are signed. Reactant gas (RG) and buffer gas (He) tubes go through the copper housing. Gases come in contact with walls which are pre-cooled by a refrigerator system or cold head. The spinning rotor gauge (SRG) is used for measurement of the pressure inside the trap. Red and blue colours of the trap poles represent opposite polarities. The figure is adopted from the paper by Gerlich et al. (2013).

After a quadrupole deflector, the ion beam enters the trap. The open pulse of the entrance electrode is synchronised with B_0 and B_1 pulses in the SIS and the guiding system, respectively. Reactant and buffer (Helium) gases can be injected through the sensitive leak valves. In some cases, we also provide the buffer gas transfer to the trap through a pulsed piezo-valve. Such transfer is applied for better confining and cooling of ions.

We control the length of the ion bunch by changing the length of the filling pulses. For more efficient confinement, the length of the beam should be comparable with the length of the trap in the axial direction. It prevents the

losses of ions from the ion trap, in reflection with created DC potential on the extraction electrode.

Confined in the pseudopotential ions form an ion cloud. The trap allows keeping ions inside the trap without any loss for more than 10 s. Potentials on the entrance and extracting electrode is usually differed by ~1 V from the potential applied to the ion trap.

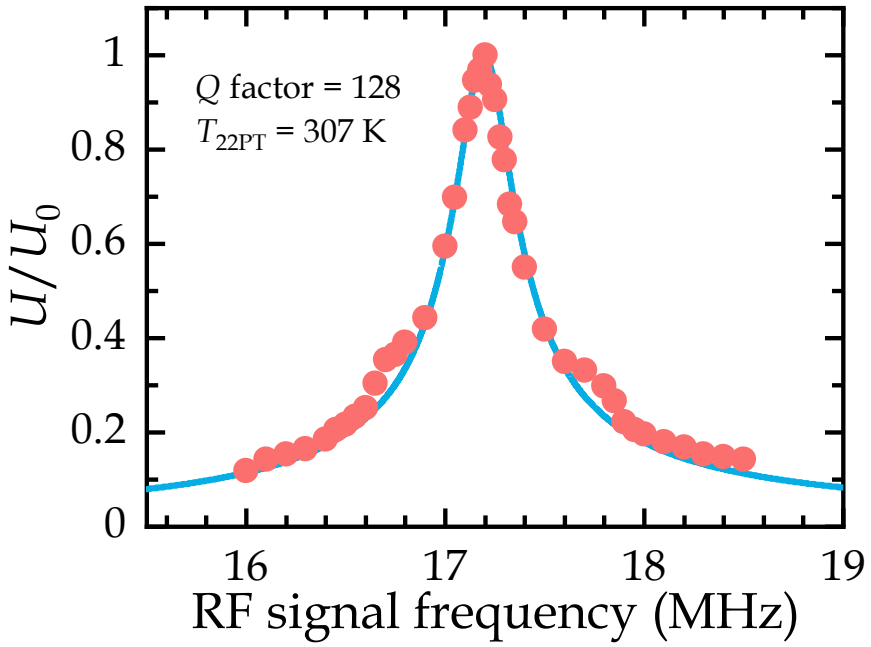

Figure 4.9: Result of measurement of resonator quality Q in the RF trap-generator system. Experimentally measured data are fitted by the universal resonance curve and shown as a solid line.

The resonance frequency of the circuit is f = 17.2 MHz. This frequency allows confining ions successfully with masses higher than 2 Da. The result of the measurement of the resonator quality is shown in Figure 4.9.

Depending on the aim, different trapping or storage time is selected for checking the ion composition after reaction in the 22PT. After opening of the extraction electrode at the chosen time by applying a voltage to this electrode, the ions pass through the analysing system. Obtained data allow us to calculate the rate of selected reactions. We repeat the same measurement two or more times to obtain a better statistic. Measurements of the dependencies of reaction rate coefficients on different trapping parameters (entrance or exit

DC potentials, trap potential, RF amplitude etc.) allow us to be sure that the experiment is carried out correctly.

4.1.5 Detection of ions

After passing the trap, ions are sent to the detection system, which analyses the composition of the ion beam after extraction from the ion trap. The detection or analyse equipment consists of a quadrupole mass spectrometer (QMS), a MicroChannel Plate Detector (MCPD), and an ion counter.

The QMS is combined with two electrodes with DC electric potential that focus ions which come from the ion trap. A generator Balzers QMH 400-5 RF is applied to generate the potential on the QMS rods.

Passing the QMS, the ion beam is focused by three electrodes with applied DC potentials to the Hamamatsu F-4655-12 microchannel plate detector. This MCPD can detect only charged particles. Interaction of the ion with microchannel walls creates the electron avalanche in a single channel, with further conversion into a digital electrical pulse. 100 MHz ion counter is used to count the digital electrical pulses. The ion counter stops at the moment of the ion extraction from the ion trap. That pulse is named "gate". The falling edge of the extraction pulse is used to control the gate pulse.

The MCPD saturation occurs when particles with a charge reach the MCPD more frequently than the counter device can count them. The ion distribution in the beam should be uniform to reduce the losses on the surface of the detector. Therefore, a slow-ramp filter is used for smoothing the extraction pulse of the ion trap. The filter allows extending the ion bunch which comes from the ion trap to avoid counter saturation. However, when it comes to the order of hundreds of trapped ions per one pulse, the effect of saturation can be negligible.

4.1.6 Cooling of the ions inside the trap

In the RF 22PT instrument, ion-molecule reactions are studied at temperatures lower than 300 K. These temperatures are relevant to some interstellar environments (see Chapter 2.1). A cooling system of the 22PT instrument is used to obtain the interstellar-relevant temperatures; therefore, ions have to be thermalised in the ion trap achieving energies of ~ 1 meV that corresponds to ~ 10 K. Cooling takes place when ions collide with the cold buffer gas resulting in kinetic energy exchange between them.

Number collisions of the thermalisation process can be evaluated from the model of elastic collisions. If we consider that kinetic energy of the ion is much higher than the kinetic energy of the buffer gas particles, the average energy that can be transmitted after one elastic collision ΔE is:

$$\Delta E = \frac{2m_{\mathrm{Ion}}m_{\mathrm{BG}}}{(m_{\mathrm{Ion}}+ m_{\mathrm{BG}})^2} E_{\mathrm{Ion}} = \gamma E_{\mathrm{Ion}} , \qquad (4.3)$$

where m_{BG} and m_{Ion} are masses of the buffer gas particle and the ion, respectively; E_{Ion} is average initial energy of the ion and γ is a linear factor which designates as mean energy decreases after j collisions. Average energy decreases after j collision:

$$\frac{E_{\mathrm{BG}}}{E_{\mathrm{Ion}}} = (1-\gamma)^j . \qquad (4.4)$$

In the same case, the collision frequency of one ion is written as:

$$f_{\mathrm{c}} = n\langle v_{\mathrm{Ion}}\sigma_{\mathrm{L}}\rangle = nk_{\mathrm{L}}, \qquad (4.5)$$

where n is gas number density and k_{L} is Langevin collisional rate constant. In equation (4.5), the brackets designate velocity averaging. Considering equation (4.5) the minimal time for cooling the ion to the energy that corresponds to the energy of the buffer gas is:

$$\Delta t = \frac{j}{f_{\mathrm{c}}} = \frac{\ln(E_{\mathrm{BG}}/E_{\mathrm{Ion}})}{\ln(1-\gamma)} \cdot \frac{1}{nk_{\mathrm{L}}} . \qquad (4.6)$$

For example, it is enough ~ 12 collisions of O^+ ions at energy 100 meV with He atoms at energy 1 meV to be thermalised. According to equation (2.25), the calculation gives $k_L \sim 6\times10^{-10}$ cm^{3}s^{-1} for O^+ + He collision. A commonly used in our experiments value of He buffer gas number density is ~ 10^{13} cm^{-3}. According to equation (4.5), collision frequency f_c has value ~ 6×10^3 s^{-1} and equation (4.6) gives a thermalisation time of O^+ ions ~ 1.5 ms.

The process of thermalisation of ions in the buffer gas can be seen when the storage time of the ions in the trap can be compared to the time of thermalisation. Examples of cooling are presented in Figures 5.5 and 5.9 (upper panel) of Chapter 5.1, where the first data points represent the situation when ions do not have enough time to cool down in collisions with pre-cooled He atoms thus have enough energy to overcome the potential barrier of the ion trap and focus electrodes of the detection system.

Additional parasitic RF heating influences the movement of the charged particles inside the trap. This effect occurs near the rods and leads to the situation when the ions temperature differs from the buffer gas temperature. The imperfection of the trap geometry may also be a cause of more intensive RF heating (Asvany & Schlemmer, 2009).

As was mentioned in 4.1.4, the cooling system of the ion trap is presented by a two-stage closed-cycle helium refrigerator system, including the compressor RW 2/3 and Leybold RGD 210 cold head. The first stage cools down to 50 K. The trap is covered in the copper housing, which is mounted on the second stage of the cold head. This configuration allows achieving temperatures around 10 K. Gas inlet system passes through the second stage of the refrigerating system to remove the impurities.

Two silicon diodes are mounted on the trap copper housing and obtained data process by Lakeshore 218 temperature monitor which also secures the 22PT from overheating. The automatic control of the heating is realised in the LabVIEW programming environment.

The difference in measured temperature of the ion trap housing walls and temperature of the ions inside the 22PT after cooling can be 5 K. This discrepancy will be discussed in the next subchapter.

4.1.7 Determination of the temperature and number densities of gases in the RF 22-pole ion trap

In this work, I mention two temperatures. The first one is the temperature of the 22PT walls, which is designated as T_{22PT}. The second one is designated simply as T, representing a collisional temperature of confined ions with reactant gas inside the trap. The temperature T is determined as the average mass-weighted value of reactants temperature. In the ion trap technics, the translational temperature of the thermalised ions (T) a bit higher than the temperature of the ion trap, this fact has also been discussed by many groups in their studies (Gerlich & Horning, 1992; Gerlich, 2008; Asvany & Schlemmer, 2009; Chakrabarty et al., 2013; Endres et al., 2017).

We used the reaction between argon ion and molecular hydrogen to determine actual temperature T and how much it is different from the temperature of the trap walls T_{22PT}. The proton transfer reaction:

$$Ar^+ + H_2 \rightarrow ArH^+ + H, \qquad (4.7)$$

has been studied by many groups before (Ervin & Armentrout, 1985; Liao et al., 1990; Rakshit & Warneck, 1980; Sizun et al., 2002) and nowadays, it is still attractive (Michaelsen et al., 2017). Since the reaction (4.7) has been studied in detail, it can be used as a testing reaction.

In this experiment, ions were not trapped, but they were led continuously in a beam. An ion beam of Ar^+ ions passed through the ion trap and reacted with H_2. We measured the numbers of primary ions $N(ArH^+)$ and products $N(Ar^+)$. The ratio $N(ArH^+)/N(Ar^+)$ was calculated as a function of the ion trap temperature T_{22PT}.

We select stable $^{36}Ar^+$ isotope (natural abundance is 0.3336%) for monitoring the flux of $^{40}Ar^+$ ions to avoid saturation of the MicroChannel Plate

Detector due to high ion current. The ratio $N(^{40}ArH^+)/N(^{36}Ar^+)$ is directly proportional to the number density of H_2, which is inversely proportional to the square root of T_{22PT}. To obtain the relative change of the number density of H_2 with the trap temperature, it is sufficient to record $N(^{40}ArH^+)/N(^{36}Ar^+)$ as a function of T_{22PT}. Molecular hydrogen was added into the trap at room temperature (312 K), and then the cooling of the trap was turned on. During the cooling, the ratio $N(^{40}ArH^+)/N(^{36}Ar^+)$ was monitored and was recorded. Measurements were done for cases when the RF field was turned on and off. When the RF voltage of the trap was turned off, data were in agreement with $1/\sqrt{T_{22PT}}$ over entire temperature range (see Figure 4.10 (a) and 4.10 (c)). In case, when RF was turned on, data were in agreement with $1/\sqrt{T_{22PT}}$ only at temperatures higher than 100 K.

When the RF field of the trap is on, measured data shows discrepancies at lower temperatures (see Figure 4.10 (b) and Figure 4.10 (d)). Although, ratio $N(^{40}ArH^+)/N(^{36}Ar^+)$ multiplied by $1/\sqrt{T_{22PT}}$ must be constant, it is constant just in case when the RF field of the ion trap is off (see Figure 4.10 (c)), and it decreases when the RF filed is on (see Figure 4.10 (d)). The decreasing can be caused by heating of the neutral gas by the RF trap filed.

Decreasing of the ratio in Figure 4.10 at the temperatures from 20 K down to 10 K, which can be seen in all graphs, is caused by hydrogen condensation on the second stage of the cooling system and further stabilisation of the number density. For more precise measurement the cooling should have been slower at these temperatures. The results of our study show that collisional temperature T is approximately 5 K higher than the measured temperature of the copper housing with inaccuracy ± 5 K. This effect is caused by heating of the ion trap rods by the RF field, which further heat the neutral atoms. In this case, the collisional temperature is defined as $T = T_{22PT} + (5 \pm 5)$ K, and in all further experimental results, this correction is taken into account. This situation has also been discussed by Plašil et al. (2012), Zymak et al. (2013), Mulin et al. (2015), and Tran et al. (2018).

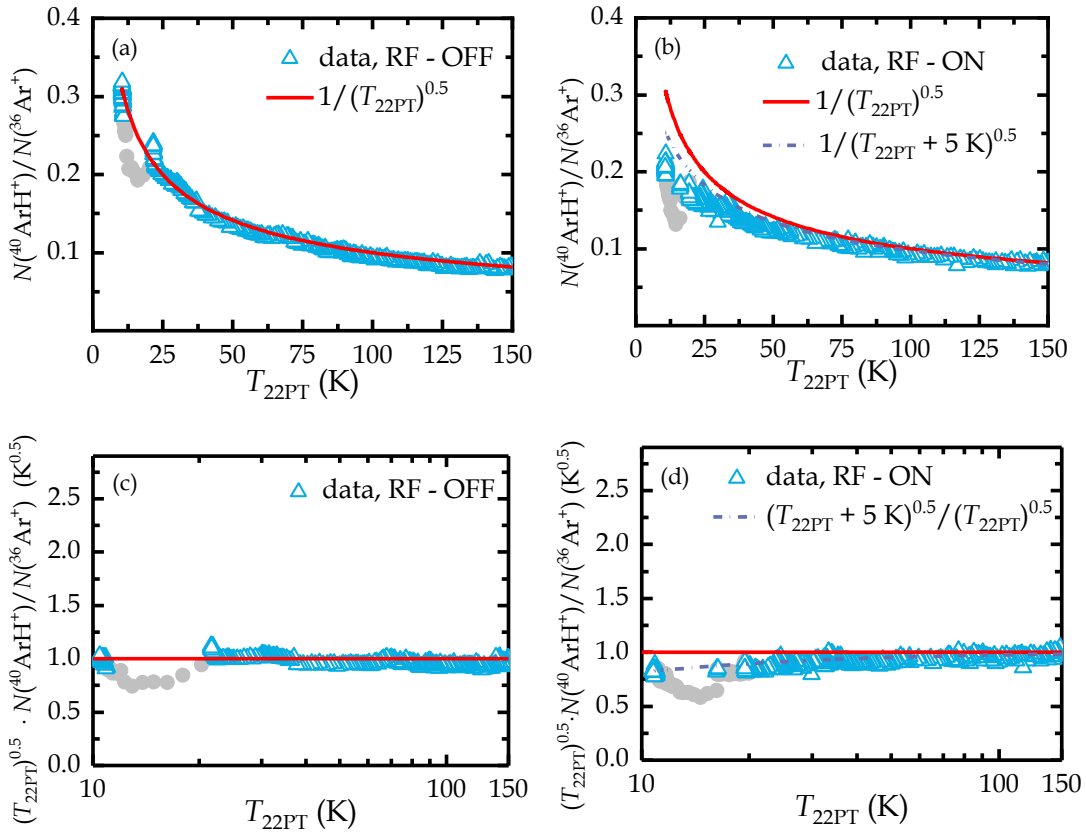

Figure 4.10: The set of graphs shows ratio $N(^{40}ArH^+)/N(^{36}Ar^+)$ as a function of the trap temperature when the radiofrequency field of the trap is turned off (a,c) or on (b,d), respectively. The ratio $N(^{40}ArH^+)/N(^{36}Ar^+)$ is directly proportional to the number density of H_2, which is inversely proportional to the square root of T_{22PT}. For better comparison, $N(^{40}ArH^+)/N(^{36}Ar^+)$ is multiplied by $\sqrt{T_{22PT}}$ (c), (d). Measurements during not stabilised conditions at the temperatures from 20 K down to 10 K are grey.

Considering all these statements, we can calculate the number density of the gas inside the 22PT trap. In case of the ideal gas, the number density n_{trap} can be calculated as follows:

$$n_{trap} = \frac{P_{SRG}}{k_B T}, \tag{4.8}$$

where P_{SRG} is gas pressure measured by the spinning rotor gauge (SRG) inside the trap and k_B is Boltzman constant. In subchapter 4.1.1, it is mentioned that the pressure inside the 22PT is measured by the calibrated spinning rotor

gauge (SRG). It is not very practical to use SRG continuously, and for routine monitoring of the pressure in the ion trap, the ionisation gauge (IG) is used.

We assume that in dynamic equilibrium conditions, the gas flow from the 22PT to its vacuum chamber is identical to the gas flow from the 22PT vacuum chamber to the turbopumps. Taking this into account, the final formula that determines the gas number density inside 22PT can be expressed as:

$$n_{\text{trap}} = \frac{C_{\text{gas}} \cdot P_{\text{IG}}}{k_{\text{B}} \sqrt{T \cdot T_{\text{IG}}}}, \tag{4.9}$$

where P_{IG} is pressure measured by the IG, T_{IG} is the temperature of the IG chamber, which is taken equal to the room temperature, C_{gas} is calibration factor between the pressures measured by SRG near the trap volume and the pressure measured by IG in the 22PT chamber. The calibration factor depends on the gas type; therefore, it is necessary to do calibration for every type of gas used in the experiment.

The examples of pressure measurements before and after injection of D_2 into 22PT volume are shown in two graphs of Figure 4.11. The lines are the linear fits which represent the pressure in time when it is constant

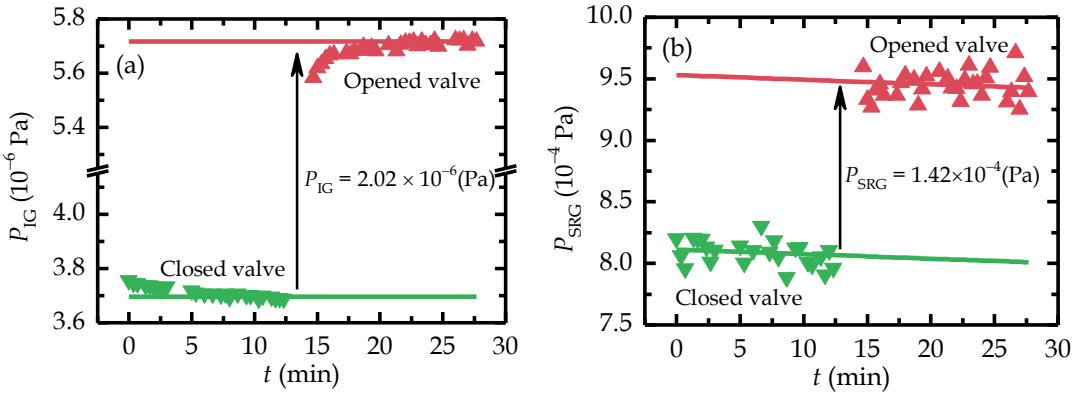

Figure 4.11: Examples of pressure measurements by ion gauge (IG) and spinning rotor gauge (SRG) at $T_{22\text{PT}}$ = 100 K. The down triangles (▼) represent background pressure before injecting of deuterium and up triangles (▲) represent pressure after injecting of deuterium into the trap volume.

Depending on gas, the data measured by the IG are different from data measured by the SRG in C_{gas} times. In the case of deuterium, the calibration factor C_{D2} from Figure 4.11. is equal to P_{SRG}/P_{IG} = 70.3 at T_{22PT} = 100 K. Therefore, the pressure of deuterium inside the trap is higher in 70.3 times than pressure measured by IG in the 22PT chamber.

The calibration factor C_{gas} can also be obtained from the dependence of the pressure measured by the SRG inside the 22PT on the pressure measured inside the trap chamber by the IG. In Figure 4.12, the dependence for deuterium that is injected directly into the trap volume is shown. It can be seen that the SRG has an offset, and after its alignment, a direct ratio between the respective pressures can be obtained.

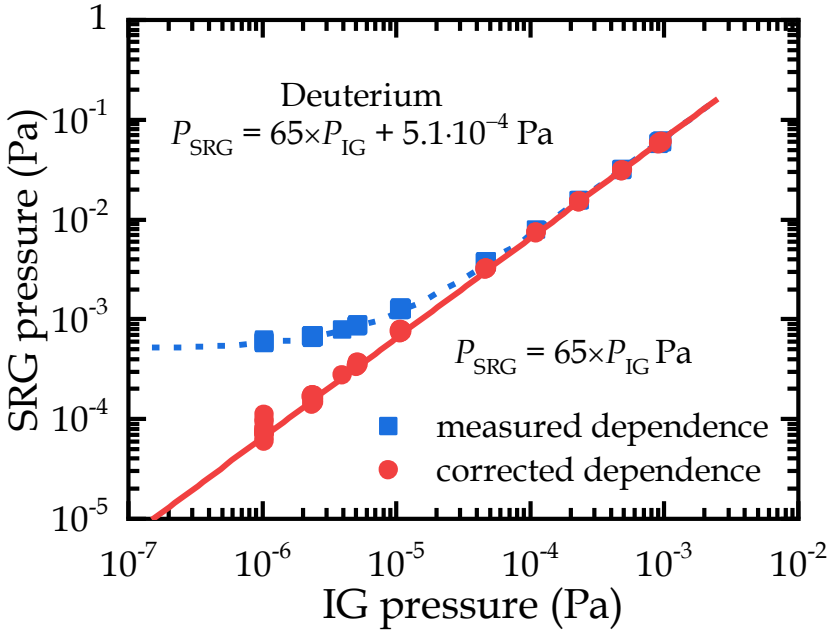

Figure 4.12: Dependence of the deuterium pressure measured by SRG inside the 22PT on the deuterium pressure measured inside trap chamber by IG at T_{22PT} = 47 K. The graph represents the ratio between the pressures measured by SRG near the trap volume and the pressure measured by IG in the 22PT chamber after the substation of the SRG offset pressure.

For some reactions, we use hydrogen in the SIS, and it is crucial to know how much H_2 penetrates the ion trap from SIS. Therefore, a similar dependence can be measured using the same algorithms, but the gas is added into the SIS chamber.

4.2 Measurement of reaction rate coefficient using the RF 22-pole ion trap

Evaluation of the reaction rate coefficients involves the standard operating procedures of the ion trap apparatus. The main routine includes the repeating injection of the ions into the trap with the determined number of ions and further analysing of the extracted ion bunch after specific trapping periods to the detection system (Gerlich & Horning, 1992).

As was mentioned in Chapter 2.2 (formula (2.12)), the reaction rate coefficient is a parameter of the rate equation of the ion-molecular system. If we solve the respective balance equation (2.12) for the simple binary ion-molecule reaction in a case when [B] >> [A^+], we derive the solution:

$$\frac{[A^+]}{[A_0^+]} = e^{-k[B]t}. \tag{4.10}$$

In our situation, we use a number of ions $N(A^+)$ counted by the ion counter after the MCPD, which is proportional to the number density of reactant ions [A^+]. After we take the logarithm of equation (4.10), the reaction rate coefficient k can be obtained.

During our experiment, we obtain the growth of the number of produced ions and the decay of the number of reactant ions. The rate coefficients of the reaction can be calculated from the decay using a simple formula:

$$k_{reaction} = \frac{1}{[B]\cdot t}\cdot \ln \frac{N(A^+)_0}{N(A^+)_t}. \tag{4.11}$$

We can also calculate the reaction rate coefficient from the growth of the number of produced ions as:

$$k_{reaction} = \frac{1}{[\mathrm{B}]\cdot t}\cdot \ln \frac{(N(\mathrm{A}^+) + N(\mathrm{C}^+))_t}{N(\mathrm{A}^+)_t}, \qquad (4.12)$$

In these formulas [B] represents the reactant gas number density inside the 22PT, defined in subchapter 4.1.7, t is storage time, $N(\mathrm{A}^+)_0$ is a number of detected primary ions at the start of the measurement, $N(\mathrm{A}^+)_t$ is a number of detected primary ions at storage time t, $(N(\mathrm{A}^+) + N(\mathrm{C}^+))_t$ is a sum of counted primary and produced ions at time t, which must be equal to the number of ions at the start of the measurement $N(\mathrm{A}^+)_0$. During the measurement and further calculation, we must consider the total loss of ions or mass discrimination.

The total inaccuracy in calculation of the rate coefficient of the ion-molecule reaction includes the statistical error and the uncertainties of the number density and reactant gas temperature measurements.

5. Experimental study of ion-molecule reactions in the RF 22-pole ion trap

5.1 OH^+ formation in the low-temperature $O^+ + H_2$ reaction

Studying the temperature dependence of the rate coefficient of the reaction $O^+ + H_2$ provides information for investigating the structure of the fundamental H_2O^+ system. The reaction of O^+ ion with H_2 molecule is important for astrochemistry as one of the possible reactions leading to water formation in the interstellar space. The experimental results of $O^+ + H_2$ study have been already published and, in this thesis, I describe our main results from the paper (Kovalenko et al., 2018). The isotope effect of replacing the reactant H_2 with D_2 and HD has also been investigated, and it is described in Chapter 5.3.

In this work, our study was focused on the determination of the dependence of reaction rate coefficients of the exoergic reaction of a ground state $O^+(^4S)$ ion with molecular hydrogen on collision temperature of reactants:

$$O^+(^4S) + H_2 \xrightarrow{k_{O+}^{H2}} OH^+ + H \qquad \Delta H^0 = -0.54 \text{ eV}, \qquad (2.6)$$

with a rate coefficient of the reaction denoted as k_{O+}^{H2}. The change of the reaction enthalpy at 0 K was calculated from tabulated enthalpies of formation, ionization potentials, and dissociation energies (Wiedmann et al., 1992; Chase, 1998; Sansonetti & Martin, 2005; Liu et al., 2009).

This reaction has also been discussed in previous papers (see e.g. Bulut et al., 2015; Gerin et al., 2016), and it has been studied, both theoretically and experimentally. Although for the astronomical modelling the reaction rate coefficient k_{O+}^{H2} at low temperatures has to be known, there are no published results of measurements at temperatures below 300 K up to now.

In this study, molecular hydrogen at room temperature was used. The molecular hydrogen consists of 75% ortho-H_2 and 25% para-H_2 fractions (normal hydrogen). The ortho-para conversation does not occur at low

temperature in our gas inlet system of the ion trap (for more details see the paper by Zymak et al. (2013)). Previous experimental studies of the reaction of O^+ ions with molecular hydrogen were carried out with H_2 at 300 K, i.e., with H_2 in thermal equilibrium.

5.1.1 Determination of a relative population of $O^+(^4S)$ and metastable $O^+(^2D)$ and $O^+(^2P)$ ions

The O^+ ions were produced by electron ionisation of N_2O molecules in the SIS. These ions can be produced in the ground state (^4S) or one of the excited metastable states (^2D or ^2P). The radiative lifetimes of these metastables are 5.6×10^3 s and 4.9 s, respectively (Godefroid & Fischer, 1984; Zeippen, 1987). Compere to the length of typical storage time, the lifetimes of metastable states of O^+ ions are relatively long. All our measurements had storage periods shorter than 0.5 s.

For determination of the population of the metastable states of O^+ ions in the 22PT, it was decided to study their reaction with molecular nitrogen. It should also be noticed that for the ground state ions $O^+(^4S)$, the charge transfer reaction is endoergic by 1.96 eV. For analysing of the measured data, we used the obtained experimental results of previous studies by Smith et al. (1978), Glosík et al. (1978), Johnsen & Biondi, (1980), Hierl et al. (1997), and Le Garrec et al. (2003). In these previous studies, the $O^+(^4S)$ ions slowly react with N_2 and form NO^+ ions:

$$O^+(^4S) + N_2 \rightarrow NO^+ + N, \qquad (5.1)$$

and for excited states $O^+(^2D, ^2P)$:

$$O^+(^2D, ^2P) + N_2 \rightarrow N_2^+ + O, \qquad (5.2)$$

the reaction proceeds with formation of N_2^+ ion. The relative populations of the ground and metastable states of the O^+ ions can be determined by monitoring the production of NO^+ and N_2^+ ions in the trap. Results of our measurements are in good agreement with results of previous studies by Hierl

et al. (1997), Glosík et al. (1978), and Le Garrec et al. (2003). The example of our measurement obtained at collisional temperature T = 72 K, gas number densities [N_2] = 3.9 ×10^{11} cm^{-3}, [He] = 5.7×10^{13} cm^{-3} and electron energy $E_{electron}(k_{O+}^{N2})$= 75 eV is shown in Figure 5.1.

From this time dependencies, it was evaluated that about 5 % of the trapped O^+ ions produced the N_2^+ ions after reaction with N_2. The measured rate coefficient of the reaction $O^+ + N_2$ is (6.6 ± 0.1)×10^{-12} cm^3s^{-1}. This value is in a very good agreement with the previously obtained experimental result at temperature T = 72 K by Le Garrec et al. (2003) in the CRESU experiment.

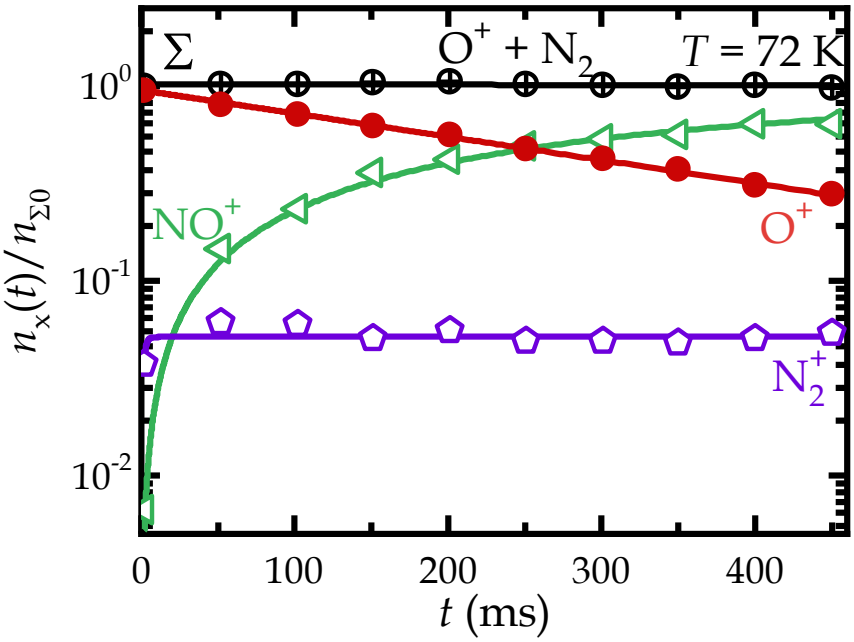

Figure 5.1: Time dependence of the normalized numbers (see explanation in subchapter 5.1.2) of trapped O^+, N_2^+, and NO^+ ions (Kovalenko et al., 2018). The sum (∑) indicates the total normalized number of ions. The experimental results were obtained at temperature T = 72 K and number densities of the gases in the 22PT [N_2] = 3.9×10^{11} cm^{-3}, [He] = 5.7×10^{13} cm^{-3}. The energy of electrons was used in the SIS as $E_{electron}(k_{O+}^{N2})$ = 75 eV.

From this evaluation, it can be concluded that over 90% of confined O^+ ions are in the (^{4}S) ground state, in a situation when $E_{electron}$ < 75 eV in the SIS. In all experiments, when the reaction rate coefficients k_{O+}^{H2} were measured as a

function of collisional temperature, we used the electrons with energy $E_{electron}$ = 50 eV in the SIS.

5.1.2 Time dependence of the number of O^+ ions in the trap after reaction with H_2

An example of the experimental result for the reaction of O^+ ions with molecular hydrogen H_2 is presented in Figure 5.2.

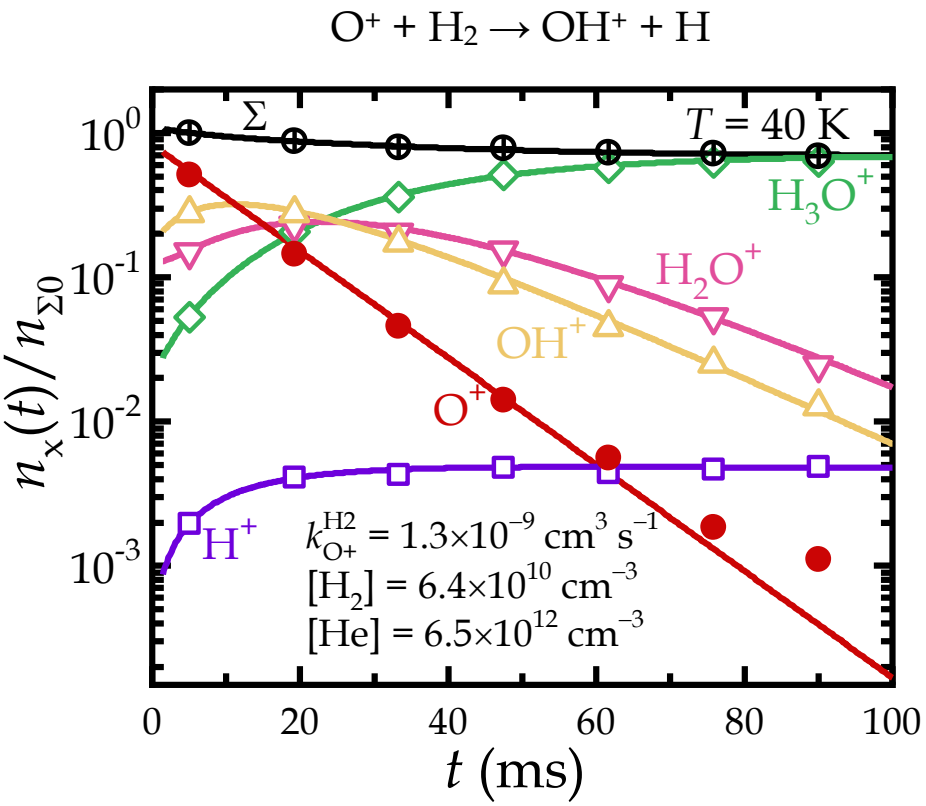

Figure 5.2: Time dependencies of the normalized numbers of the indicated ions after injecting O^+ ions into the 22PT. All lines indicate the results from the fits. The experiment was performed with electron energy $E_{electron}(k_{O+}^{H2})$ = 50 eV. The collisional temperature was T = 40 K. The number density of hydrogen gas was $[H_2] = 6.4\times10^{10}$ cm^{-3}, and the helium number density was $[He] = 6.5\times10^{12}$ cm^{-3}. The calculated reaction rate coefficients for OH^+ production is k_{O+}^{H2} (40 K) = $(1.3 \pm 0.5)\times10^{-9}$ cm^{3}s^{-1}.

Ions were counted after passing the analysing system at determining trapping times t and denoted as $n_x(t)$. The index x defines the specific ion type,

e.g., $n_{O+}(t)$ refers to the number of O^+ ions. The sum of the number of counted ions at the storage time t is denoted as $n_{\Sigma 0} = \Sigma n_x(t)$. We divided the ion numbers by the total number of ions measured at the beginning of storage t_0. Obtained normalized values $n_x(t)/n_{\Sigma 0}$ are plotted in Figure 5.2.

Almost all injected O^+ ions are converts into H_3O^+ ions via sequential hydrogen atom abstraction from H_2. The small amount of produced H^+ ions (growing to ≈ 0.5 % of Σ) is an indicator of the relative population of metastable $O^+(^2D, ^2P)$ ions.

The calibration reaction $H^+ + CH_4$ with products CH_3^+ and CH_4^+ was used for correction of shown normalized numbers of H^+ ions for the difference in detection efficiency, which relates to O^+ ions.

The decreasing of sum $\Sigma = n_x(t)/n_{\Sigma 0}$ with time indicates that the detection efficiencies for other produced ions OH^+, H_2O^+, and H_3O^+ is smaller relative to O^+ ions. The fits of increases of these OH^+, H_2O^+, and H_3O^+ ions are plotted with treating them as free parameters; therefore, they are not corrected in Figure 5.2.

Analysis of Figure 5.2 indicates that O^+ ions react with H_2, forming OH^+ ions. The produced OH^+ ions also react with H_2 continue a sequence of additional exothermic reactions with H_2:

$$OH^+ + H_2 \xrightarrow{k^{H2}_{OH+}} H_2O^+ + H \qquad \Delta H^0 = -1.02\ \text{eV}, \qquad (5.3)$$

$$H_2O^+ + H_2 \xrightarrow{k^{H2}_{H2O+}} H_3O^+ + H \qquad \Delta H^0 = -1.70\ \text{eV}, \qquad (5.4)$$

with the reaction rate coefficients k^{H2}_{OH+} and k^{H2}_{H2O+}. The final ion product in this sequence is H_3O^+. The given reaction 0 K enthalpy changes were calculated from relevant enthalpies of formation given by Haney & Franklin, (1969) and Chase, (1998), dissociation energies given by Liu et al. (2009), and ionization potentials given by Wiedmann et al. (1992) and Lauzin et al. (2015). The detailed study of these reactions was performed in our ion trap technique for temperatures down to 15 K by Tran et al. (2018).

Observed H^+ ions can not be efficiently produced in the reaction of ground state $O^+(^4S)$ ions with molecular hydrogen as this reaction is endoergic by 0.06 eV and also spin forbidden (Flesch & Ng, 1991; Li et al., 1997). The H^+ ions and H_2^+ ions can be simultaneously produced with OH^+ in reactions of excited metastable $O^+(^2D)$ and $O^+(^2P)$ ions with H_2:

$$\rightarrow OH^+ + H, \tag{5.5a}$$

$$O^+(^2D, ^2P) + H_2 \rightarrow H_2^+ + O, \tag{5.5b}$$

$$\rightarrow H^+ + OH. \tag{5.5c}$$

The $O^+(^2D, ^2P)$ specifies an unidentified mixture of $O^+(^2D)$ and $O^+(^2P)$ metastable ions, with respective reaction enthalpy changes for the channel (5.5a) $\Delta H^0(^2D) = -3.27$ eV and $\Delta H^0(^2P) = -4.96$ eV. Calculated reaction enthalpy of changes of the other channels can be found in the paper by Li et al. (1997). The produced H_2^+ ions further react with H_2 and produce protonated molecular hydrogen ions H_3^+. This situation is shown in Figure 5.3, where the detected products for reaction of O^+ ions coming from the ion source, with molecular hydrogen are indicated.

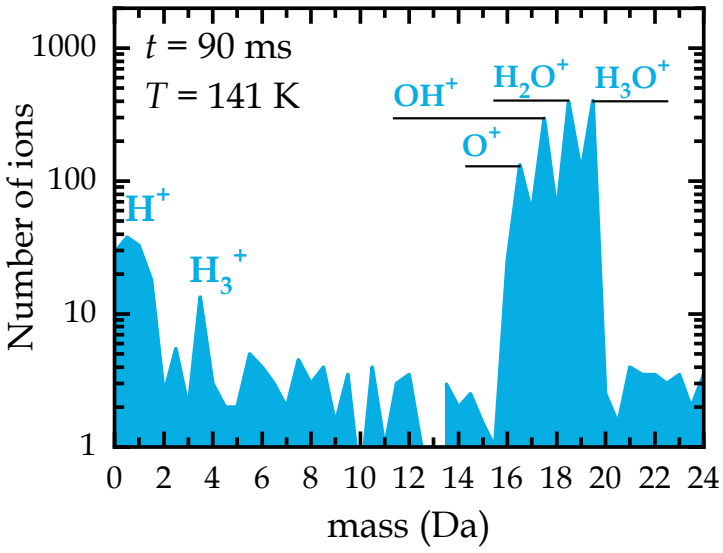

Figure 5.3: Integral spectrum with indicated ions for the reaction of O^+ ions coming from the SIS with H_2 at T = 141 K. The ion composition was analysed after being stored for 90 ms in the ion trap.

Despite the higher fraction ratio for production of H_2^+ ions than for H^+ ions (Li et al., 1997) we prefer for characterization of the fraction of metastable $O^+(^2D, ^2P)$ ions in 22PT monitoring the production of H^+ ions which do not react with H_2.

In comparison with the population of $O^+(^2D, ^2P)$ metastable ions obtained in experiments with N_2, the fraction of produced H^+ ions is low. Therefore, OH^+ ions are also produced in reactions of metastable $O^+(^2D, ^2P)$ ions with hydrogen. For above-studied reactions (2.6), (5.3 − 5.5), the data obtained for primary O^+ ions and all products were fitted using a kinetic model. Obtained fits (solid lines) are in good agreement with our measured data. The reaction rates, the initial number of all ions and the detection efficiencies were selected as free parameters of the model. The decrease in the number of O^+ ions in time illustrates that the decay is mono-exponential over almost 3 orders of magnitude.

Figure 5.4 demonstrate the increase of the fraction F of metastable $O^+(^2D)$ and $O^+(^2P)$ ions with increasing energy of electrons $E_{electron}$ in the range from 21 eV to 145 eV. We assume that the fraction of H^+ ions is produced via reaction (5.5c). The number of produced H^+ ions corresponds to the population of metastable $O^+(^2D)$ and $O^+(^2P)$ ions. The produced fraction of H^+ ions in the reaction of $O^+(^2D)$ and $O^+(^2P)$ metastable ions with hydrogen in the 22PT reaches up to 1 % of Σ (see inset of Figure 5.4). This result confirms the conclusion obtained in the test with N_2. Thus, I can confidently say that over 90 % of injected O^+ ions from the SIS are in the (^4S) ground state for the used electron energies in the SIS lower than 75 eV.

To reduce the effect of $O^+(^2D)$ and $O^+(^2P)$ ions, the energy of electrons in the SIS was maintained at $E_{electron}$ = 50 eV in all measurements of $k_{O^+}^{H2}$. The fraction of H^+ ions was also checked during all measurements.

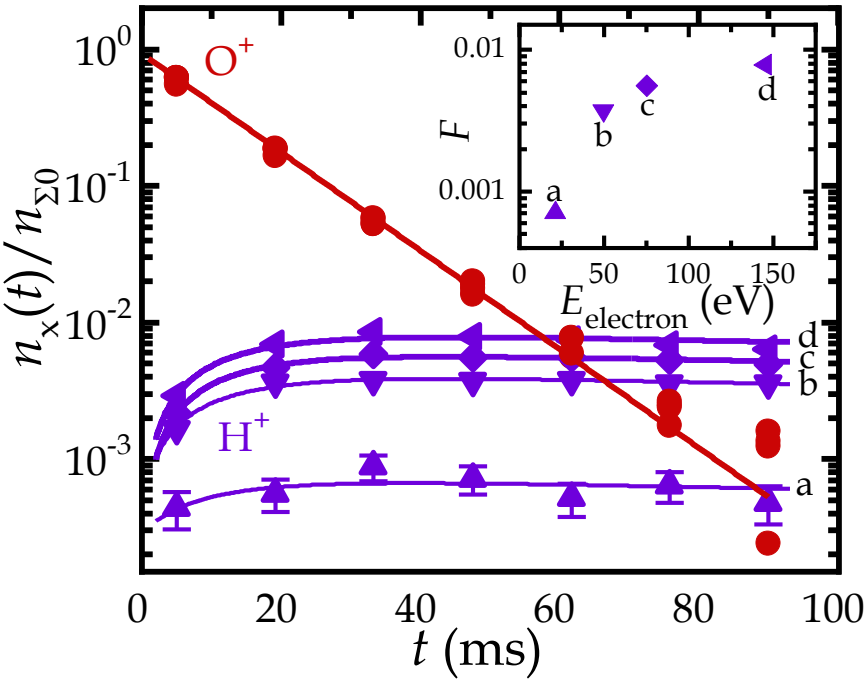

Figure 5.4: The O^+ decays, and H^+ growth were taken at four different electron energies $E_{electron}$ ranging from 21 eV to 145 eV at T = 56 K, $[H_2] = 5.4\times10^{10}$ cm^{-3}, and [He] = 5.5×10^{12} cm^{-3}. The calculated reaction rate coefficient for production of OH^+ ions is k_{O+}^{H2} (56 K) = $(1.5 \pm 0.3)\times10^{-9}$ cm^{3}s^{-1}. The inset: dependence of the fraction F of produced H^+ ions for reaction O^+ with H_2 on the electron energy in the SIS (Kovalenko et al., 2018).

Another example of time dependence for the studied reaction is given in Figure 5.5, together with the results from fits. The measurements were performed at collisional temperatures T = 25 K and T = 77 K. Analogically to Figure 5.2, the sequential addition of hydrogen atoms to O^+ ions leads to final production of H_3O^+ ions. Also, it can be seen that less than one percent of H^+ ions is produced. The first data point represents the situation when ions do not have enough time to cool down in collisions with pre-cooled He atoms (see subchapter 4.1.6). These points were not considered in further fitting.

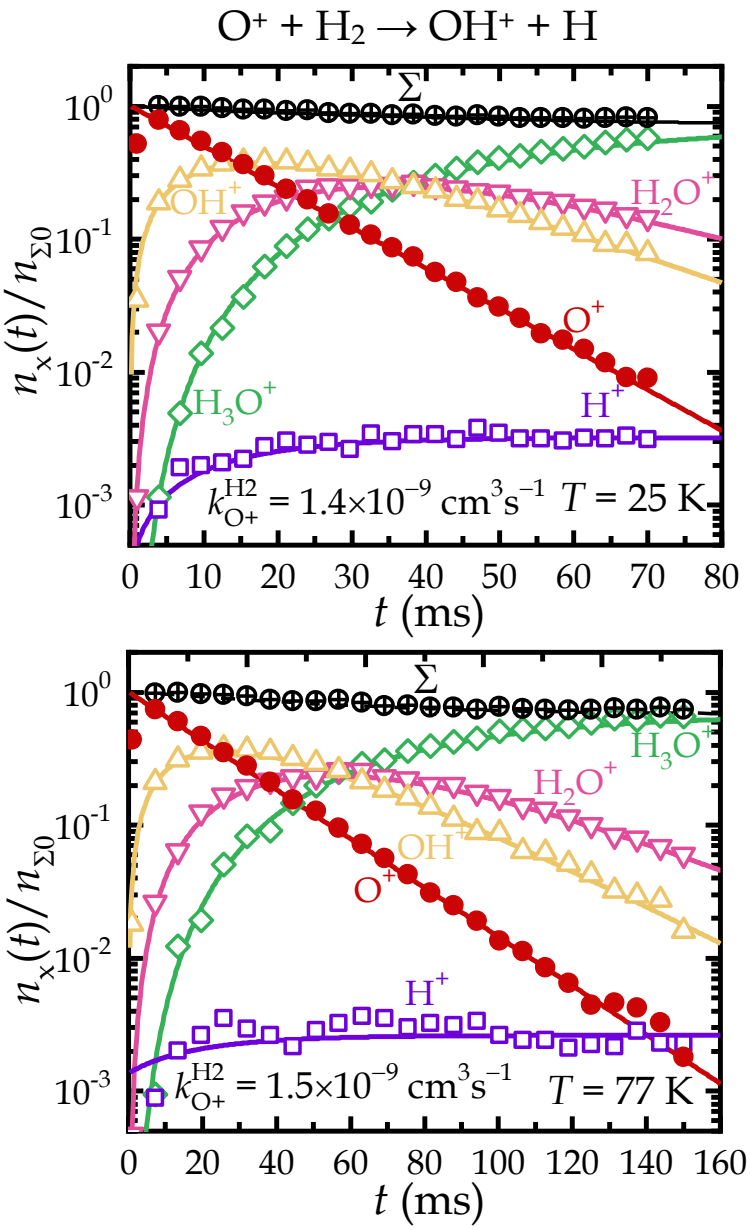

Figure 5.5: Time dependencies of the normalized numbers of shown ions after injection of O^+ ions into the 22PT. Upper panel: experimental results were obtained at collision temperature $T = 25$ K and gas number densities $[H_2] = 4.9\times10^{10}$ cm^{-3}, $[He] = 1.2\times10^{13}$ cm^{-3}. Lower panel: $T = 77$ K, $[H_2] = 2.8\times10^{10}$ cm^{-3}, $[He] = 6.7\times10^{12}$ cm^{-3}. The $\oplus$ symbols indicate the normalized total number of ions (Σ). The experimental results are fitted with a kinetic model (solid lines). The calculated reaction rate coefficients k^{H2}_{O+} are given at the bottom inside the plots.

All measured decays of the number of O^+ ions have been experimentally studied at collisional temperatures, ranging from 300 K to 15 K.

5.1.3 Dependence of rate of $O^+ + H_2$ reaction on the number density of H_2

The dependencies of the reaction rates r^{H2}_{O+}, r^{H2}_{OH+} and r^{H2}_{H2O+} on the number density of the reactant gas [H_2] were measured at temperature T = 259 K, these dependencies can be seen in Figure 5.6. The linear character of obtained dependencies confirms that the loss processes of O^+ ions in the 22PT are caused predominantly by a binary reaction with molecular hydrogen. Therefore, the rate for this binary ion-molecular reaction can be written as $r^{H2}_{O+} = k^{H2}_{O+}$ [H_2] + r_{bg}. Where r_{bg} is a level of the background loss rate which is measured in the 22PT with pure He without H_2.

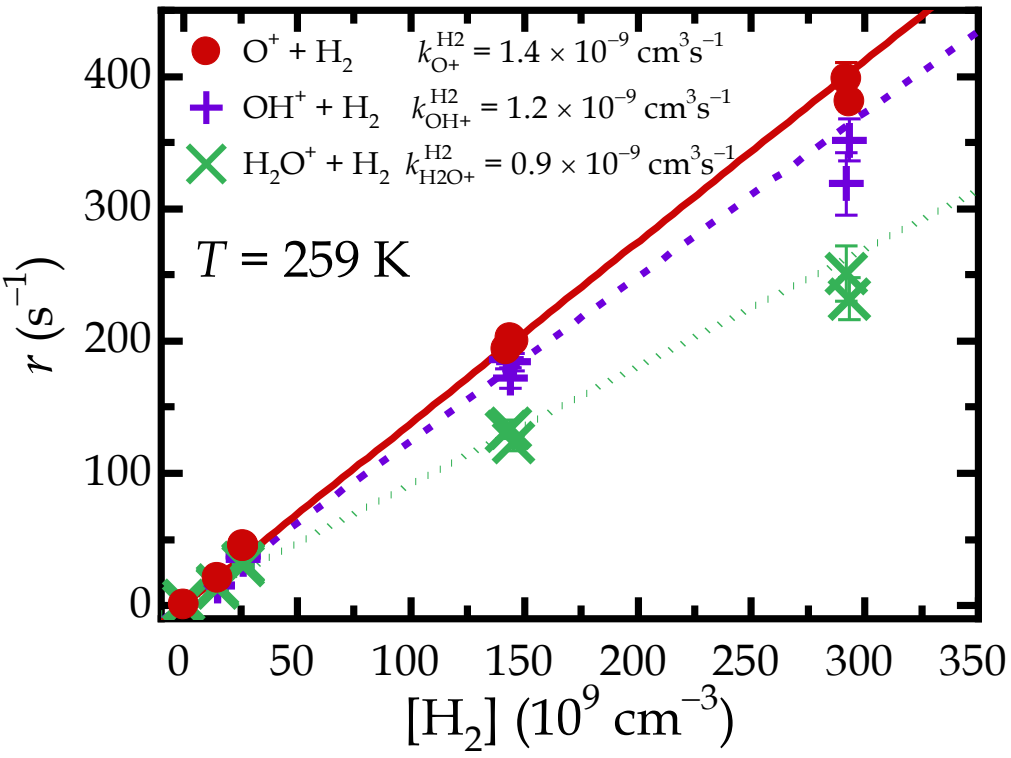

Figure 5.6: Dependencies of the loss rates r^{H2}_{O+}, r^{H2}_{OH+}, and r^{H2}_{H2O+} of the reaction of O^+, OH^+, and H_2O^+ ions with H_2 on the number density of the reactant gas [H_2]. The collisional temperature was maintained at 259 K. The slope of the plotted dependencies gives the corresponding binary reaction rate coefficients k^{H2}_{O+}, k^{H2}_{OH+}, and k^{H2}_{H2O+} (Kovalenko et al., 2018).

The obtained value of the background loss rate from the fits is r_{bg} = 0.9 s^{-1}. At temperatures lower than 150 K, the cooling system is able to reduce the residual background gases more efficient (in our case these gases mostly are N_2O and H_2O coming from the ion source). Figure 5.6 also contains the rate coefficients k^{H2}_{OH+} and k^{H2}_{H2O+} of reactions (5.3) and (5.4), respectively.

The rate coefficients of reactions (2.6), (5.3), and (5.4) were obtained from the linear regression model of the measured data in Figure 5.6. The obtained values are: k^{H2}_{O+} (259 K) = (1.4 ± 0.3)×10^{-9} cm^3s^{-1}, k^{H2}_{OH+} (259 K) = (1.2 ± 0.2)×10^{-9} cm^3s^{-1}, and k^{H2}_{H2O+} (259 K) = (0.90 ± 0.18)×10^{-9} cm^3s^{-1}. These values are in a good agreement with results from previous experiments at temperature 300K (see e.g. ref. FA (Fehsenfeld et al., 1967), ICR (Kim et al., 1975), SIFT (Jones et al., 1981), and VT-SIFT (Martínez et al., 2015)).

5.1.4 Temperature dependence of reaction rate coefficient of $O^+ + H_2$ reaction

The obtained dependence of the reaction rate coefficient k^{H2}_{O+} on temperature can be seen in Figure 5.7. The results from theories and previous experiments are also plotted.

As we expected, Figure 5.7 demonstrates a typical temperature dependence of an exothermic ion-molecule reaction where the experimentally determined rate coefficients, k^{H2}_{O+}, are close to the Langevin rate coefficient $k_L(H_2)$ ($k_L(H_2)$ = 1.56×10^{-9} cm^3s^{-1}).

We summarize 50 years of $O^+ + H_2$ reaction study in a grope of filled points around 300 K. Previous experimental results were achieved using different experimental methods. The first results were obtained at 300 K with the flowing afterglow technique (FA) (Fehsenfeld et al., 1967). Then the reaction of O^+ ions with molecular hydrogen was studied in an ion cyclotron resonance (ICR) experiment by Kim et al. (1975) and the selected ion flow tube (SIFT) experiment by Smith et al. (1978). In the selected ion flow-drift tube (SIFDT) experiment, Federer et al. (1984) obtained the value of the reaction rate

coefficient at the mean relative kinetic energy of 0.07 eV. These previous studies did not give any measured results for temperatures below 300 K.

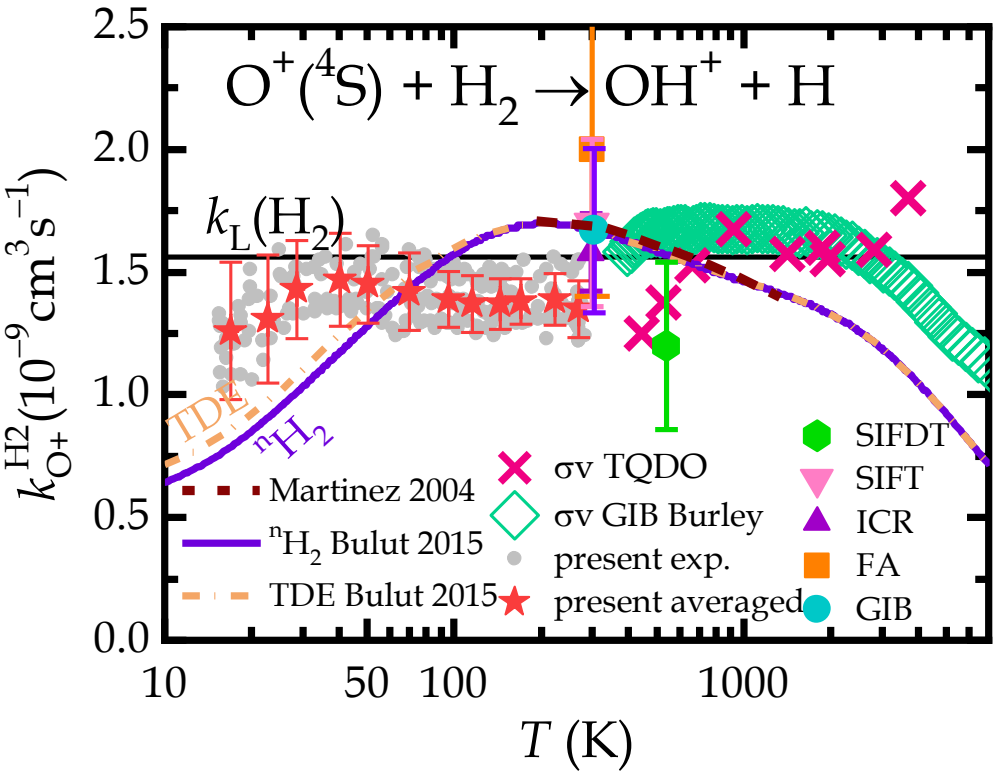

Figure 5.7: Temperature dependence of the binned average reaction rate coefficient k_{O+}^{H2} (full red stars) from the measured data (full grey circles) of the reaction of the ground state $O^+(^4S)$ ions with H_2. (Kovalenko et al., 2018). The horizontal straight line ($k_L(H_2)$) indicates the value of the Langevin collisional rate coefficient. The error bars show the total uncertainty of our measurements. The filled symbols at 300 K and 500 K are results from the measurements at one temperature in the previous experiments. The points extended from 400 K to 7000 K are effective rate coefficients, measured with the guided ion beam technique GIB (300 − 7000 K) by Burley et al. (1987) and a triple quadrupole double octupole technique TQDO (400 − 3500 K) by Li et al. (1997). The dashed line shows the theoretically calculated rate coefficients by Martínez et al. (2004). The solid and dash-dotted lines show reaction rate coefficients for normal-H_2 and for H_2 with thermal populated nuclear spin states, respectively, based on theoretical cross-sections of Bulut et al. (2015).

Our calculated rate coefficients are slightly below $k_L(H_2)$. This situation can be explained by a systematic uncertainty of our data, which is estimated to be up to 20 % for our ion trap experiment.

Two sets of previously measured data were obtained above room temperature by Burley et al. (1987) in the GIB experiment, and by Li et al. (1997) in the TQDO experiment, where the ion beam was guided through a target gas cell with temperature 300 K. These results are below $k_L(H_2)$, and the discussions of deviations of $k_L(H_2)$ above 0.3 eV are given in the paper by Bulut et al. (2015). Measured effective cross-sections from these experiments were converted to the effective reaction rate coefficients after multiplying them with the mean relative velocity. For data obtained by Li et al. (1997), we applied a correction of the centre of mass-energy for the thermal motion of the neutral target with $T_{GAS} \approx 300$ K by adding a term $3/2 \cdot k_B \cdot T_{GAS} \cdot m_{O+}/(m_{O+} + m_{H2})$, where m_{O+} and m_{H2} are the O^+ and H_2 masses, respectively.

For temperatures from 300 K to 30 K, our calculated reaction rate coefficients are independent on temperature, and for temperatures from 30 K to 15 K, the behaviour shows the slight decrees. A similar effect is also predicted by the theoretical model, which is given as a solid line by Bulut et al. (2015). This model by Bulut et al. (2015) applied the TDWP calculations (time-dependent wave packet) for determining the integral cross-sections of reactive collisions of O^+ ions with $H_2(j)$. The energies of collisions were ranged from 1 meV up to 1 eV and for the rotation states $j = 0$, 1, and 2. In these calculations, Bulut et al. (2015) used a concept of global potential energy surface (PES) which was determined for the ground state of electrons $1^4A'$ of H_2O^+ ions by Martínez et al. (2004). On this PES, reactants can proceed to the formation of OH^+ ions and H atoms without a potential barrier. According to this information, the calculated cross-sections are in a very good agreement with a prediction from the Langevin model for the population of the rotational energy states at temperature 300 K (see Bulut et al., (2015), Figure 8). Moreover, in this case, the results from the temperature dependence

of k_{O+}^{H2} show that the obtained in the theoretical calculations cross-sections align below collision energy 10 meV. Considering the *T*-dependent *j*-populations of the normal-H_2, the thermal rate coefficients were calculated from data obtained by Bulut et al. (2015). This result is demonstrated by the already described solid line in Figure 5.7, extended for temperatures from 10 K to 7000 K.

It is too early to make a conclusion about decreasing of the rate coefficients of reaction (2.6) at low temperatures through the fact that we have not yet known why the TDWP cross-sections depart from the Langevin model below the energy of 10 meV (Bulut et al., 2015). The thermal reaction rate coefficients were provided by Bulut et al., (2015) only above 200 K. The align may be caused by inaccuracies in the theoretical calculations or due to the wrong long-range behaviour of the global potential energy surface.

5.2 Reaction of N^+ with HD and D_2 at low temperatures

The importance of ammonia and its deuterated isotopologues in interstellar medium has been discussed in subchapter 2.1.1 and 2.1.3. As their formation starts from the reaction of N^+ ions with H_2 or HD and D_2, the kinetic of title reactions has to be well studied. We investigate the formation of NH^+ and ND^+ ions in endothermic hydrogen (or deuterium) abstraction reactions of N^+ ions with HD and D_2 at temperatures from 300 K down to 15 K. In this work I present temperature dependencies and Arrhenius plots of measured reaction rate coefficients, from which the activation energies of all reaction channels are determined.

Our study focuses on the reactions:

$$N^+ + HD \xrightarrow{k_{N+}^{HDa}} ND^+ + H \qquad (5.6a)$$

$$N^+ + HD \xrightarrow{k_{N+}^{HDb}} NH^+ + D \qquad (5.6b)$$

$$N^+ + D_2 \xrightarrow{k_{N+}^{D2}} ND^+ + D \qquad (5.7)$$

where k_{N+}^{HDa}, k_{N+}^{HDb}, and k_{N+}^{D2} are the rate coefficients of listed reactions. The overall reaction rate coefficient of N^+ ions with HD is $k_{N+}^{HD} = (k_{N+}^{HDa} + k_{N+}^{HDb})$ and the branching ratio is determined as $BR_{NH+}^{HD} = k_{N+}^{HDb} / (k_{N+}^{HDa} + k_{N+}^{HDb})$. The previously studied reaction of N^+ ions with H_2 by Zymak et al. (2013) and reactions with D_2 and HD, which are presented in this work, have activation energies comparable with the energies of rotational excitation of the reactant molecules. It has been observed that the available rotational energy allows promoting to the reactions. However, some of the previous studies of these reactions suggest that their activation energies can be partly caused by barriers on the reaction paths (Gerlich, 1993; Tosi et al., 1994). Moreover, the actual endothermicities of these reactions have been not known yet, and they need to be determined.

The reaction (5.6) of N^+ ions with HD was studied at low temperature in the uniform supersonic flow or the CRESU experiment by Marquette et al. (1988). At 300 K and above, the reaction was also studied in the SIFDT experiment by Adams & Smith (1985), the GIB experiments by Ervin & Armentrout (1987), and Sunderlin & Armentrout (1994). Mentioned experimental techniques were described in Chapter 2.3.

The reaction (5.7) of N^+ ions with D_2 was studied at low temperatures in the CRESU experiment by Marquette et al. (1988) and in the ion trap experiment by Gerlich (1993). At thermal energies and above, the reaction of N^+ ions with D_2 was studied in the SIFDT experiment by Adams & Smith (1985), in the GIB experiment by Sunderlin & Armentrout (1994), and in the merged molecular beams (MB) and the crossed molecular beams (CB) experiments by Tosi et al. (1994).

In the present experiment, normal deuterium was used. In the normal-D_2, the para-D_2 to ortho-D_2 ratio is 1:2. The populations of the rotational states correspond to thermal equilibrium at 300 K. Our previous experiments with H_2 gas indicate that the para to ortho ratio does not change when H_2 flows from the bottle into the trap, for more discussion see Hejduk et

al. (2012) and Zymak et al. (2013). It can be assumed that the same situation applies to deuterium.

It must be noticed that the effect of contributions of HD and H_2 admixtures in D_2 and H_2 in HD needs to be considered for more precise evaluation of the activation energy from the Arrhenius fit model. We have calculated this effect, and we prepare these corrected results for publication. I would also like to admit that difference between values presented in these work and values that take into account the correction for contributions of HD and H_2 is no more than 7–10%.

5.2.1 Time dependence of the number of N^+ ions in the trap after reaction with HD, and D_2

Nitrogen ions were formed by electron impact ionization of N_2 gas with further confining them in the SIS. The volume of the ion trap was filled with a mixture of reactant gas (HD or D_2) and He buffer gas. Number densities of D_2 and HD in the trap were varied from 10^{10} cm^{-3} up to 10^{12} cm^{-3}. The number density of helium during the experiments varied in the range of $10^{12} - 10^{14}$ cm^{-3}.

A time dependence measurement of the normalised number of trapped N^+ ions after reaction with molecular D_2 is shown in Figure 5.8. The experiment was performed at the temperature T = 266 K after storage of N^+ ions in the 22PT which was already filled with D_2 reactant gas and He buffer gas.

The plotted data were normalized by dividing the number of ions of the specific ion mass $n_x(t)$ at trapping or storage time t by the total number of detected ions $n_{\Sigma 0}$ at the beginning of the experiment.

The ND^+ ions are produced right after storage of N^+ ions in the ion trap and their reaction with D_2. Similarly, to $NH^+ + H_2$ reaction (Rednyk et al., 2019), ND^+ ions react with D_2. The reaction of ND^+ with D_2 has two channels where D_3^+ and ND_2^+ ions are produced. The ND_2^+ ions consequently react with D_2 forming ND_3^+ ions. Finally, ND_4^+ ions are slowly

formed in the reaction of ND_3^+ ions with D_2. The ND_4^+ production can be neglected due to the low rate of formation at high temperatures.

From the time dependence of the normalized number of D_3^+ ions, it can be noticed that at relatively long storage times the number of D_3^+ ions slowly decreases due to reactions with N_2 molecules where N_2D^+ ions are formed. The N_2 gas penetrates the ion trap volume from the ion source.

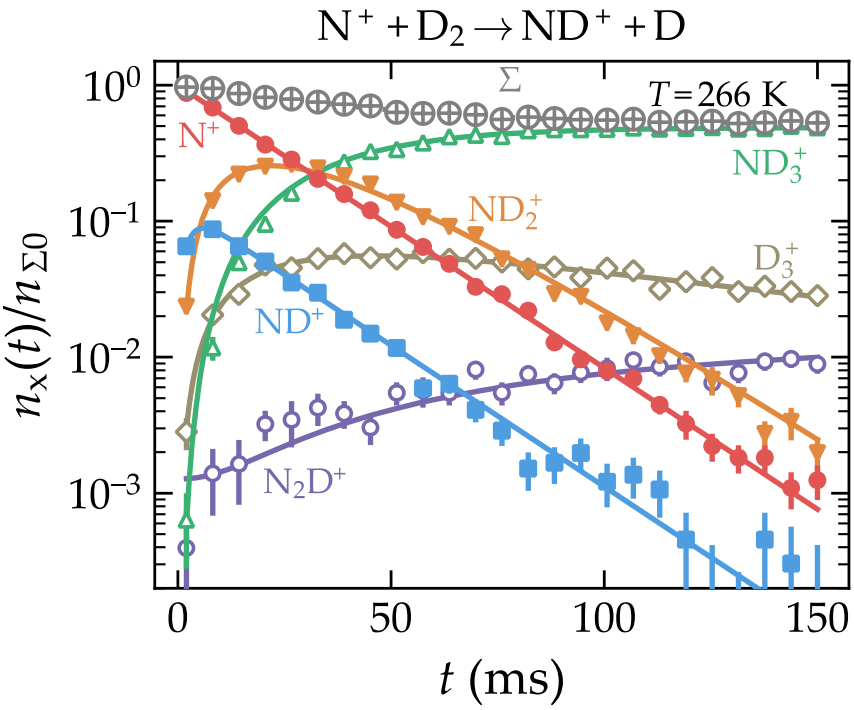

Figure 5.8: Measured time dependence of the normalized numbers ($n_x(t)/n_{\Sigma 0}$) of N^+, ND^+, ND_2^+, ND_3^+, D_3^+, and N_2D^+ ions. The collisional temperature was $T = 266$ K the number density of deuterium gas was $[D_2] = 2.9\times10^{11}$ cm^{-3}, and the number density of the buffer gas was $[He] = 1.4\times10^{13}$ cm^{-3}. The fit solutions of the interconnected system of the rate equations are indicated with the solid lines. The $\oplus$ symbol indicates the time dependence of the normalized total number of ions in the ion trap, $\Sigma(t) = \Sigma\, n_x(t)/n_{\Sigma 0}$. The reaction rate coefficient obtained from the decay of N^+ ions is $k_{N^+}^{D2} = 1.7\times10^{-10}$ cm^{3}s^{-1}.

The results of the kinetic-fit model are given in Figure 5.8. For fitting procedures, the mass discrimination of the produced ions, represented by the

slight decrease in the total number of ions over time, was considered. Obtained reaction rate coefficient from the decay of N^+ ions is $k_{N^+}^{D2} = 1.7\times10^{-10}$ cm^{3}s^{-1}.

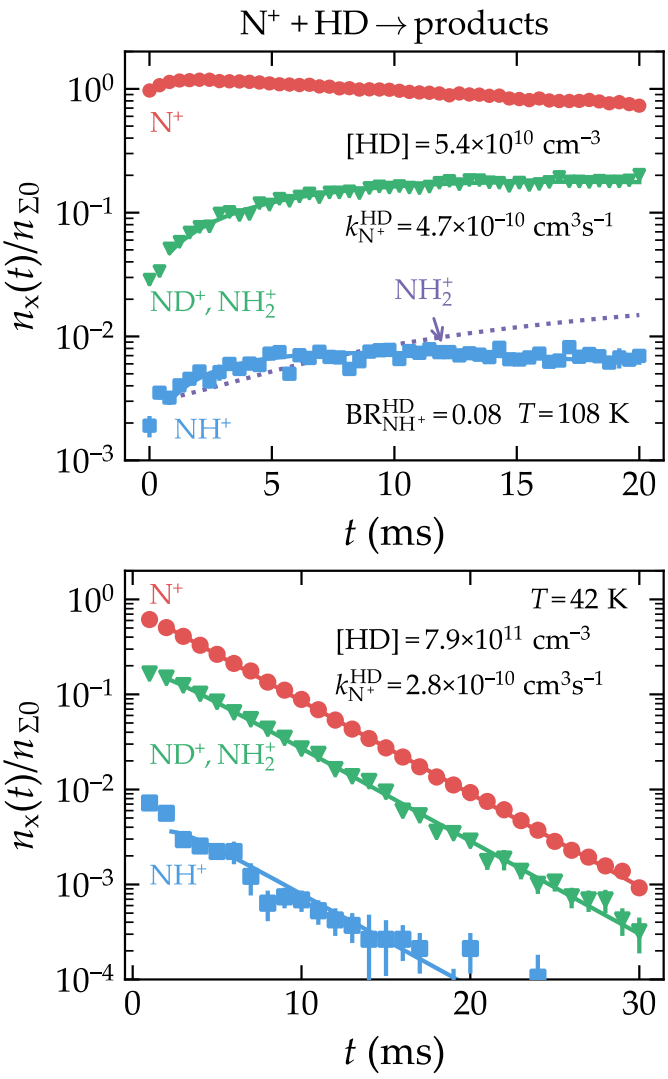

Figure 5.9: Measured time dependencies of the normalized numbers ($n_x(t)/n_{\Sigma 0}$) of the primary N^+ ions and the produced ND^+ and NH^+ ions. Our measurements were performed at T = 108 K and T = 42 K. Buffer gas number densities were [He] = 1.1×10^{13} cm^{-3} and [He] = 2.7×10^{13} cm^{-3}, respectively. The solid lines are fits of the measured data. Upper panel: The time dependencies were measured with a low reactant gas number density. The dotted line indicates the amount of secondary NH_2^+ ions estimated from the fit. Lower panel: The time dependencies measured with a higher reactant gas number density. Measured rate coefficients and number densities of reactant gas are shown on the graph together with the value of the branching ratio for the upper panel.

Examples of the measurements for reaction (5.6) at 108 K and 42 K are shown in Figure 5.9. Measured data were fitted using a kinetic model for ions with masses 14 Da (N^+), 15 Da (NH^+), and 16 Da (ND^+, NH_2^+). The time dependencies of the relative number of all ionic species in the ion trap were measured. For simplicity, the time dependencies of the relative number of ions which correspond to secondary products are not plotted in Figure 5.9.

In the upper panel of Figure 5.9, the time dependencies of the normalized numbers ($n_x(t)/n_{\Sigma 0}$) of the primary N^+ ions and the formed ND^+ and NH^+ ions measured with the low number density of HD ([HD] = 5.4×10^{10} cm^{-3}) are shown. In the lower panel of Figure 5.9, the time dependencies of the normalized numbers of the primary N^+ and the formed NH_2^+, ND^+, and NH^+ ions measured with the higher number density of HD ([HD] = 7.9×10^{11} cm^{-3}) are shown. The mono-exponential decrease of the normalized numbers of N^+ ions in the lower panel is over three orders of magnitude. It indicates that the relaxation of N^+ ions does not have an influence on the measured data during the experiment.

5.2.2 Dependence of the rate of N^+ + HD reaction on the number density of HD

In the experiment at the constant temperature of the ion trap, we measured the dependence of the loss rate of N^+ ions in reaction with HD molecule on the number density of HD gas. It was confirmed that the dominant loss process for the trapped N^+ ions is the binary reaction with HD.

It shows that the decay of the number of N^+ ions in the 22PT in time is controlled by the binary reactions with HD molecules. The slope of the obtained linear dependence is given by the reaction rate coefficient (according to the expression $r_{N+}^{HD} = (k_{N+}^{HD} \cdot [HD] + r_{bg})$, where r_{bg} is the background loss rate of N^+ ions).

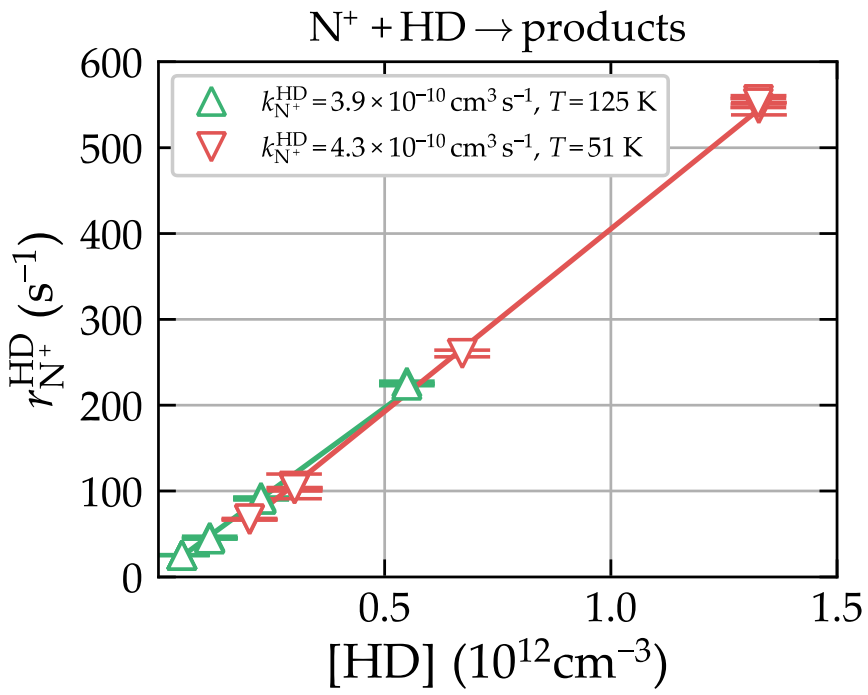

Figure 5.10: Dependencies of the loss rates r_{N+}^{HD} of the reaction of N^+ ions with HD molecule on the number density of the reactant gas [HD]. Measurements were performed at collisional temperatures, T = 51 K and T = 125 K (with [He] = 1.6×10^{13} cm^{-3} and [He] = 2.1×10^{13} cm^{-3}, respectively). The values of the binary reaction rate coefficient k_{N+}^{HD} (indicated in the figure) are given by the slopes of the plotted dependencies.

5.2.3 Temperature dependencies of the branching ratio and the rate coefficients of N^+ + HD reaction

The obtained temperature dependence of the calculated branching ratio BR_{NH+}^{HD} of the production of NH^+ ions is plotted in Figure 5.11. The reaction rate coefficients k_{N+}^{HDa} and k_{N+}^{HDb} were calculated for the production of ND^+ and NH^+ by multiplying the total reaction rate coefficient k_{N+}^{HD} by $(1 - BR_{NH+}^{HD})$ and BR_{NH+}^{HD}, respectively.

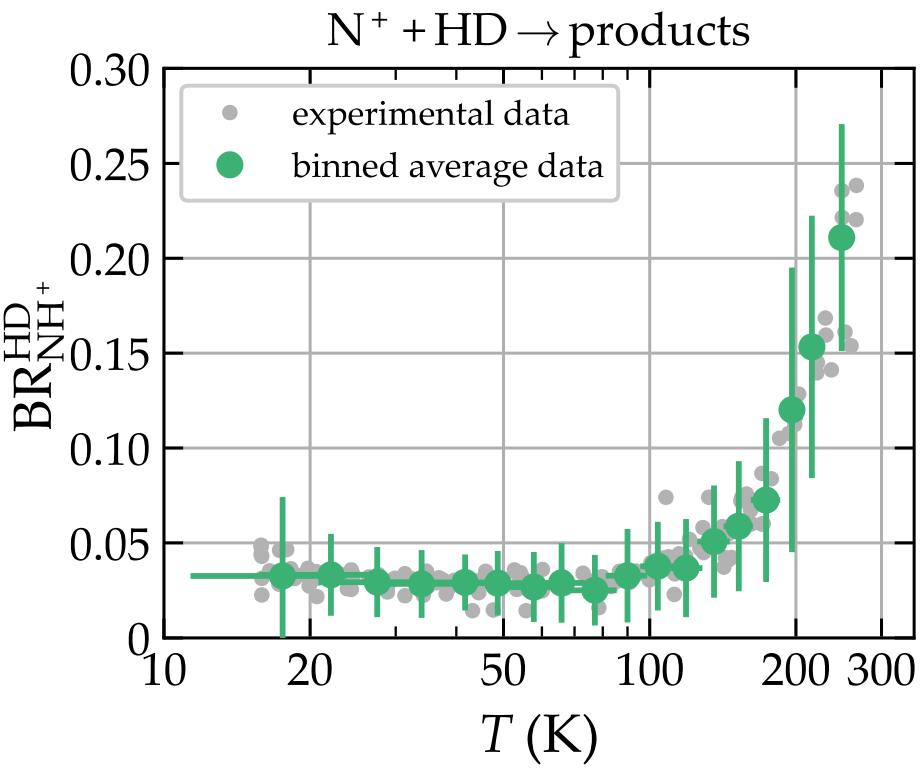

Figure 5. 11: Temperature dependence of the calculated branching ratio BR_{NH+}^{HD} of the production of NH^+ channel. The data obtained in experiments from the time dependencies are indicated with the smaller grey points, larger green points indicate the binned average values.

The obtained temperature dependencies of the rate coefficients k_{N+}^{HD}, k_{N+}^{HDa}, and k_{N+}^{HDb} are shown in Figure 5.12, together with results measured in previous experiments.

The value measured at 20 K in the CRESU experiment by Marquette et al. (1988) is in a good agreement with our value k_{N+}^{HDa} at this temperature. The reaction rate coefficients from the SIFDT experiment (Adams & Smith, 1985) and the GIB experiment (Ervin & Armentrout, 1987) were obtained as a function of mean collision energy $\langle E \rangle$. These data are presented as a function of effective temperature $T_{ef} = 2/3\langle E \rangle / k_B$.

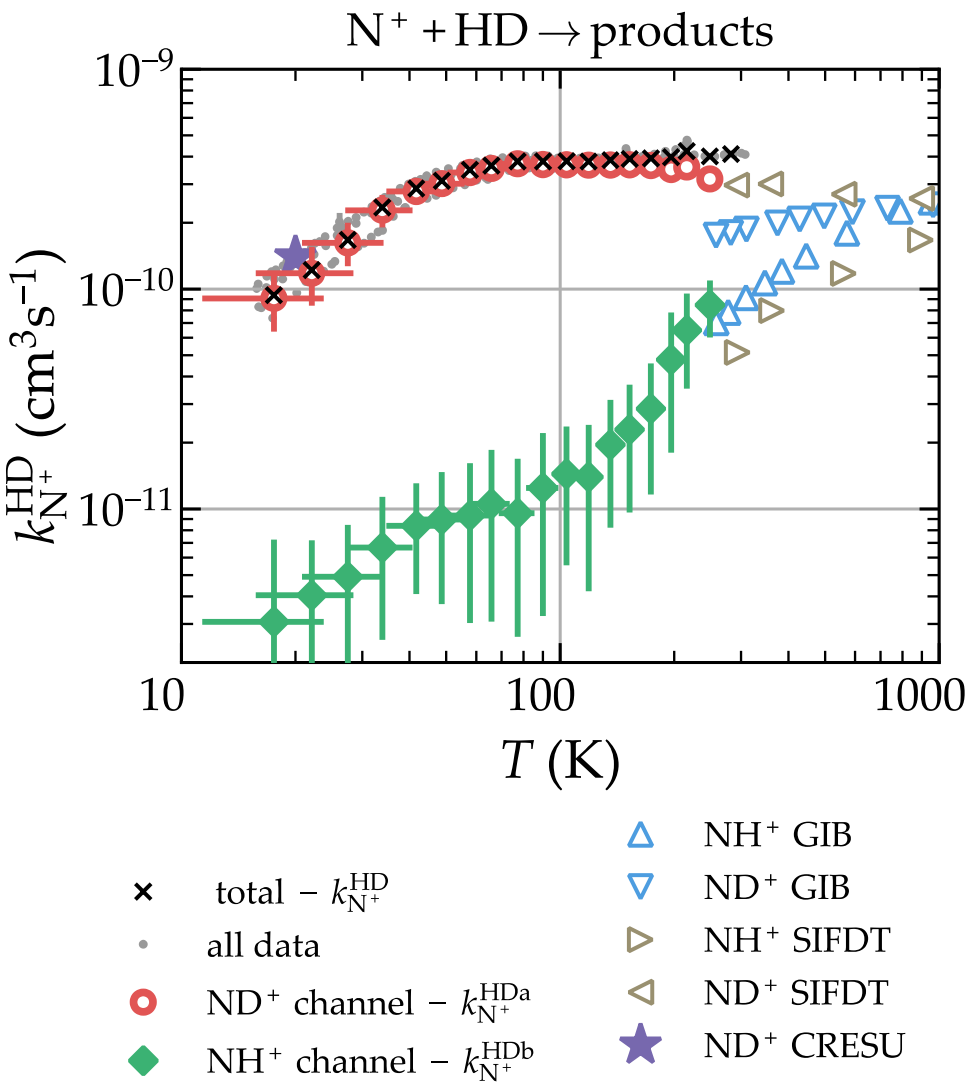

Figure 5.12: Temperature dependencies of the binned average reaction rate coefficients k_{N+}^{HD} (black crosses), k_{N+}^{HDa} for ND^+ channel (open red circles) and k_{N+}^{HDb} for NH^+ channel (full green diamonds). The k_{N+}^{HD} were obtained from data point (small grey circles). The results of Marquette et al. (1988) (CRESU), Ervin & Armentrout (1987) (GIB), and Adams & Smith (1985) (SIFDT) are also shown.

From extrapolation of the obtained temperature dependencies of k_{N+}^{HDa} and k_{N+}^{HDb} towards 300 K, it is obvious that our measured data are in a good agreement with values obtained previously in the SIFDT and the GIB experiments at ~300 K.

Arrhenius plot of the temperature dependence of k_{N+}^{HDa} is shown in Figure 5.13. The plot also includes the reaction rate coefficients of this channel from previous studies (Marquette et al., 1988; Ervin & Armentrout, 1987; Adams & Smith, 1985).

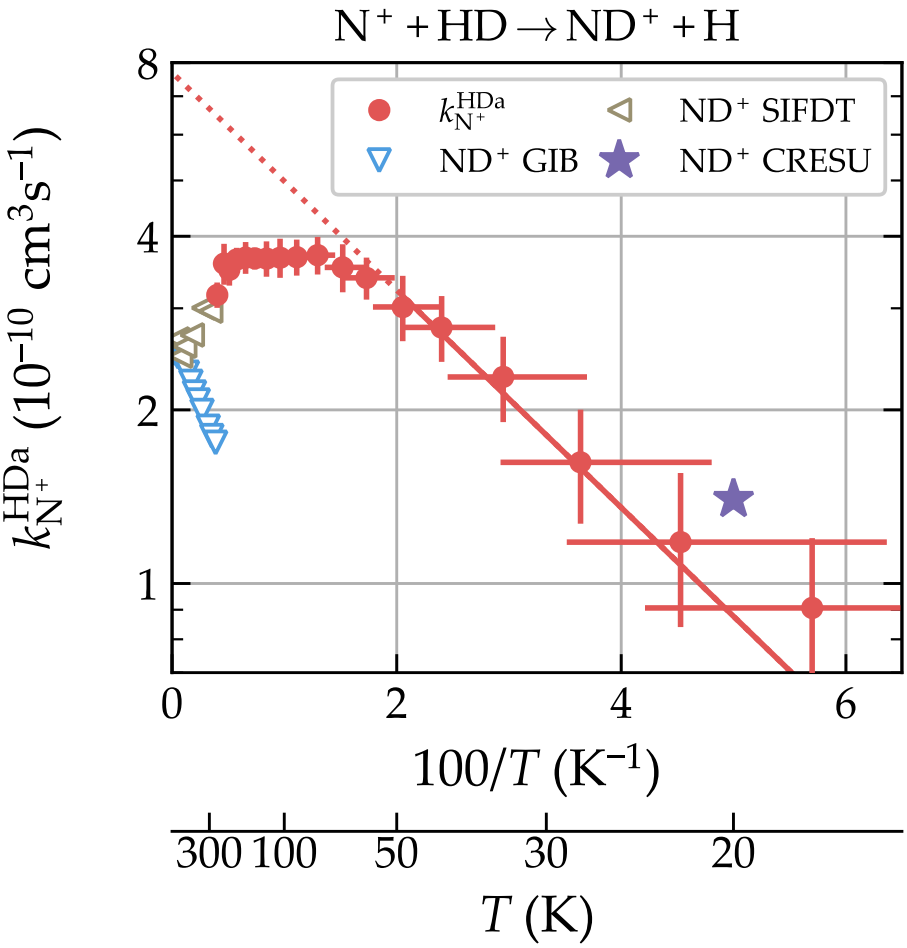

Figure 5.13: Arrhenius plot of the temperature dependence of the reaction rate coefficients k_{N+}^{HDa} (full red circles). A full straight line represents the fit of the temperature dependence of k_{N+}^{HDa} (for T<50 K) by Arrhenius function $k(T) = A \cdot \exp(-E_a/kT)$. The dotted line indicates an extrapolation to the higher temperatures. Values of k_{N+}^{HDa} obtained in previous experimental studies of Marquette (1988) (CRESU), Ervin & Armentrout (1987) (GIB), and Adams & Smith (1985) (SIFDT) are also shown.

A pre-exponential factor A and the activation energy E_a can be obtained from the fit of measured data by simple Arrhenius function $k(T) = A \cdot \exp(-E_a/kT)$. For k_{N+}^{HDa}, the fit can give reliable parameters only for

temperatures from 50 K to 15 K. The obtained activation energy from the fit of k_{N+}^{HDa} for temperatures from 15 K to 50 K is $E_a^{HD}(ND^+)$ = (3.1±0.7^{sys}±0.2^{stat}) meV. The systematic error is caused by temperature uncertainty. This obtained result for activation energy is collected in Table 5.1 together with results of previous studies which are presented for comparison. The rate coefficient k_{N+}^{HDa} is nearly constant at temperatures above 80 K and it starts decreasing at temperatures above 200 K with increasing temperature. The same character of temperature (kinetic energy) dependence was observed by Adams & Smith (1985) at temperatures above 300 K.

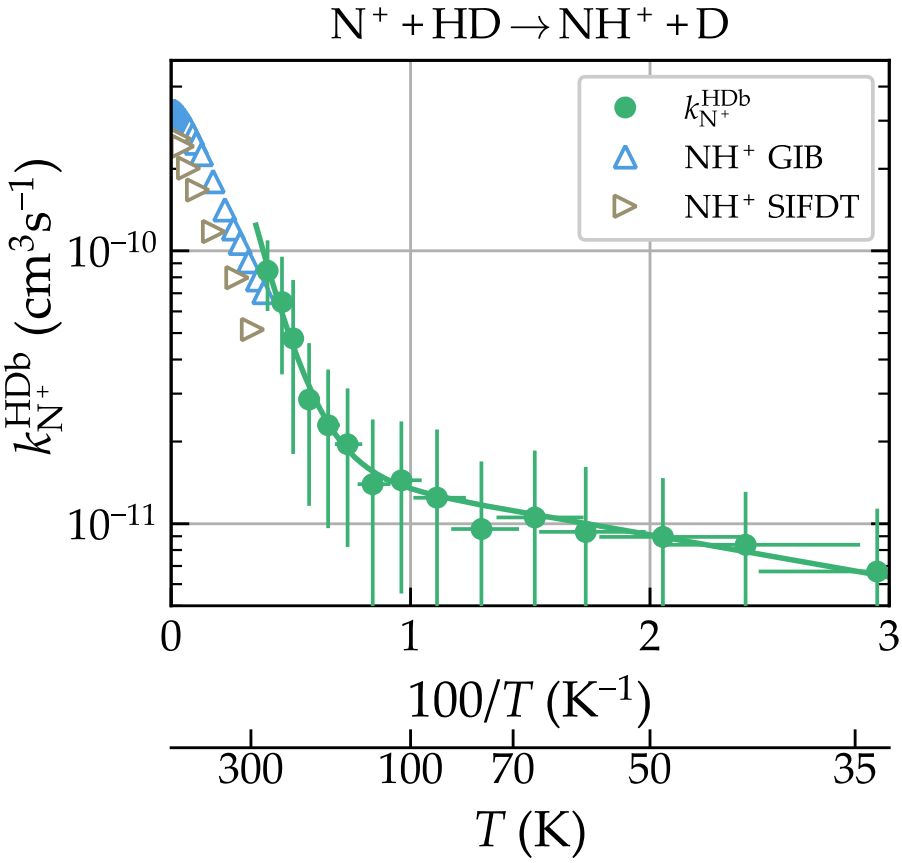

Figure 5.14: Arrhenius plot of the temperature dependence of the reaction rate coefficients k_{N+}^{HDb} (full green circles). The temperature dependence for k_{N+}^{HDb} is fitted by Arrhenius function $k(T) = A \cdot \exp(-E_a/kT) + k_{bg}$ and indicated by full line. Values of k_{N+}^{HDb} obtained in previous experimental studies by Adams & Smith (1985) (SIFDT), and by Ervin & Armentrout (1987) (GIB) are also indicated.

Figure 5.14 shows the Arrhenius plot of the temperature dependence of the rate coefficient k_{N+}^{HDb}. The temperature dependence of the rate coefficient k_{N+}^{HDb} is fitted by Arrhenius function $k(T) = A \cdot \exp(-E_a/kT) + k_{bg}$, where k_{bg} represents the rate coefficient of reactions with residual gases. The activation energy E_a of k_{N+}^{HDb} obtained from the fit is $E_a^{HD}(NH^+) = (67 \pm 5^{sys} \pm 5^{stat})$ meV. Figure 5.14 also includes the results from previous studies by Adams & Smith (1985) and Ervin & Armentrout (1987). For comparison, obtained activation energy of k_{N+}^{HDb} together with results from previous studies are also presented in Table 5.1.

5.2.4 Temperature dependence of $N^+ + D_2$ reaction rate coefficients

The temperature dependence of $N^+ + D_2$ reaction rate coefficient k_{N+}^{D2} is presented in Figure 5.15. From the plotted experimental data, it can be seen that at temperatures below ~ 80 K, k_{N+}^{D2} does not continue to fall similar to what can be seen at temperatures from 300 K to 80 K. The reaction rate coefficients k_{N+}^{D2} obtained in our study (closed red circles) are compared with previously obtained results of other experimental studies.

The losses of N^+ ions in the trap are also caused by the reaction with HD admixture (up to 3%) that comes with deuterium (≈ 97%) from the bottle. These losses are already comparable with losses in reactions with D_2 at temperatures around ~ 70 K. At temperatures below 60 K, the reaction with HD admixture is the main loss process of N^+ ions in the 22PT.

Previously measured experimental values were obtained in the CRESU experiment by Marquette et al. (1988), in the 22-pole RF ion trap experiment by Gerlich (1993), in the crossed molecular beams (CB) and the merged molecular beams (MB) experiments by Tosi et al. (1994), in the guided ion beam (GIB) experiment by Ervin & Armentrout (1987), and the SIFDT experiment by Adams & Smith (1985). The data from the paper by Gerlich (1993) have a very steep decrease at temperatures above 70 K;

however, they align below 70 K. In the original paper this situation was qualitatively explained by the presence of HD admixture in the D_2 gas that had been used. The data from the beams experiments MB and CB of Tosi et al. (1994) have similar shifted alignment at low temperatures. The reason of this shifts is probably due to a higher temperature of the neutral beam of D_2 and presence of the admixture of HD (see discussion of Gerlich (1993) and Tosi et al. (1994)).

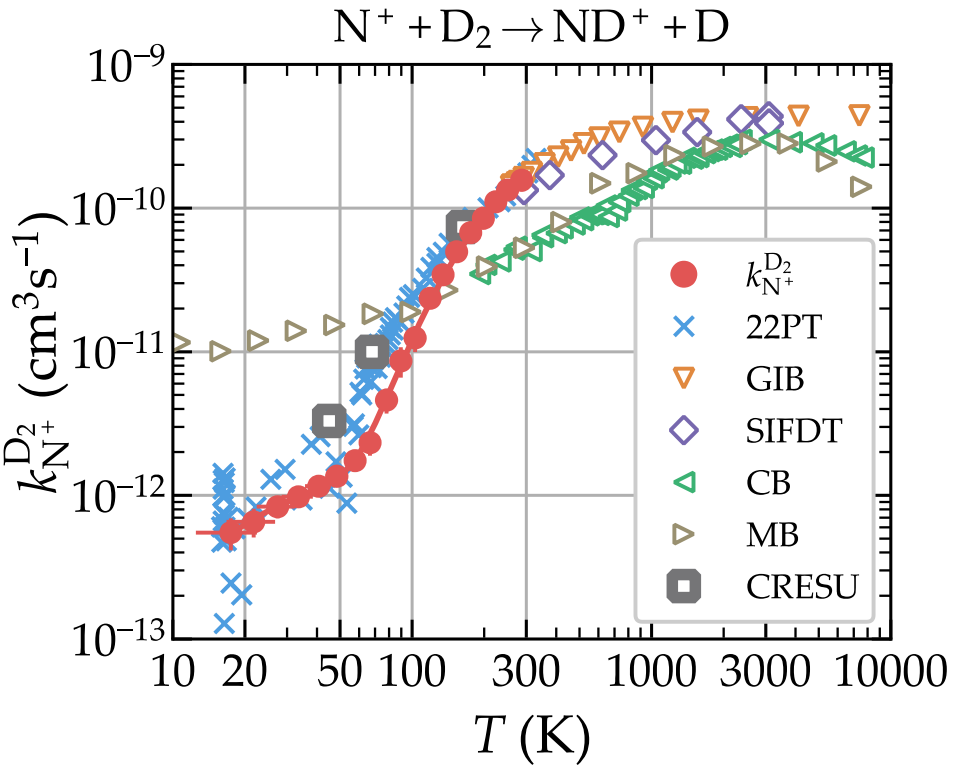

Figure 5.15: Temperature dependence of the binned average reaction rate coefficient k_{N+}^{D2} (full red circles) from the measured data of the reaction of N^+ ions with D_2. Comparison of the temperature dependence of k_{N+}^{D2} obtained in the present study with the values of k_{N+}^{D2} measured in the previous experiments CRESU (Marquette et al., 1988), 22PT (Gerlich, 1993), MB and CB (Tosi et al., 1994), GIB (Ervin & Armentrout, 1987), and SIFDT (Adams & Smith, 1985).

The Arrhenius plot of the obtained temperature dependence of k_{N+}^{D2} is presented in Figure 5.16. The values obtained in the previous experiments

which are included in Figure 5.15 are also shown in the Arrhenius plot of Figure 5.16. For clearness, the data of Tosi et al. (1994), plotted in Figure 5.15, were deliberately excluded. The obtained parameters of the fit are pre-exponential factor $A^{D2} = (6.9\pm0.7^{sys}\pm0.3^{stat})\times10^{-10}$ cm^{3}s^{-1}, activation energy $E_a^{D2} = (35.9\pm2.5^{sys}\pm0.9^{stat})$ meV and $k^{D2}_{bg} = (1.8\pm0.1^{sys}\pm0.2^{stat})\times10^{-12}$ cm^{3}s^{-1}.

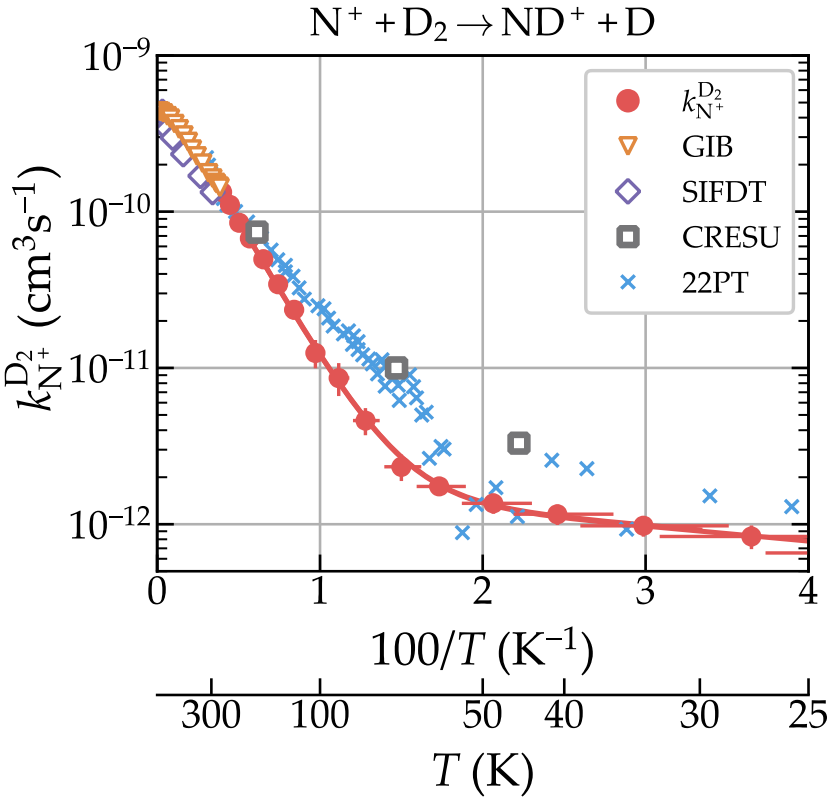

Figure 5.16: Arrhenius plot of the temperature dependence of the reaction rate coefficients k^{D2}_{N+}. The obtained binned average results (full red circles) are fitted by Arrhenius function with a background. Data obtained in the previous experiments CRESU (Marquette et al., 1988), 22PT (Gerlich, 1993), GIB (Ervin & Armentrout, 1987), and SIFDT (Adams & Smith, 1985) are also shown.

5.2.5 Summary of the experimentally determined activation energies

The obtained values of the activation energy E_a from the Arrhenius fits with the validity ranges are summarised in Table 5.1. The activation energies

of reactions with ortho-H_2, para-H_2, and H_2 in Thermodynamic Equilibrium (TDE) were evaluated from the data published by Zymak et al. (2013).

Table 5.1: The summarizing of the experimentally determined activation energies of reactions (2.2), (5.6), and (5.7). The numerical column shows the activation energies obtained from our and other experiments. The last column indicates the interval of temperatures or energies, where the original data were obtained.

Reference	Reactant	E_a, ΔH^0 (meV)	T, E range
$N^+ + H_2 \rightarrow NH^+ + H$			
Zymak 2013	para-H_2	20.9	15 − 25 K
Zymak 2013	ortho-H_2	3.1#	20 − 110 K
Zymak 2013	H_2(TDE)	19.3	15 − 110 K
Marquette 1985	normal H_2	3.4#	8 − 70 K
Adams 1985	H_2(TDE)	11	300 K − 500 meV
$N^+ + HD \rightarrow ND^+ + H$			
this work	HD(TDE)	3.1	15 − 50 K
Gerlich 1993	HD(TDE)	0.9	~ 15 − 50 K
$N^+ + HD \rightarrow NH^+ + D$			
this work	HD(TDE)	67	180 − 250 K
Adams 1985	HD(TDE)	43	300 K − 500 meV
$N^+ + D_2 \rightarrow ND^+ + D$			
this work	normal D_2	35.9#	80 − 300 K
Tosi 1994	normal D_2	29$	~ 20 − 100 meV
Adams 1985	D_2(TDE)	33	300 K − 500 meV

$ Indicates that the value corresponds to ΔH^0 instead of E_a, i.e., the cross-section threshold was evaluated.

# Indicates the measurements with rotationally excited molecules. Note that in case of reaction with normal-D_2, the activation energies were fitted at temperatures above 50 K, where the rotational populations are still close to equilibrium. However, it follows from the phase space theory calculations of Gerlich (1993) that the rotationally excited D_2 is the dominant reactant at temperatures higher than 50 K.

Assuming that there are no barriers on the reaction paths of the studied reactions, the obtained activation energies, E_a, should be close to the 0 K reaction endothermicities. Nevertheless, we have to consider that the Arrhenius dependence is not a good approximation if the mean collision energy is close to the value of the activation energy.

At the intermediate temperatures ($k_B T \sim> E_a/10$), the activation energy is strongly influenced by the shape of the reaction cross-section near the threshold (Menzinger & Wolfgang, 1969). The Arrhenius behaviour can further break down due to contributions of the internal states of reactants with different reactivities; thus, the observed thermal reaction rate coefficient can vary with temperature. The activation energy is equal to the cross-section threshold energy of the ground-state reactants in the low-temperature limit only. Thus, for reactions with lower activation energies (k_{N+}^{oH2} (Zymak et al., 2013) and k_{N+}^{HDb} in the present study), the temperature-dependent rate coefficients cannot be fitted with a single Arrhenius function in the entire temperature range. Therefore, the low-temperature linear parts of the measured temperature dependencies in the Arrhenius plots were selected manually for evaluation of the activation energies. The appropriate temperature ranges are also given in Table 5.1.

The results of our experimental studies of endothermic reactions of N^+ ions with H_2, HD, and D_2 at low temperatures are summarised in Figure 5.17. In Figure 5.17, the temperature dependencies (a) and the Arrhenius plots (b) of the reaction rate coefficients k_{N+}^{pH2} of the reaction of N^+ ions with para-H_2, k_{N+}^{oH2} of the reaction of N^+ ions with ortho-H_2, k_{N+}^{HDa} (production of ND^+ in reaction with HD), and k_{N+}^{HDb} (production of NH^+ in reaction with HD), and k_{N+}^{D2} (the reaction of N^+ ions with D_2) are plotted. The plotted temperature dependencies of k_{N+}^{pH2} and k_{N+}^{oH2} in both figures were calculated from the data published in the previous study by Zymak et al. (2013).

We also measured the dependence of reaction rate coefficients on the number density of helium. The deviations from the mono-exponential decay

of the number of N^+ ions does not show an influence of N^+ fine structure (FS) relaxation. Therefore, we can assume that the relaxation process proceeds fast in comparison with the reactive processes.

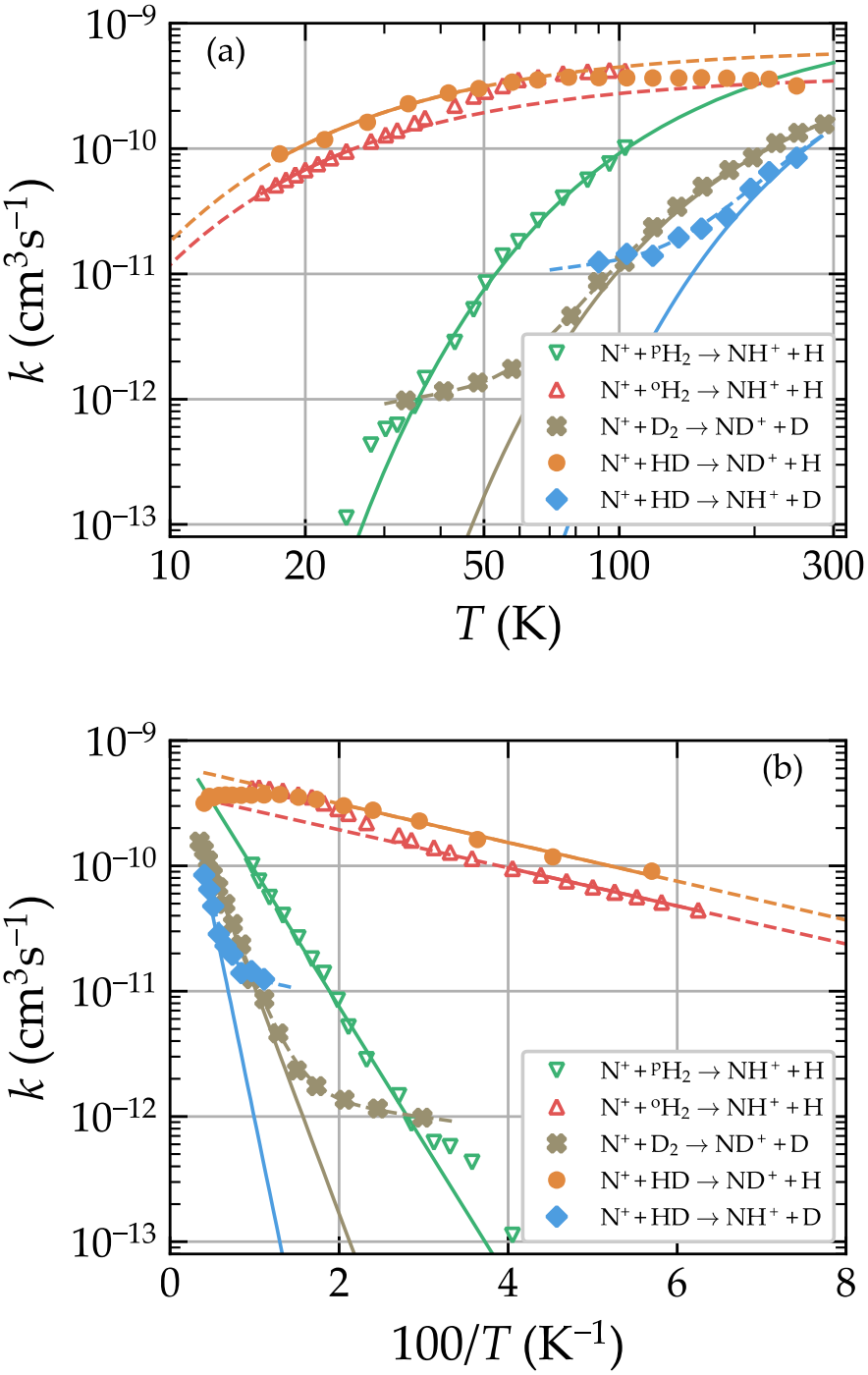

Figure 5.17: Temperature dependencies (a) and the Arrhenius plots (b) of the reaction rate coefficients k_{N+}^{HDa}, k_{N+}^{HDb}, and k_{N+}^{D2} obtained in the present work in comparison with k_{N+}^{pH2} and k_{N+}^{oH2} obtained by Zymak et al. (2013).

All our results are coherent with a model which assumes that there is no barrier on the reaction path. Although in some previous studies (Gerlich et al., 1993; Tosi et al., 1994) it is suggested that there must be a reaction barrier, it has to be indicated that those experiments have been carried out at higher energies (Tosi et al., 1994) and the electronic isotopic shifts are not taken into account. For more precise evaluation of activation energy, the contributions of HD and H_2 admixtures in D_2 and H_2 in HD need to be concerned.

5.2.6 Influence of admixture of [HD] in [D_2]

The deuterium from the bottle contains a small admixture of HD, and the actual fraction f_{HD} of HD in the deuterium gas is $f_{HD} = (0.375 \pm 0.004)\%$. The HD fraction in the bottle was checked in our laboratory using a Cavity Ring-Down Spectrometer CRDS (Macko et al., 2004; Hlavenka et al., 2006; Plašil et al., 2018). The number density [HD] was measured by probing the R(1) overtone transition of HD molecule at 7241.8493 cm^{-1} (line position and transition probability were taken from high-resolution transmission molecular absorption database (HITRAN database, Gordon et al., 2017)). The fraction was calculated as $f_{HD} = [HD]/[D_2]$, where $[D_2]$ was determined from the pressure measured using a capacitive pressure gauge. Our calculated reaction rate coefficients were obtained using HD or D_2 gases with a small admixture of D_2 and H_2 in HD or HD and H_2 in D_2. The number density of D_2 with subtracted HD fraction is denoted as [sub-D_2].

The data of the rate coefficients of N^+ + HD reaction (Figure 5.12) were multiplied by the experimentally obtained fraction value of HD in D_2, and the calculated rate coefficients for this fraction were substrated from the rate coefficient data of N^+ + D_2 reaction, $k_{N+}^{sub\text{-}D2} = k_{N+}^{D2} - f_{HD} \cdot k_{N+}^{HD}$.

As an example, the obtained in the present study rate coefficients k_{N+}^{HD} and expressed contribution of the HD admixture as $f_{HD} \cdot k_{N+}^{HD}$, are shown as full and open squares in Figure 5.18. The corrected temperature dependence of

$k_{N+}^{sub\text{-}D2}$ after subtraction of $f_{HD} \cdot k_{N+}^{HD}$ is shown in Figure 5.18 as red open circles. The behaviour continues to fall to the temperature of 50 K, where it starts lying between 1×10^{-12} cm^3 s^{-1} and 2×10^{-12} cm^3 s^{-1} reaction rate coefficients.

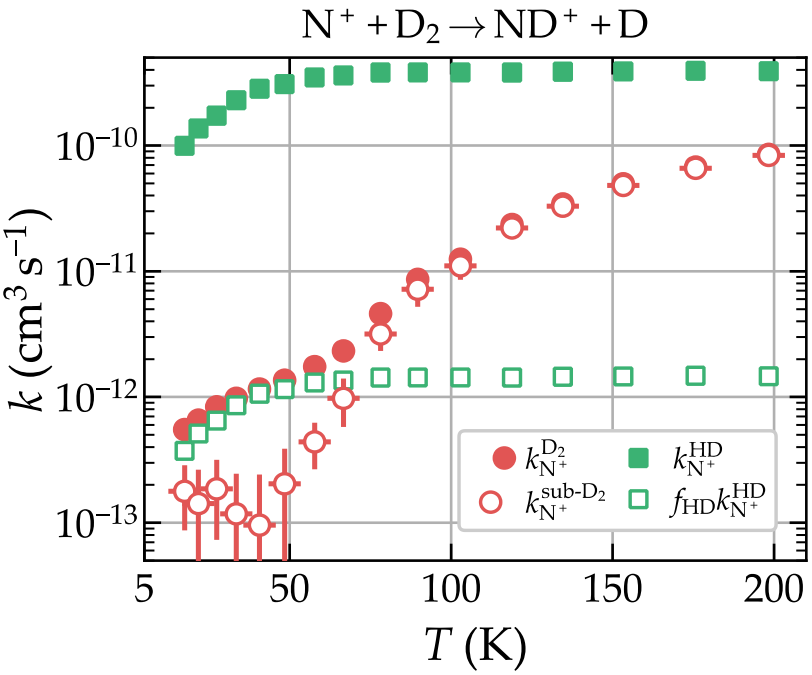

Figure 5.18: Correction of the rate coefficients of the reaction $N^+ + D_2$. The temperature dependence of the binned average reaction rate coefficients k_{N+}^{D2} and k_{N+}^{HD} are presented as full red circles and green squares, respectively. Indicated open red circles demonstrate the temperature dependence of $k_{N+}^{sub\text{-}D2}$ obtained after the correction of k_{N+}^{D2} for the admixture of HD in D_2 gas by subtracting $f_{HD} \cdot k_{N+}^{HD}$ (open green squares).

The correction allows us to clarify the obtained values of the rate coefficients of $N^+ + D_2$ reaction for more than one order of magnitude. These corrections will be used for more precise determination of activation energy of studied reactions, and we will publish this clarified data in a further publication.

5.3 Reaction of O^+ ions with HD and D_2 at low temperatures

Our 22PT apparatus was also involved in the study of the isotope effect of reaction of O^+ ions with HD and D_2 molecules. This investigation was a continuation of the early studied reaction of $O^+(^4S)$ ions with H_2 (Kovalenko et al., 2018):

$$O^+ + H_2 \xrightarrow{k_{O+}^{H2}} OH^+ + H. \qquad (2.6)$$

Measured temperature dependence of the reaction rate coefficient k_{O+}^{H2} was obtained for temperature in the range from 300 K to 15 K and presented in this work in Chapter 5.1 (see, Figure 5.7 or paper Kovalenko et al., 2018).

Presented in this chapter study is aimed to determine the temperature dependencies of the rate coefficients of the reaction of oxygen ions with hydrogen isotopologues. Also, I would like to notice that the results described in this chapter have been sent for publication.

Reactions that have been studied:

$$O^+ + D_2 \xrightarrow{k_{O+}^{D2}} OD^+ + D, \quad \Delta H^0 = -0.51 \text{ eV}, \qquad (5.8)$$

with the reaction rate coefficient k_{O+}^{D2}, and the reaction

$$O^+ + HD \xrightarrow{k_{O+}^{HDa}} OD^+ + H \quad \Delta H^0 = -0.55 \text{ eV} \qquad (5.9a)$$

$$O^+ + HD \xrightarrow{k_{O+}^{HDb}} OH^+ + D, \quad \Delta H^0 = -0.51 \text{ eV} \qquad (5.9b)$$

with reaction rate coefficients k_{O+}^{HDa} and k_{O+}^{HDb}, respectively. The total reaction rate coefficient k_{O+}^{HD} determines as a sum of the rate coefficients of the separate channels (5.9a) and (5.9b), $k_{O+}^{HD} = k_{O+}^{HDa} + k_{O+}^{HDb}$.

The reaction change of enthalpy at 0 K was calculated from tabulated enthalpies of formation, dissociation energies and ionization potentials (Wiedmann et al., 1992; Sunderlin & Armentrout, 1990; Li et al., 1997; Chase, 1998; Sansonetti & Martínez, 2005; Liu et al., 2009).

The primary O^+ ions were produced in the same way as they were prepared for the study of $O^+ + H_2$ reaction and production processes were described in detail in Chapter 5.1.

5.3.1 Time dependence of number of O^+ ions in the trap after reaction with HD and D_2

A typical example of a time dependence obtained for reaction of O^+ ions with D_2 at T = 37 K is shown in Figure 5.19.

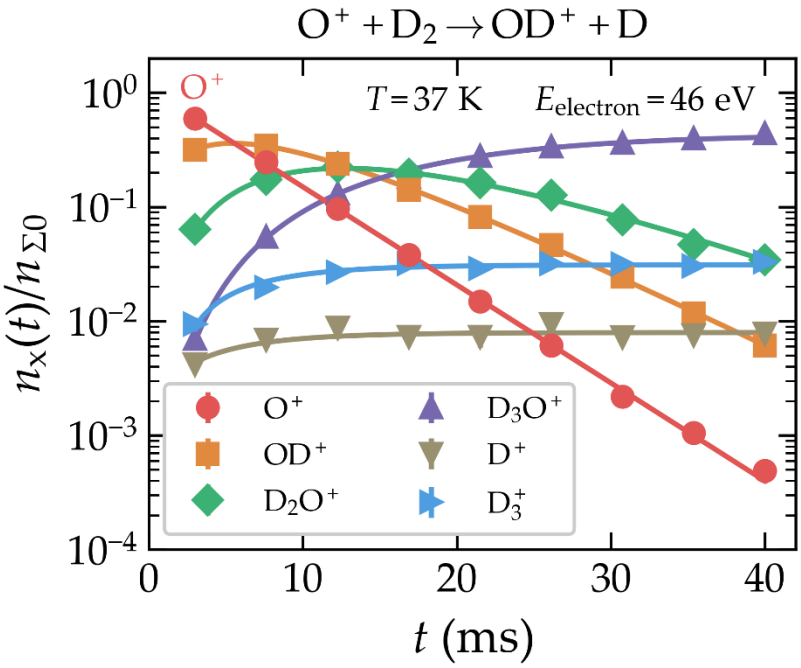

Figure 5.19: Measured time dependence of normalized numbers ($n_x(t)/n_{\Sigma 0}$) of the indicated ions after injection of O^+ ions into the 22PT ($O^+ + D_2$ reaction). The time dependence is measured at T = 37 K with the number density of $[D_2] = 1.9\times10^{11}$ cm^{-3} and $[He] = 2.9\times10^{13}$ cm^{-3}. The electron energy $E_{electron}(k_{O+}^{D2})$ for producing of O^+ ions in the ion source was 46 eV. The obtained reaction rate coefficient from the fit of decay of O^+ ions (solid line) is $k_{O+}^{D2}(37\ K) = 1\times10^{-9}$ cm^{3}s^{-1}.

The plotted data are normalized by dividing the number of ions of the specific ion mass $n_x(t)$ at trapping or storage time t by the total number of detected ions $n_{\Sigma 0}$ at the beginning of the measurement. In Figure 5.19, the time

dependence of normalized primary O^+ ions and OD^+, D_2O^+, D_3O^+, D_3^+, D^+ product ions are plotted.

From these measured time dependencies, it can be seen that formed OD^+ ions continue to react with D_2 with the formation of D_2O^+ ions which then react with D_2 molecules, and D_3O^+ ions are finally produced (the same way as for reaction of $O^+ + H_2$).

The decay of the normalized number of O^+ ions is mono-exponential for almost three orders of magnitude. The reaction rate coefficients $k_{O^+}^{D2}(T)$ were calculated from the fits at preselected temperatures (T) with known D_2 and He partial number densities.

Unambiguous evidence of observation of metastable $O^+(^2D, ^2P)$ ions in the 22PT is the production of D^+ and D_2^+ ions. Formation of these ions is endothermic for the ground state $O^+(^4S)$ ions but exothermic for metastable $O^+(^2D, ^2P)$ ions, (see ref. Li et al., 1997). The D^+ and D_2^+ ions can be formed in the reaction of metastable $O^+(^2D, ^2P)$ ions with D_2. The production of D_3^+ indicates that the D_2^+ ions are also formed in the reaction of metastable $O^+(^2D, ^2P)$ ions with D_2. As the reaction $D_2^+ + D_2$ proceeded fast (Langevin rate coefficient is $1.45\times10^{-9}\,cm^3s^{-1}$), we made a decision to observe the formation of D_3^+ instead of D_2^+ ions. We calculate the fraction of excited $O^+(^2D, ^2P)$ ions in the 22PT by monitoring the formation of D^+ ions which do not react with D_2 (prolonged ternary association can be neglected). However, the fraction of production D_2^+ ions is higher than for D^+ ions, (see Li et al., 1997).

As in the previous similar experiment (Chapter 5.1), the rate coefficients are dependent on the fraction of metastable $O^+(^2D, ^2P)$ ions which come from the SIS to the 22PT. The same situation is also inherent for the branching ratios of reaction O^+ ions with HD. This situation can be seen in Figure 5.20. Used gas and electron energy give the number of produced $O^+(^2D, ^2P)$ ions in the ion source. It can be assumed that the same fraction (F) of metastable $O^+(^2D, ^2P)$ ions present in the 22PT as in the previous experiment (Chapter 5.1). In our measuring routine, we also studied the dependence of the formation of D^+ ions in reaction of O^+ ions with D_2 on the applied energy of electrons in the SIS

$E_{electron}$. We investigated that the fraction of exited $O^+(^2D, ^2P)$ ions in the 22PT is lower than 5 % for electron energies used in the SIS < 50 eV.

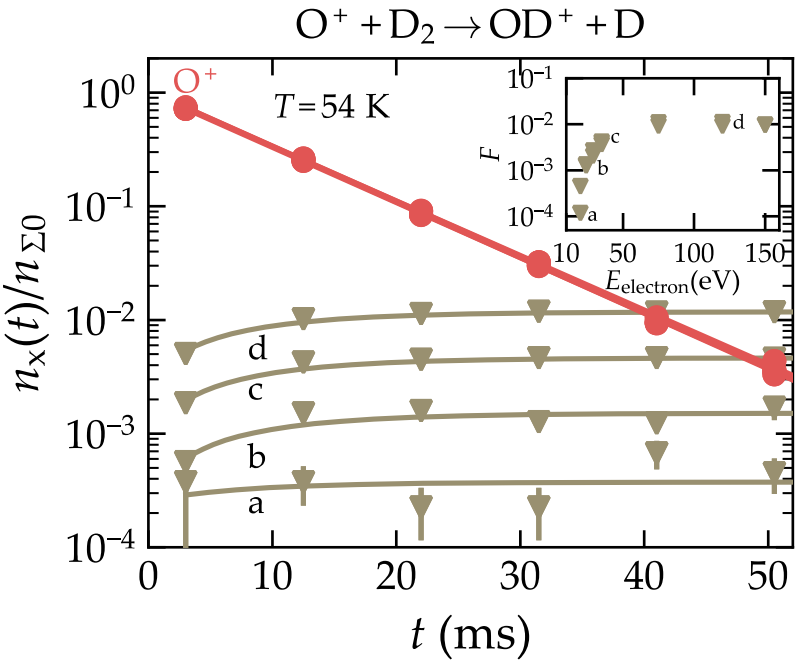

Figure 5.20: The measured time dependencies at several electron energies $E_{electron}$ used in the SIS of normalized numbers of primary O^+ ions and produced D^+ ions (O^+ + D_2 reaction). The electron energies $E_{electron}$ were changed in the range from 20 eV up to 150 eV. The obtained data were measured at T = 54 K with [D_2] = 9.2×10^{10} cm^{-3} and [He] = 2.4×10^{13} cm^{-3} gas number densities respectively. The obtained reaction rate coefficients k_{O+}^{D2}(37 K) from the decays of O^+ ions have almost the same value around 1.2×10^{-9} cm^{3}s^{-1}. The inset shows the dependence of the fraction F of produced D^+ ions on applied electron energy $E_{electron}$ used in the SIS (Kovalenko et al., 2021, submitted).

It was already mentioned at the beginning of Chapter 5.3 that the reaction of $O^+(^4S)$ ion with HD molecule has two reaction channels (5.9a) and (5.9b) with the ion products OD^+ and OH^+, respectively. The corresponding reaction rate coefficients are denoted as k_{O+}^{HDa} and k_{O+}^{HDb} and the total reaction rate coefficient is $k_{O+}^{HD} = k_{O+}^{HDa} + k_{O+}^{HDb}$. The branching ratios of the production of OD^+ and OH^+ ions are denoted as BR_{OD+}^{HD} and BR_{OH+}^{HD}, respectively. The BR_{OD+}^{HD} and

BR_{OH+}^{HD} are defined as $BR_{OD+}^{HD} = k_{O+}^{HDa} / (k_{O+}^{HDa} + k_{O+}^{HDb})$ and $BR_{OH+}^{HD} = k_{O+}^{HDb} / (k_{O+}^{HDa} + k_{O+}^{HDb})$. For calculation of k_{O+}^{HDa} and k_{O+}^{HDb}, the decays of the number of primary O^+ ions and the increases of the number of OD^+ and OH^+ produced ions in the trap were measured.

Figure 5.21 presents the measured time dependencies of the normalized numbers of the primary reactant ions and the secondary produced ions of $O^+ + HD$ reaction. In the ion trap, both OD^+ and OH^+ products continue to react with HD and form H_2O^+, OHD^+, and D_2O^+ ions. The products with the same mass to charge ratio complicate the measurement as it is hard to distinguish them during the measurements. In our data analysis, the balance equations for the productions and the losses of all ions must be considered.

In the experiment, the low electron energy ($E_{electron}(k_{O+}^{HD})$ = 37 eV) was applied in the ion source to minimize the population of the $O^+(^2D, ^2P)$ metastable ions in the ion trap. The data presented in the upper panel of Figure 5.21 were measured during the shorter trapping time to fit the increases of OH^+ and OD^+ products and calculate k_{O+}^{HDa} and k_{O+}^{HDb}. At the short trapping time, the decay of the number of oxygen ions is relatively small, and the formation of OH^+ and OD^+ ions is distinguishable from the formation of the secondary products. The total reaction rate coefficient k_{O+}^{HD} was calculated from the decay of O^+ ions in the lower panel of Figure 5.21. Measured decay of O^+ ions in reaction with HD has a decrease for almost 2 orders of magnitude. Secondary products of mass 19 and 20 Da are shown in Figure 5.21 and denoted as A_{19}^+ and A_{20}^+, respectively.

We considered the efficiency of the detection system in the data analysis (extraction from the ion trap, mass selection, and detection), which is dependent on the mass of the ion (mass discrimination). These fitted detection efficiencies were used in the analysis of the $O^+ + HD$ data. The difference between detection efficiencies for O^+ and D^+ ions was measured using a calibration reaction of D^+ ions with CH_4 (for details, see Kovalenko et al., 2018). The measured relative numbers of ions presented in this work are corrected for the mass discrimination.

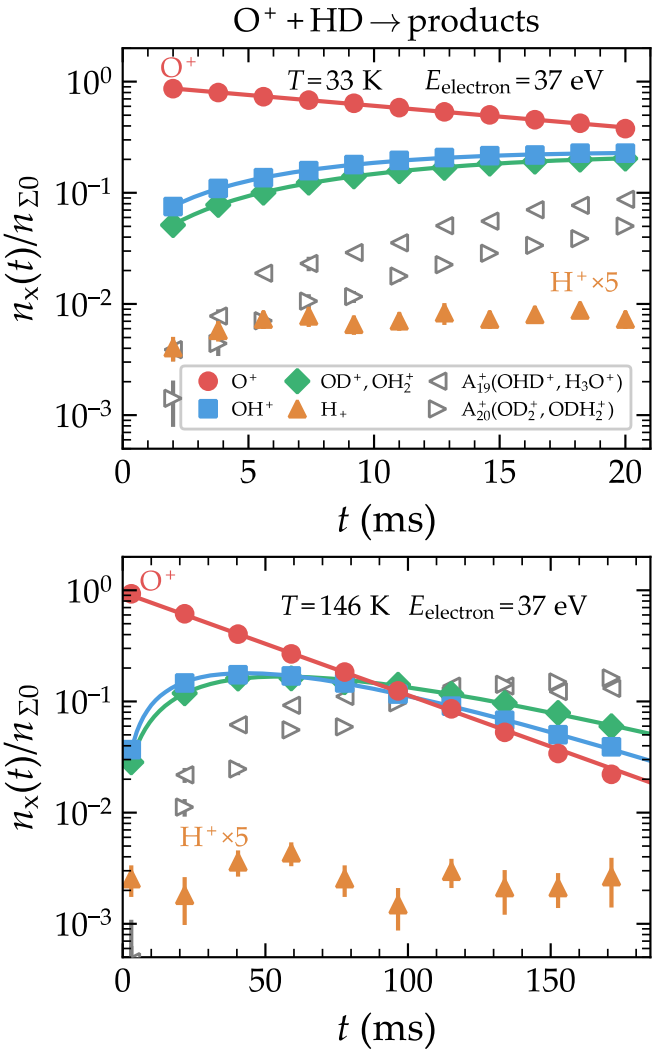

Figure 5.21: **T**ime dependencies of the normalized numbers ($n_x(t)/n_{\Sigma 0}$) of the indicated ions after the injection of O^+ ions into the ion trap (O^+ + HD reaction). Oxygen ions were produced in SIS with electron energy 37 eV. Upper panel (shorter trapping time): the time dependencies of the normalized numbers of the primary O^+ ions and the produced ions obtained at T = 33 K, [HD] = 3.4×10^{10} cm^{-3}, [He] = 3.1×10^{13} cm^{-3}. The values plotted for H^+ ions are multiplied by factor 5. All lines indicate the fit results calculated from a kinetic model. The calculated total reaction rate coefficient is k_{O+}^{HD} (33 K) = 1.3×10^{-9} cm^{3}s^{-1}. Lower panel (longer trapping time): the time dependencies of the normalized numbers of the O^+ primary ions and produced ions measured at T = 146 K, [HD] = 1.6×10^{10} cm^{-3}, [He] = 1.5×10^{13} cm^{-3}. The calculated total reaction rate coefficient is k_{O+}^{HD}(146 K) = 1.3×10^{-9} cm^{3}s^{-1}.

5.3.2 Dependence of rate of O^+ + D_2 reaction on the number density of D_2

We also confirmed the binary character of the O^+ + D_2 reaction by measuring the dependence of the reaction lose rate r_{O+}^{D2} on the number density of deuterium at several temperatures. In Figure 5.22 the example of dependencies of reaction rate r_{O+}^{D2} on [D_2] number densities obtained at T = 104 K and T = 62 K is demonstrated.

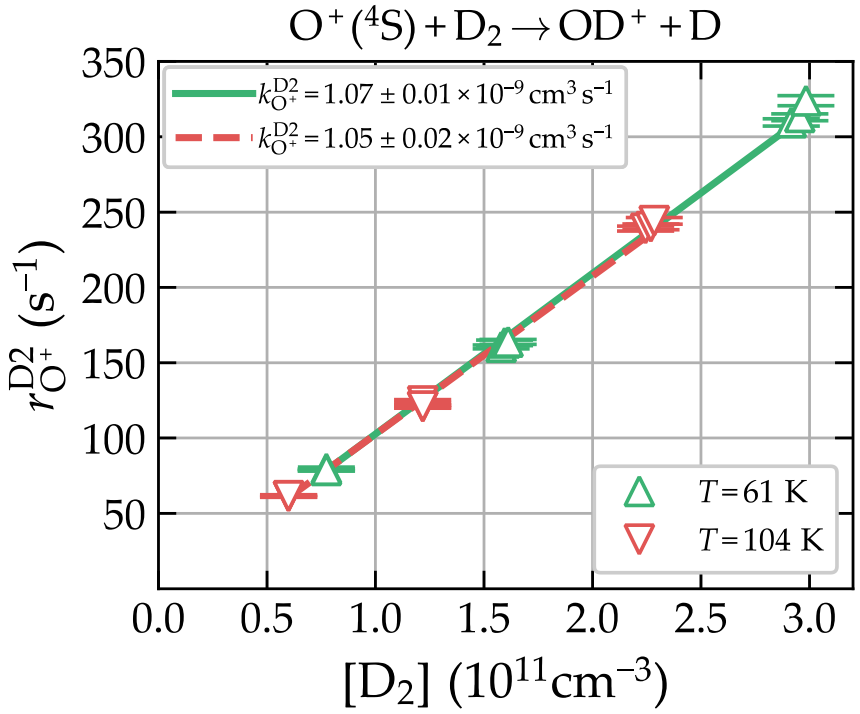

Figure 5.22: Dependencies of the loss rates r_{O+}^{D2} of $O^+(^4S)$ ions on D_2 number density at collisional temperatures T = 61 K (green triangles up, [He] = 1.65×10^{13} cm^{-3}) and T = 104 K (red triangles down, [He] = 2.15×10^{13} cm^{-3}) (Kovalenko et al., 2021, submitted).

In this measurement, the initial O^+ ions were produced using the energy of electrons in the SIS as 46 eV. The linear character of the measured dependencies, $r_{O+}^{D2} = k_{O+}^{D2} \cdot [D_2] + r_{bgO+}^{D2}$, confirms that the reaction proceeds by binary reaction with D_2. The values of the rate coefficient k_{O+}^{D2} of the reaction of O^+ ions with D_2 are given by the slopes of the plotted dependencies. The influence of reactions with molecules of background gases is neglectable as the

level of the background loss rate (r_{bgO+}^{D2}) obtained in the measurement with pure He without D_2 is very low.

Obtained reaction rate coefficients from the linear fits of measured dependencies of reaction rate on the number density of D_2 are: $k_{O+}^{D2}(61\ K) = 1.07\times10^{-9}\ cm^3s^{-1}$ and $k_{O+}^{D2}(104\ K) = 1.05\times10^{-9}\ cm^3s^{-1}$. These results are in agreement with measured rate coefficients from subchapter 5.3.1. Note that in the fits, the uncertainty caused by the measurements of the number density was not considered.

5.3.3 Temperature dependencies of the rate coefficients of $O^+ + D_2$ and $O^+ + HD$ reactions

The temperature dependencies of rate coefficients k_{O+}^{D2} and k_{O+}^{HD} of the reactions $O^+ + D_2$ and $O^+ + HD$ were obtained by measuring the time dependencies of particular ions at collision temperatures from 300 K to 15 K and 235 K to 15 K, respectively. The electrons with low energies ($E_{electron}(k_{O+}^{D2}) = 46$ eV, $E_{electron}(k_{O+}^{HD}) = 37$ eV) were emitted in the SIS to achieve the dominant population of ground state $O^+(^4S)$ ions inside the ion trap.

In Figure 5.23, the temperature dependence of the binned average reaction rate coefficients k_{O+}^{D2} obtained in the present study (open red circles) is compared with previous experimental results and theoretical studies.

The presented results are compared with the temperature dependencies of converted reaction rate coefficients from cross-sections obtained in GIB experiments by Li et al. (1997) and Burley et al. (1987). The experimental value obtained by Burley et al. (1987) at temperature $T = 305$ K is $1.04\times10^{-9}\ cm^3s^{-1}$.

The cross-sections results obtained in other theoretical calculations by Martínez et al. (2006), Xu et al. (2012), Wang et al. (2018), and Zhu et al. (2020) were converted to the reaction rate coefficients $k = <\sigma v>$ (see equation (2.11)) as the function of a mean relative kinetic energy of the reactants (E_r). Calculated values of these rate coefficients are also included in Figure 5.22 as the function of the kinetic temperature, defined as $T_{ef} = 2E_r/(3k_B)$.

For theoretical values of cross-sections, we obtained two temperature dependencies of rate coefficients of the reaction of O^+ ions with D_2 by continuously extrapolating the cross-section by a constant value or by a function proportional to $1/\sqrt{E_r}$ (Langevin behaviour). I assume that the actual rate coefficients (within the theoretical approximation) lie between these extreme values in the hatched areas indicated in Figure 5.23.

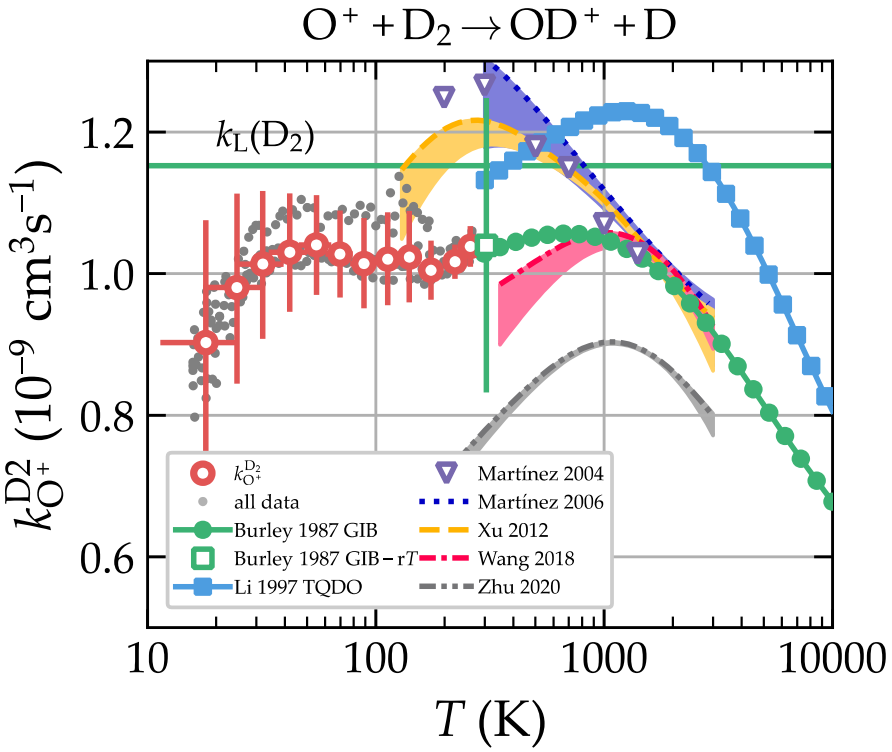

Figure 5.23: Temperature dependence of the reaction rate coefficient k_{O+}^{D2} of the reaction of $O^+(^4S)$ ions with D_2 (Kovalenko et al., 2021, submitted). The larger red open circles indicate the binned average values from the measure data (small grey circles). The horizontal straight line ($k_L(D_2)$) shows the value of the Langevin collisional rate coefficient. Converted reaction rate coefficients from cross-sections obtained in the GIB (Burley et al., 1987) and the TQDO (Li et al., 1997) experiments are also shown. Obtained values of the reaction rate coefficients were converted from the cross-sections which were theoretically obtained by Martínez et al. (2006), Xu et al. (2013), Wang et al. (2018), and by Zhu et al. (2020).

The total reaction rate coefficient k_{O+}^{HD} was calculated from the fits of time decays of O^+ ions. All experimental results were obtained for temperatures in the range from 235 K to 15 K.

The calculated binned average results of the total reaction rate coefficient k_{O+}^{HD} are shown in Figure 5.24 as red open circles.

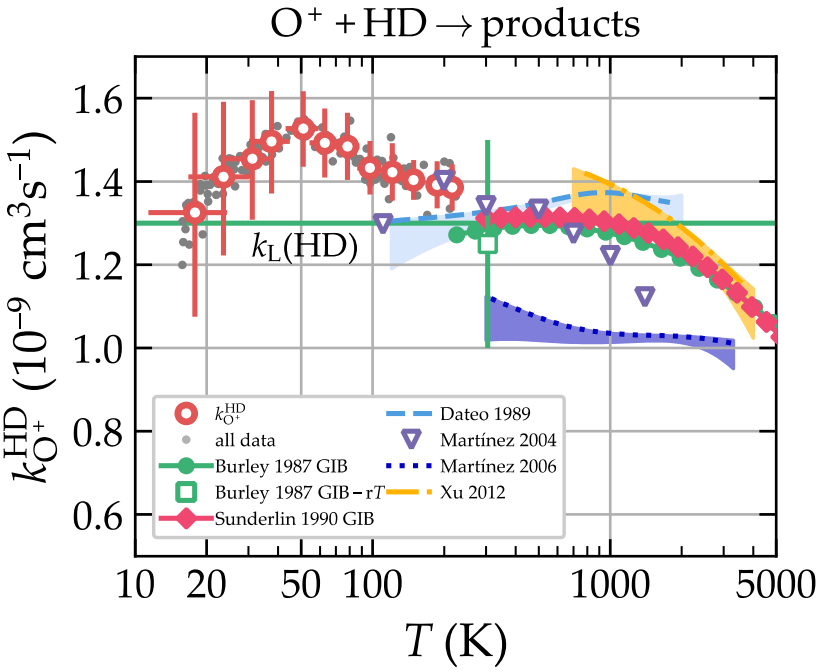

Figure 5.24: Temperature dependence of the total rate coefficient k_{O+}^{HD} of the reaction of $O^+(^4S)$ ion with HD molecule (Kovalenko et al., 2021, submitted). The larger open circles indicate the binned average values from measured data (small grey circles). The horizontal straight line (k_L(HD)) shows the value of the Langevin collisional rate coefficient. Converted reaction rate coefficients from cross-sections obtained in the GIB experiments by Sunderlin & Armentrout (1990) and Burley et al. (1987) are also shown. The rate coefficients were converted from the theoretical cross-sections, obtained by Dateo et al. (1989), Martínez et al. (2004), (2006), and by Xu et al. (2012).

The presented results are compared with the temperature dependencies of phenomenological reaction rate coefficients obtained in the GIB experiments by Sunderlin & Armentrout (1990) and Burley et al. (1987). The experimental value obtained by Burley et al. (1987) at temperature T = 305 K is 1.25×10^{-9} cm^{3}s^{-1}. The cross-sections result obtained in other theoretical

studies by Dateo et al. (1989), Martínez et al. (2004), (2006), and by Xu et al. (2012) were converted to phenomenological rate coefficients $k = <\sigma v>$ in the same way as it was also done for reaction $O^+ + D_2$. Theoretical results of González et al. (1993) were not presented in Figure 5.24 as obtained cross-sections were calculated for energies from 0.4 eV to 10 eV ($\approx 4\times10^3 - 1\times10^5$ K).

5.3.4 Temperature dependence of the branching ratio of $O^+ + HD$ reaction and summary

The trapping times for dependencies of the number of formed OH^+ and OD^+ ions in the ion trap were chosen to have recognizable increases of the production of these two channels (see Figure 5.21). The branching ratios BR^{HD}_{OH+} and BR^{HD}_{OD+} were obtained for the collisional temperatures from 235 K down to 15 K.

Calculated values of $BR^{HD}_{OH+} = k^{HDb}_{O+} / (k^{HDa}_{O+} + k^{HDb}_{O+})$ are shown in Figure 5.25. The obtained values were compared with data from previous experiments (GIB (Burley, 1987; Sunderlin & Armentrout, 1990) and VT-SIFDT (Viggiano et al., 1991)) and with calculated theoretical temperature dependencies (Dateo et al., 1989; González et al. 1993; Martínez et al., 2006; Xu et al., 2012). Branching ratios from listed sources (except data from SIFDT experiment (Viggiano et al., 1991)) were calculated from theoretically or experimentally obtained cross-sections using the formula $f(OH^+) = \sigma(OH^+)/(\sigma(OH^+) + \sigma(OD^+))$, where f designates the fraction. Obtained branching ratios from cross-sections can not be compared directly with the branching ratios obtained from the rate coefficient of the reactions. Discrepancies between these two BR can be seen at much lower energies (lower than 300 K or 0.04 eV). Therefore, our data can be reliably compared to data with temperatures higher than 300 K. However, it can be seen that the present data are in good agreement with previous experimental results which were measured at temperatures/collision energies above ~100 K (GIB (Burley 1987), GIB (Sunderlin & Armentrout, 1990) and VT-SIFDT (Viggiano et al.,

1991). It has to be noticed that there are no previous experimental results for temperature below 100 K for both reactions (5.8) and (5.9).

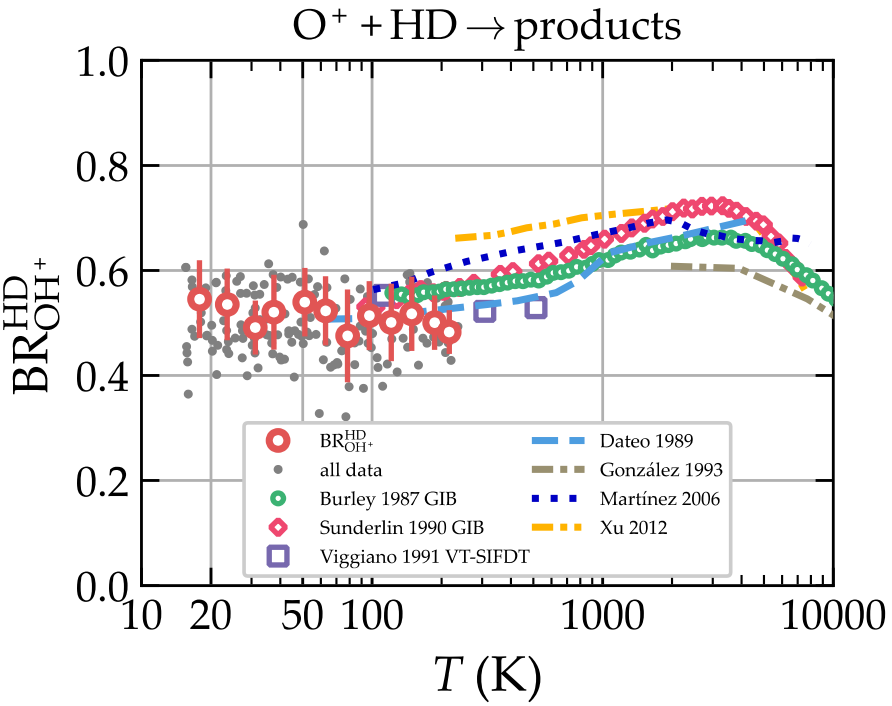

Figure 5.25: The temperature dependence of the branching ratio $BR_{OH+}^{HD} = k_{O+}^{HDb} / (k_{O+}^{HDa} + k_{O+}^{HDb})$ for the production of OH^+ ions in the reaction of O^+ ions with HD (Kovalenko et al., 2021, submitted). Each independent measurement is indicated with a small full circle; the large open circles indicate the binned average values. The present data are compared with experimental results obtained in the GIB (Burley et al., 1987; Sunderlin & Armentrout, 1990) and the VT-SIFDT (Viggiano et al., 1991) experiments and with temperature dependencies of BR_{OH+}^{HD} obtained from theoretically calculated cross-sections (Dateo et al., 1989; González et al., 1993; Martínez et al., 2006; Xu et al., 2012).

Figure 5.26 demonstrates the investigated isotope effect of the reactions of O^+ ions with normal-H_2, HD, and with normal-D_2. The data of the reaction of O^+ with normal-H_2 were taken from our previous study (Kovalenko et al., 2018 or see Chapter 5.1). The dependencies are shown for collision temperatures ranging from 15 K up to 300 K.

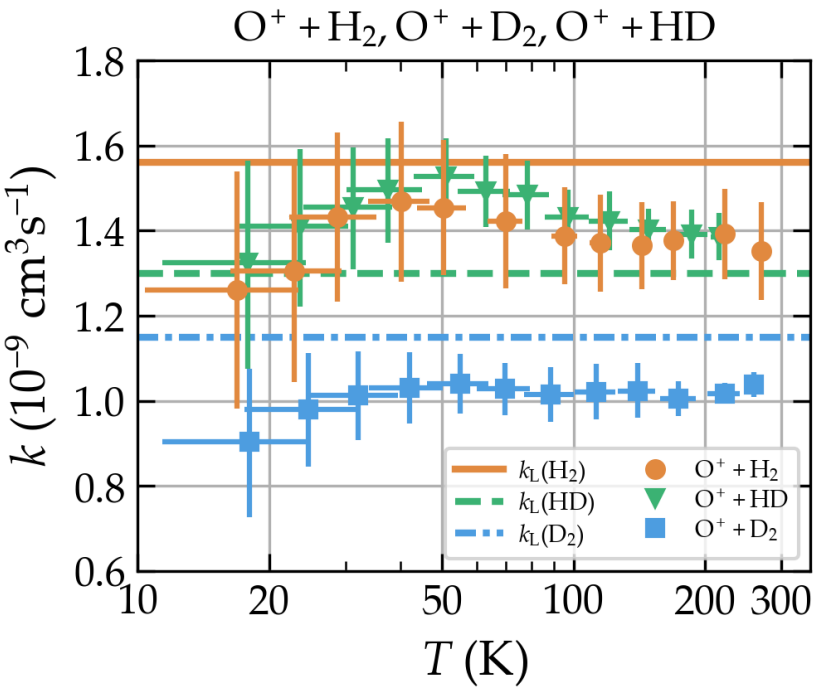

Figure 5.26: Demonstration of the isotope effect of the reactions of O^+ ions with normal-H_2, HD, and with normal-D_2 (Kovalenko et al., 2021, submitted). The horizontal lines indicate the values of the Langevin collisional rate coefficients of these reactions. Previously obtained data of $O^+ + H_2$ reaction was taken from our study (Kovalenko et al., 2018, or see chapter 5.1).

From the figure, I can conclude that the rate coefficients of these reactions are nearly constant, and their values are in a good agreement with the values of corresponding Langevin collisional rate coefficients. Slight deviations between Langevin collision rate coefficients and our measured reaction rate coefficients are within the accuracy of our experimental results.

For this study, we have prepared a deep discussion to explain the results of our study, and the final results have been sent for publication (Kovalenko et al., 2021, submitted).

6. Summary

My work is represented by the experimental study of several reactions of molecular hydrogen and its isotopologues with oxygen and nitrogen ions. These experiments are conducted under laboratory astrophysical conditions which are relevant to molecule-forming regions of the dense or diffuse molecular clouds. The thesis is focused on the study of the formation of OH^+ ions which take part in the chemical network of water formation in the interstellar medium. Also, the isotope effect in reactions of N^+ and O^+ ions with HD and D_2 was studied. In our group, these 5 reactions were experimentally studied, and I was involved in measurements, data analysis and the preparation of the experimental results for publications.

The work is aimed to understand the kinetic of the reaction of O^+ ions with molecular hydrogen. By dint of our RF 22-pole ion trap technique, we extended the range of the experimentally determined temperature dependence of reaction rate coefficient down to a collisional temperature of 15 K. Obtained behaviour is similar to many exothermic reactions of ions with molecular hydrogen, which can be described by a simple Langevin capture model. The value of the rate coefficient obtained at 300 K is in a good agreement with the results from previous experimental studies. From the temperature dependence (Figure 5.7), it can be seen that the reaction rate coefficients slightly decrease below 30 K. This result is in a good agreement with the TDWP cross-sections which level off below 10 meV (Bulut et al., 2015). Nevertheless, we need more experiments with re-examination for collision energies relevant to 10 K. Some measurements with para-H_2 could help to discover the additional changes at temperatures from 10 K to 30 K. I would like to remind that the measured reaction rate coefficients for temperatures from 300 K to 15 K of this reactions are essential for modelling and understanding the chemical processes of water formation in the interstellar medium. The main results for $O^+ + H_2$ reaction are presented in Figure 5.7 (see also paper Kovalenko et al., 2018, in the attachment).

Temperature dependencies of reaction rate coefficients and the activation energies of reactions of N^+ ions with HD and D_2 were obtained from the experimental study of these reactions. Table 5.1 collects our experimentally determined values of activation energies in comparison, with those obtained in other experiments. The main results for these reactions are presented in Figure 5.17. Our results do not prove the absence of barriers, however, I can conclude that the barriers are either negligible or identical for all reactions (relative to product channels). Study of the reverse reactions can help to prove or deny the presence of the barriers. Using our RF 22-pole ion trap apparatus in combination with the source of H atoms, a study of the reaction $NH^+ + H \rightarrow N^+ + H_2$ (reverse to reaction (2.2)) has been performed. The results are now being prepared for publication.

The reactions of O^+ ions with hydrogen isotopologues HD and D_2 were experimentally studied to see the changes in reaction kinetics due to isotope exchange in comparison to $O^+ + H_2$ reaction. All three reactions show the same character of the temperature dependence of reactions rate coefficients, and their values are close to Langevin rate coefficients. Our results are in good agreement with previously obtained results from theoretic calculations or experiments. The ratio of rate coefficient of the OH^+ production channel to the total reaction rate coefficient is close to 0.5 in the studied temperature range 15 — 237 K. Our result is in agreement with the values of branching ratio of OH^+ fraction derived from previous experimental and theoretical studies where the branching ratio of OH^+ fraction is calculated from cross-sections of the separate channels. The main results for these reactions are presented in Figure 5.25 and 5.26 (see also submitted paper Kovalenko et al., 2021, in the attachment).

The experimental results of our studies were presented at international conferences and published in impacted scientific journals (see section List of Publications). The experimental results for reactions $O^+ + D_2$, HD have been submitted to The Journal of Chemical Physics and are under review. Results of $N^+ + D_2$, HD study, have been submitted to The Astrophysical Journal.

Bibliography

Acharyya, K., & Herbst, E. (2015). Molecular development in the Large Magellanic Cloud. *The Astrophysical Journal*, *812*(2), 142(1–17). https://doi.org/10.1088/0004-637x/812/2/142

Adams, N., & Smith, D. (1976). The selected ion flow tube (SIFT); A technique for studying ion-neutral reactions. *International Journal of Mass Spectrometry and Ion Physics*, *21*(3–4), 349–359. https://doi.org/10.1016/0020-7381(76)80133-7

Adams, N., Smith, D., Lister, D., Rakshit, A., Tichý, M., & Twiddy, N. (1979). The rate coefficients for several ternary association reactions of CH_3^+ in the temperature range 100 – 300 K. *Chemical Physics Letters*, *63*(1), 166–170. https://doi.org/10.1016/0009-2614(79)80482-0

Adams, N., & Smith, D. (1985). A study of the nearly thermoneutral reactions of N with H_2, HD and D_2. *Chemical Physics Letters*, *117*(1), 67–70. https://doi.org/10.1016/0009-2614(85)80407-3

Adams, N. G., Smith, D., & Paulson, J. F. (1980). An experimental survey of the reactions of NH_n^+ ions (n = 0 to 4) with several diatomic and polyatomic molecules at 300 K. *The Journal of Chemical Physics*, *72*(1), 288–297. https://doi.org/10.1063/1.438893

Albertsson, T., Semenov, D. A., Vasyunin, A. I., Henning, T., & Herbst, E. (2013). New Extended Deuterium Fractionation Model: Assessment at dense ISM conditions and sensitivity analysis. *The Astrophysical Journal Supplement Series*, *207*(2), 27(1–29). https://doi.org/10.1088/0067-0049/207/2/27

Aleman, I., Ueta, T., Ladjal, D., Exter, K. M., Kastner, J. H., Montez, R., … Zijlstra, A. A. (2014). Herschel Planetary Nebula Survey (HerPlaNS). *Astronomy & Astrophysics*, *566*, A79(1–9). https://doi.org/10.1051/0004-6361/201322940

Asvany, O. (2003). Experiments with ions and clusters in a variable temperature 22-pole ion trap. Doctoral thesis, Chemnitz University of Technology, Faculty of Natural Sciences.

Asvany, O., & Schlemmer, S. (2009). Numerical simulations of kinetic ion temperature in a cryogenic linear multipole trap. *International Journal of Mass Spectrometry*, *279*(2–3), 147–155. https://doi.org/10.1016/j.ijms.2008.10.022

Awad, Z., & Shalabiea, O. M. (2017). Deuterium chemistry in the young massive protostellar core NGC 2264 CMM3. *Astrophysics and Space Science*, *363*(1), 12 (1–29). https://doi.org/10.1007/s10509-017-3232-7

Awad, Z., Viti, S., Bayet, E., & Caselli, P. (2014). Deuterium chemistry of dense gas in the vicinity of low-mass and massive star-forming regions. *Monthly Notices of the Royal Astronomical Society*, *443*(1), 275–287. https://doi.org/10.1093/mnras/stu1141

Barlow, M. J., Swinyard, B. M., Owen, P. J., Cernicharo, J., Gomez, H. L., Ivison, R. J., … Polehampton, E. T. (2013). Detection of a noble gas molecular ion, $^{36}ArH^+$, in the Crab Nebula. *Science*, *342*(6164), 1343–1345. https://doi.org/10.1126/science.1243582

Benitez, F., Duclut, C., Chaté, H., Delamotte, B., Dornic, I., & Muñoz, M. A. (2016). Langevin equations for reaction-diffusion processes. *Physical Review Letters*, *117*(10), 100601(1–6). https://doi.org/10.1103/PhysRevLett.117.100601

Borodi G. (2008). On the combination of a low energy hydrogen atom beam with a cold multipole ion trap. Doctoral thesis, Chemnitz University of Technology, Faculty of Natural Sciences.

Bulut, N., Castillo, J., Jambrina, P. G., Kłos, J., Roncero, O., Aoiz, F. J., & Bañares, L. (2015). Accurate time-dependent wave packet calculations for the $O^+ + H_2 \rightarrow OH^+ + H$ ion-molecule reaction. *The Journal of Physical Chemistry A*, *119*(50), 11951–11962. https://doi.org/10.1021/acs.jpca.5b00815

Burley, J., Ervin, K. M., & Armentrout, P. (1987). Translational energy dependence of $O^+(^4S)$ + $H_2(D_2, HD)$ → $OH^+(OD^+)$ + H(D) from thermal energies to 30 eV c.m. *International Journal of Mass Spectrometry and Ion Processes*, *80*, 153–175. https://doi.org/10.1016/0168-1176(87)87027-1

Butner, H. M., Charnley, S. B., Ceccarelli, C., Rodgers, S. D., Pardo, J. R., Parise, B., … Davis, G. R. (2007). Discovery of interstellar heavy water. *The Astrophysical Journal*, *659*(2), L137–L140. https://doi.org/10.1086/517883

Böhringer, H., & Arnold, F. (1986). Temperature and pressure dependence of the reaction of He^+ ions with H_2. *The Journal of Chemical Physics*, *84*(3), 1459–1462. https://doi.org/10.1063/1.450490

Campbell, E., Maier, J., Gerlich, D., Banerjee, A., Holz, M., & Chakrabarty, S. (2014). A novel method to measure spectra of cold molecular ions. *Proceedings of the 69th International Symposium on Molecular Spectroscopy*. https://doi.org/10.15278/isms.2014.rh01

Caselli, P., Walmsley, C. M., Terzieva, R., & Herbst, E. (1998). The ionization fraction in dense cloud cores. *The Astrophysical Journal*, *499*(1), 234–249. https://doi.org/10.1086/305624

Caselli, P., Sipilä, O., & Harju, J. (2019). Deuterated forms of H_3^+ and their importance in astrochemistry. *Philosophical Transactions of the Royal Society A: Mathematical, Physical and Engineering Sciences*, *377*(2154), 20180401–20180410. https://doi.org/10.1098/rsta.2018.0401

Ceccarelli, C., Loinard, L., Castets, A., Tielens, A. G. G. M., Caux, E., Lefloch, B., & Vastel, C. (2001). Extended D_2CO emission: The smoking gun of grain surface-chemistry. *Astronomy & Astrophysics*, *372*(3), 998 – 1004. https://doi.org/10.1051/0004-6361:20010559

Ceccarelli, C., Caselli, P., Bockelée-Morvan, D., Mousis, O., Pizzarello, S., Robert, F., & Semenov, D. (2014). Deuterium Fractionation: The Ariadne's Thread from the Precollapse Phase to Meteorites and Comets Today. In Protostars and Planets VI. University of Arizona Press. p. 859. https://doi.org/10.2458/azu_uapress_9780816531240-ch037

Ceccarelli, C. (2002). Millimeter and infrared observations of deuterated molecules. *Planetary and Space Science*, *50*(12–13), 1267–1273. https://doi.org/10.1016/s0032-0633(02)00093-4

Cernicharo, J., Tercero, B., Fuente, A., Domenech, J. L., Cueto, M., Carrasco, E., … Pearson, J. (2013). Detection of the ammonium ion in space. *The Astrophysical Journal*, *771*(1), 1–4. https://doi.org/10.1088/2041-8205/771/1/l10

Chase, M. W. (1998). NIST-JANAF thermochemical tables. Woodbury (New York): American Chemical Society and the American Institute of Physics for the National Institute of Standards and Technology.

Chesnavich, W., Su, T., & Bowers, M. (1980). Collisions in a noncentral field: a variational and trajectory investigation of ion-dipole capture. *The Journal of Chemical Physics*, *72*(4), 2641–2655. https://doi.org/10.1063/1.439409

Cheung, A. C., Rank, D. M., Townes, C. H., Thornton, D. D., & Welch, W. J. (1968). Detection of NH_3 molecules in the interstellar medium by their microwave emission. *Physical Review Letters*, *21*(25), 1701–1705. https://doi.org/10.1103/physrevlett.21.1701

Crapsi, A., Caselli, P., Walmsley, C. M., Myers, P. C., Tafalla, M., Lee, C. W., & Bourke, T. L. (2005). Probing the evolutionary status of starless cores through N_2H and N_2D observations. *The Astrophysical Journal*, *619*(1), 379–406. https://doi.org/10.1086/426472

Dateo, C. E., & Clary, D. C. (1989). Isotopic branching ratio for the O^+ + HD reaction. *Journal of the Chemical Society, Faraday Transactions 2*, *85*(10), 1685–1696. https://doi.org/10.1039/f29898501685

Dishoeck, E. F. V., Jansen, D. J., Schilke, P., & Phillips, T. G. (1993). Detection of the interstellar NH_2 radical. *The Astrophysical Journal*, *416*, L83–L86. https://doi.org/10.1086/187076

Draine, B. T. (2011). Physics of the interstellar and intergalactic medium. Princeton, N.J: Princeton University Press.

Endres, C. P., Schlemmer, S., Schilke, P., Stutzki, J., & Müller, H. S. (2016). The Cologne Database for Molecular Spectroscopy, CDMS, in the Virtual Atomic and Molecular Data Centre, VAMDC. *Journal of Molecular Spectroscopy*, *327*, 95–104. https://doi.org/10.1016/j.jms.2016.03.005

Endres, E., Egger, G., Lee, S., Lakhmanskaya, O., Simpson, M., & Wester, R. (2017). Incomplete rotational cooling in a 22-pole ion trap. *Journal of Molecular Spectroscopy*, *332*, 134–138. https://doi.org/10.1016/j.jms.2016.12.006

Ervin, K. M., & Armentrout, P. B. (1985). Translational energy dependence of $Ar^+ + XY \rightarrow ArX^+ + Y$ ($XY = H_2, D_2$, HD) from thermal to 30 eV c.m. *The Journal of Chemical Physics*, *83*(1), 166–189. https://doi.org/10.1063/1.449799

Ervin, K. M., & Armentrout, P. B. (1987). Energy dependence, kinetic isotope effects, and thermochemistry of the nearly thermoneutral reactions $N^+(^3P) + H_2(HD, D_2) \rightarrow NH^+(ND^+) + H(D)$. *The Journal of Chemical Physics*, *86*(5), 2659–2673. https://doi.org/10.1063/1.452068

Federer, W., Villinger, H., Howorka, F., Lindinger, W., Tosi, P., Bassi, D., & Ferguson, E. (1984). Reaction of O^+, CO^+, and CH^+ Ions with Atomic Hydrogen. *Physical Review Letters*, *52*(23), 2084–2086. https://doi.org/10.1103/physrevlett.52.2084

Fehsenfeld, F. C., Schmeltekopf, A. L., & Ferguson, E. E. (1967). Thermal-energy ion-neutral reaction rates. VII. some hydrogen-atom abstraction reactions. *The Journal of Chemical Physics*, *46*(7), 2802–2808. https://doi.org/10.1063/1.1841117

Ferguson, E., Fehsenfeld, F., & Schmeltekopf, A. (1969). Flowing afterglow measurements of ion-neutral reactions. *Advances in Atomic and Molecular Physics Advances in Atomic and Molecular Physics Volume 5*, 1–56. https://doi.org/10.1016/s0065-2199(08)60154-2

Ferrière, K. M. (2001). The interstellar environment of our galaxy. *Reviews of Modern Physics*, *73*(4), 1031–1066. https://doi.org/10.1103/RevModPhys.73.1031

Flesch, G. D., & Ng, C. Y. (1991). Absolute total cross-sections for the charge transfer and dissociative charge transfer channels in the collisions of $O^+(^4S) + H_2$. *The Journal of Chemical Physics*, *94*(3), 2372–2373. https://doi.org/10.1063/1.459859

Gal, R. L., Hily-Blant, P., Faure, A., Forêts, G. P. D., Rist, C., & Maret, S. (2014). Interstellar chemistry of nitrogen hydrides in dark clouds. *Astronomy & Astrophysics*, *562,* A83(1–20). https://doi.org/10.1051/0004-6361/201322386

Garrec, J.-L. L., Carles, S., Speck, T., Mitchell, J., Rowe, B., & Ferguson, E. (2003). The ion-molecule reaction of O^+ with N_2 measured down to 23 K. *Chemical Physics Letters*, *372*(3–4), 485–488. https://doi.org/10.1016/s0009-2614(03)00377-4

Gerin, M., Luca, M. D., Black, J., Goicoechea, J. R., Herbst, E., Neufeld, D. A., … Lorenzani, A. (2010). Interstellar OH^+, H_2O^+ and H_3O^+ along the sight-line to G10.6–0.4. *Astronomy & Astrophysics*, *518,* L110(1–5). https://doi.org/10.1051/0004-6361/201014576

Gerin, M., Neufeld, D. A., & Goicoechea, J. R. (2016). Interstellar Hydrides. *Annual Review of Astronomy and Astrophysics*, *54*(1), 181–225. https://doi.org/10.1146/annurev-astro-081915-023409

Gerlich, D., & Horning, S. (1992a). Experimental investigation of radiative association processes as related to interstellar chemistry. *Chemical Reviews*, *92*(7), 1509–1539. https://doi.org/10.1021/cr00015a003

Gerlich, D. (1992b)., private communication, May 17, (2008).

Gerlich, D. (1993). Experimental investigations of ion-molecule reactions relevant to interstellar chemistry. *J. Chem. Soc., Faraday Trans.*, *89*(13), 2199–2208. https://doi.org/10.1039/ft9938902199

Gerlich, D. (1995). Ion-neutral collisions in a 22-pole trap at very low energies. *Physica Scripta*, *T59*, 256–263. https://doi.org/10.1088/0031-8949/1995/t59/035

Gerlich, D. (2008). The production and study of ultra-cold molecular ions, chapter 6: Low temperatures and cold molecules (ed. I.W.M. Smith), Imperial College Press, Singapore, 295–343.

Gerlich, D., Plašil, R., Zymak, I., Hejduk, M., Jusko, P., Mulin, D., & Glosík, J. (2013). State Specific Stabilization of $H^+ + H_2(j)$ Collision Complexes. *The Journal of Physical Chemistry A*, 117(39), 10068–10075. https://doi.org/10.1021/jp400917v

Glosík, J., Rakshit, A. B., Twiddy, N. D., Adams, N. G., & Smith, D. (1978). Measurement of the rates of reaction of the ground and metastable excited states of O_2^+, NO^+ and O^+ with atmospheric gases at thermal energy. *Journal of Physics B: Atomic and Molecular Physics*, *11*(19), 3365–3379. https://doi.org/10.1088/0022-3700/11/19/013

Glosík, J., Hejduk, M., Dohnal, P., Rubovič, P., Kálosi, Á., & Plašil, R. (2015). State selective study of H_3 recombination in Cryo-FALP and SA-CRDS experiments at 77 K. *EPJ Web of Conferences*, *84*, 01002(1–10). https://doi.org/10.1051/epjconf/20158401002

Godefroid, M., & Fischer, C. F. (1984). MCHF-BP fine-structure splittings and transition rates for the ground configuration in the nitrogen sequence. *Journal of Physics B: Atomic and Molecular Physics*, *17*(5), 681–692. https://doi.org/10.1088/0022-3700/17/5/008

González, M., Gilibert, M., Aguilar, A., & Sayós, R. (1993). A comparison between experimental and theoretical excitation functions for the $O^+ + H_2$ ($^4A'$) system using trajectory calculations over a wide energy range. *The Journal of Chemical Physics*, 98(4), 2927–2935. https://doi.org/10.1063/1.464120

Gómez-Carrasco, S., Godard, B., Lique, F., Bulut, N., Kłos, J., Roncero, O., … Cernicharo, J. (2014). OH^+ in astrophysical media: state-to-state formation rates, Einstein coefficients and inelastic collision rates with He. *The Astrophysical Journal*, *794*(1), 33(1–16). https://doi.org/10.1088/0004-637x/794/1/33

Gordon, I. E., Rothman, L. S., Hill, C., Kochanov, R. V., Tan, Y., Bernath, P. F., … Zak, E. J. (2017). The HITRAN2016 molecular spectroscopic database. *Journal of Quantitative Spectroscopy and Radiative Transfer*, *203*, 3–69. https://doi.org/10.1016/j.jqsrt.2017.06.038

Haney, M. A., & Franklin, J. L. (1969). Mass spectrometric determination of the proton affinities of various molecules. *The Journal of Physical Chemistry*, *73*(12), 4328–4331. https://doi.org/10.1021/j100846a049

Harju, J., Daniel, F., Sipilä, O., Caselli, P., Pineda, J. E., Friesen, R. K., … Shirley, Y. L. (2017). Deuteration of ammonia in the starless core Ophiuchus/H-MM1. *Astronomy & Astrophysics*, *600*, A61(1–18). https://doi.org/10.1051/0004-6361/201628463

Hejduk, M., Dohnal, P., Varju, J., Rubovič, P., Plašil, R., & Glosík, J. (2012). Nuclear spin state-resolved cavity ring-down spectroscopy diagnostics of a low-temperature H_3^+-dominated plasma. *Plasma Sources Science and Technology*, *21*(2), 024002(1–9). https://doi.org/10.1088/0963-0252/21/2/024002

Henchman, M., Smith, D., Adams, N. G., Paulson, J. F., & Herman, Z. (1989). The mechanism of the reaction $CH_4^+ + CH_4 = CH_5^+ + CH_3$ as a function of energy: rate constants and product distributions for the reactions of $CH_4^+ + CD_4$ and $CD_4^+ + CH_4$ at 80 and 300 K. *International Journal of Mass Spectrometry and Ion Processes*, *92*, 15–36. https://doi.org/10.1016/0168-1176(89)83016-2

Herbst, E., & Klemperer, W. (1973). The formation and depletion of molecules in dense interstellar clouds. *The Astrophysical Journal*, *185*, 505–533. https://doi.org/10.1086/152436

Herbst, E., Defrees, D. J., & Mclean, A. D. (1987). A detailed investigation of proposed gas-phase syntheses of ammonia in dense interstellar clouds. *The Astrophysical Journal*, *321*, 898–906. https://doi.org/10.1086/165682

Herbst, E. (1995). Chemistry in the Interstellar Medium. *Annual Review of Physical Chemistry*, *46*(1), 27–54. https://doi.org/10.1146/annurev.pc.46.100195.000331

Herbst, E. (2005). Molecular ions in interstellar reaction networks. *Journal of Physics: Conference Series*, *4*, 17–25. https://doi.org/10.1088/1742-6596/4/1/003

Hierl, P. M., Dotan, I., Seeley, J. V., Doren, J. M. V., Morris, R. A., & Viggiano, A. A. (1997). Rate constants for the reactions of O^+ with N_2 and O_2 as a function of temperature (300–1800 K). *The Journal of Chemical Physics*, *106*(9), 3540–3544. https://doi.org/10.1063/1.473450

Hily-Blant, P., Bonal, L., Faure, A., & Quirico, E. (2013). The ^{15}N-enrichment in dark clouds and Solar System objects. *Icarus*, *223*(1), 582–590. https://doi.org/10.1016/j.icarus.2012.12.015

Hlavenka, P., Plašil, R., Bánó, G., Korolov, I., Gerlich, D., Ramanlal, J., … Glosík, J. (2006). Near infrared second overtone cw-cavity ringdown spectroscopy of D_2H^+ ions. *International Journal of Mass Spectrometry*, *255–256*, 170–176. https://doi.org/10.1016/j.ijms.2006.02.002

Hollenbach, D., Kaufman, M. J., Bergin, E. A., & Melnick, G. J. (2008). Water, O_2, and ice in molecular clouds. *The Astrophysical Journal*, *690*(2), 1497–1521. https://doi.org/10.1088/0004-637x/690/2/1497

Hollenbach, D., Kaufman, M. J., Neufeld, D., Wolfire, M., & Goicoechea, J. R. (2012). The chemistry of interstellar OH^+, H_2O^+, and H_3O^+: inferring the cosmic-ray ionization rates from observations of molecular ions. *The Astrophysical Journal*, *754*(2), 105(1–22). https://doi.org/10.1088/0004-637x/754/2/105

Hunter, E. P. L., & Lias, S. G. (1998). Evaluated gas phase basicities and proton affinities of molecules: an update. *Journal of Physical and Chemical Reference Data*, *27*(3), 413–656. https://doi.org/10.1063/1.556018

Jackson, D. M., Stibrich, N. J., Adams, N. G., & Babcock, L. M. (2005). A selected ion flow tube study of the reactions of a sequence of ions with amines. *International Journal of Mass Spectrometry*, *243*(2), 115–120. https://doi.org/10.1016/j.ijms.2005.02.004

Jensen, M. J., Bilodeau, R. C., Heber, O., Pedersen, H. B., Safvan, C. P., Urbain, X., … Andersen, L. H. (1999). Dissociative recombination and excitation of H_2O^+ and HDO^+. *Physical Review A*, *60*(4), 2970–2976. https://doi.org/10.1103/physreva.60.2970

Johnsen, R., & Biondi, M. A. (1980). Charge transfer coefficients for the $O^+(^2D)$ + N_2 and $O^+(^2D)$ + O_2 excited ion reactions at thermal energy. *The Journal of Chemical Physics*, *73*(1), 190–193. https://doi.org/10.1063/1.439913

Jones, J., Birkinshaw, K., & Twiddy, N. (1981). Rate coefficients and product ion distributions for the reactions of OH^+ and H_2O^+ with N_2, O_2, NO. N_2O, Xe, CO, CO_2, H_2S and H_2 at 300 K. *Chemical Physics Letters*, *77*(3), 484–488. https://doi.org/10.1016/0009-2614(81)85191-3

Jusko, P., Roučka, Š., Mulin, D., Zymak, I., Plašil, R., Gerlich, D., … Glosík, J. (2015). Interaction of O^- and H_2 at low temperatures. *The Journal of Chemical Physics*, *142*(1), 014304(1–7). https://doi.org/10.1063/1.4905078

Kim, J. K., Theard, L. P., & Huntress, W. T. J. (1975). ICR studies of some hydrogen atom abstraction reactions: $X^+ + H_2 \rightarrow XH^+ + H$. *The Journal of Chemical Physics*, *62*(1), 45–52. https://doi.org/10.1063/1.430236

Kovalenko, A., Tran, T. D., Rednyk, S., Roučka, Š., Dohnal, P., Plašil, R., … Glosík, J. (2018). OH^+ formation in the low-temperature $O^+(^4S)$ + H_2 reaction. *The Astrophysical Journal*, *856*(2), 100(1–6). https://doi.org/10.3847/1538-4357/aab106 (see attachment)

Langevin, M. (1905). Une formule fondamentale de théorie cinétique. *In Annales de chimie et de physique, 5*, 245–288.

Lauzin, C., Jacovella, U., & Merkt, F. (2015). Threshold ionization spectroscopy of H_2O, HDO and D_2O and low-lying vibrational levels of HDO and D_2O. *Molecular Physics*, *113*(24), 3918–3924. https://doi.org/10.1080/00268976.2015.1049971

Li, A., & Draine, B. T. (2001). Infrared emission from interstellar dust. II. the diffuse interstellar medium. *The Astrophysical Journal*, *554*(2), 778–802. https://doi.org/10.1086/323147

Li, T. (2020). Chemical Langevin equation for complex reactions. *The Journal of Physical Chemistry A*, 124(5), 810–816. https://doi.org/10.1021/acs.jpca.9b10108

Li, X., Huang, Y. L., Flesch, G. D., & Ng, C. Y. (1997). Absolute state-selected total cross-sections for the ion–molecule reactions $O^+(^4S, ^2D, ^2P)$ + $H_2(D_2)$. *The Journal of Chemical Physics*, *106*(2), 564–571. https://doi.org/10.1063/1.473395

Liao, C. -L., Xu, R., Flesch, G. D., Baer, M., & Ng, C. Y. (1990). Experimental and theoretical total state-selected and state-to-state absolute cross-sections. I. The $H_2^+(X,v')$ + Ar reaction. *The Journal of Chemical Physics*, *93*(7), 4818–4831. https://doi.org/10.1063/1.458673

Liu, J., Salumbides, E. J., Hollenstein, U., Koelemeij, J. C. J., Eikema, K. S. E., Ubachs, W., & Merkt, F. (2009). Determination of the ionization and dissociation energies of the hydrogen molecule. *The Journal of Chemical Physics*, *130*(17), 174306(1-8). https://doi.org/10.1063/1.3120443

Macko, P., Bánó, G., Hlavenka, P., Plašil, R., Poterya, V., Pysanenko, A., … Glosík J. (2004). Afterglow studies of H_3^+ (v = 0) recombination using time resolved cw-diode laser cavity ring-down spectroscopy. *International Journal of Mass Spectrometry*, *233*(1–3), 299–304. https://doi.org/10.1016/j.ijms.2003.12.035

Major, F. G., Gheorghe, V. N., & Werth, G. (2005) Charged Particle Traps: Physics and Techniques of Charged Particle Field Confinement; Springer: Berlin/Heidelberg, Germany.

March, R. E., & Todd, J. F. J. (2005). Quadrupole ion trap mass spectrometry. Hoboken (N.J.): Wiley.

Marquette, J. B., Rebrion, C., & Rowe, B. R. (1988). Reactions of $N^+(^3P)$ ions with normal, para, and deuterated hydrogens at low temperatures. *The Journal of Chemical Physics*, *89*(4), 2041–2047. https://doi.org/10.1063/1.455101

Martínez, O., Ard, S. G., Li, A., Shuman, N. S., Guo, H., & Viggiano, A. A. (2015). Temperature-dependent kinetic measurements and quasi-classical trajectory studies for the $OH^+ + H_2/D_2 \rightarrow H_2O^+/HDO^+ +$ H/D reactions. *The Journal of Chemical Physics*, *143*(11), 114310(1–5). https://doi.org/10.1063/1.4931109

Martínez, R., Sierra, J. D., Gray, S. K., & González, M. (2006). Time dependent quantum dynamics study of the $O^+ + H_2(v = 0, j = 0) \rightarrow OH^+ +$ H ion-molecule reaction and isotopic variants (D_2, HD). *The Journal of Chemical Physics*, *125*(16), 164305(1–7). https://doi.org/10.1063/1.2359727

Martínez, R., Millán, J., & González, M. (2004). Ab initio analytical potential energy surface and quasiclassical trajectory study of the $O^+(^4S) + H_2(X^1\Sigma_g^+) \rightarrow OH^+(X^3\Sigma^-) + H(^2S)$ reaction and isotopic variants. *The Journal of Chemical Physics*, *120*(10), 4705–4714. https://doi.org/10.1063/1.1638735

Menzinger, M., & Wolfgang, R. (1969). The meaning and use of the Arrhenius activation energy. *Angewandte Chemie International Edition in English*, *8*(6), 438–444. https://doi.org/10.1002/anie.196904381

Meyer, D. M., & Roth, K. C. (1991). Discovery of interstellar NH. *The Astrophysical Journal*, *376*, L49–L52. https://doi.org/10.1086/186100

Michaelsen, T., Bastian, B., Carrascosa, E., Meyer, J., Parker, D. H., & Wester, R. (2017). Imaging state-to-state reactive scattering in the $Ar^+ + H_2$ charge transfer reaction. *The Journal of Chemical Physics*, *147*(1), 013940(1–8). https://doi.org/10.1063/1.4983305

Mulin, D., Roučka, Š., Jusko, P., Zymak, I., Plašil, R., Gerlich, D., … Glosík, J. (2015). H/D exchange in reactions of OH^- with D_2 and of OD^- with H_2 at low temperatures. *Physical Chemistry Chemical Physics*, *17*(14), 8732–8739. https://doi.org/10.1039/c5cp00516g

Muller, S., Müller, H. S. P., Black, J. H., Beelen, A., Combes, F., Curran, S., … Zwaan, M. A. (2016). OH^+ and H_2O^+ absorption toward PKS 1830–211. *Astronomy & Astrophysics*, *595,* A128(1–10). https://doi.org/10.1051/0004-6361/201629073

Neau, A., Khalili, A. A., Rosén, S., Padellec, A. L., Derkatch, A. M., Shi, W., … Ugglas, M. A. (2000). Dissociative recombination of D_3O^+ and H_3O^+: Absolute cross-sections and branching ratios. *The Journal of Chemical Physics*, *113*(5), 1762–1770. https://doi.org/10.1063/1.481979

Neill, J. L., Crockett, N. R., Bergin, E. A., Pearson, J. C., & Xu, L.-H. (2013). Deuterated molecules in Orion Kl from Herschel/HIFI. *The Astrophysical Journal*, *777*(2), 85(1–20). https://doi.org/10.1088/0004-637x/777/2/85

Neufeld, D. A., & Wolfire, M. G. (2016). The chemistry of interstellar argonium and other probes of the molecular fraction in diffuse clouds. *The Astrophysical Journal*, *826*(2), 183(1–12). https://doi.org/10.3847/0004-637x/826/2/183

Oliveira, C. M., Hebrard, G., Howk, J. C., Kruk, J. W., Chayer, P., & Moos, H. W. (2003). GD 246, WD 2331−475, HZ 21, and Lanning 23: Results from Interstellar Deuterium, Nitrogen, and Oxygen Abundances toward the FUSE Mission. *The Astrophysical Journal*, *587*(1), 235–255. https://doi.org/10.1086/368019

Ossenkopf, V., Müller, H., Lis, D., Schilke, P., Bell, T., Bruderer, S., . . . Ceccarelli, C. (2010). Detection of interstellar oxidaniumyl: Abundant H_2O^+ towards the star-forming regions DR21, Sgr B2, and NGC6334. *Astronomy & Astrophysics*, 518, L111(1–5). https://doi.org/10.1051/0004-6361/201014577

Pilbratt, G. L., Riedinger, J. R., Passvogel, T., Crone, G., Doyle, D., Gageur, U., . . . Schmidt, M. (2010). Herschel Space Observatory: An ESA facility for far-infrared and submillimetre astronomy. *Astronomy & Astrophysics*, 518, L1(1–6). https://doi.org/10.1051/0004-6361/201014759

Plašil, R., Dohnal, P., Kálosi, Á., Roučka, Š., Shapko, D., Rednyk, S., … Glosík, J. (2018). Stationary afterglow apparatus with CRDS for study of processes in plasmas from 300 K down to 30 K. *Review of Scientific Instruments*, *89*(6), 063116(1–10). https://doi.org/10.1063/1.5036834

Plašil, R., Zymak, I., Jusko, P., Mulin, D., Gerlich, D., & Glosík, J. (2012). Stabilization of H^+–H_2 collision complexes between 11 and 28K. *Philosophical Transactions of the Royal Society A: Mathematical, Physical and Engineering Sciences*, *370*(1978), 5066–5073. https://doi.org/10.1098/rsta.2012.0098

Pratap, P., Dickens, J. E., Snell, R. L., Miralles, M. P., Bergin, E. A., Irvine, W. M., & Schloerb, F. P. (1997). A study of the physics and chemistry of TMC-1. *The Astrophysical Journal*, *486*(2), 862–885. https://doi.org/10.1086/304553

Rakshit, A. B., & Warneck, P. (1980). Thermal rate coefficients for reactions involving $^2P_{1/2}$ and $^2P_{3/2}$ argon ions and several neutral molecules. *The Journal of Chemical Physics*, *73*(6), 2673–2679. https://doi.org/10.1063/1.440480

Rebrion, C., Rowe, B. R., & Marquette, J. B. (1989). Reactions of A^+ with H_2, N_2, O_2, and CO at 20, 30, and 70 K. *The Journal of Chemical Physics*, *91*(10), 6142–6147. https://doi.org/10.1063/1.457433

Rednyk, S., Roučka, Š., Kovalenko, A., Tran, T. D., Dohnal, P., Plašil, R., & Glosík, J. (2019). Reaction of NH^+, NH_2^+, and NH_3^+ ions with H_2 at low temperatures. *Astronomy & Astrophysics, 625*, A74(1–8). https://doi.org/10.1051/0004-6361/201834149 (see attachment)

Rist, C., Faure, A., Hily-Blant, P., & Gal, R. L. (2013). Nuclear-spin selection rules in the chemistry of interstellar nitrogen hydrides. *The Journal of Physical Chemistry A*, *117*(39), 9800–9806. https://doi.org/10.1021/jp312640a

Rist, C., Faure, A., Hily-Blant, P., & Gal, R. L. (2013). Nuclear-Spin Selection Rules in the Chemistry of Interstellar Nitrogen Hydrides. *The Journal of Physical Chemistry A*, *117*(39), 9800–9806. https://doi.org/10.1021/jp312640a

Roberts, H., Herbst, E., & Millar, T. J. (2003). Enhanced Deuterium Fractionation in Dense Interstellar Cores Resulting from Multiply Deuterated H_3^+. *The Astrophysical Journal*, *591*(1), L41–L44. https://doi.org/10.1086/376962

Roueff, E., Lis, D. C., F. F. S. Van Der Tak, Gerin, M., & Goldsmith, P. F. (2005). Interstellar deuterated ammonia: from NH_3 to ND_3. *Astronomy & Astrophysics*, *438*(2), 585–598. https://doi.org/10.1051/0004-6361:20052724

Roueff, E. (2015). (New) molecular ions in the interstellar medium. EPJ Web of Conferences, 84, 06004(1–9). https://doi.org/10.1051/epjconf/20158406004

Rowe, B. R., Dupeyrat, G., Marquette, J. B., & Gaucherel, P. (1984). Study of the reactions $N_2^+ + 2N_2 \rightarrow N_4^+ + N_2$ and $O_2^+ + 2O_2 \rightarrow O_4^+ + O_2$ from 20 to 160 K by the CRESU technique. *The Journal of Chemical Physics*, *80*(10), 4915–4921. https://doi.org/10.1063/1.446513

Rowe, B., Marquette, J., Dupeyrat, G., & Ferguson, E. (1985). Reactions of He^+ and N^+ ions with several molecules at 8 K. *Chemical Physics Letters*, *113*(4), 403–406. https://doi.org/10.1016/0009-2614(85)80391-2

Rowe, B., Canosa, A., & Page, V. L. (1995). FALP and CRESU studies of ionic reactions. *International Journal of Mass Spectrometry and Ion Processes*, *149-150*, 573–596. https://doi.org/10.1016/0168-1176(95)04292-s

de Ruette, N., Miller, K. A., O'Connor, A. P., Urbain, X., Buzard, C. F., Vissapragada, S., & Savin, D. W. (2015). Merged-beams reaction studies of $O + H_3^+$. *The Astrophysical Journal*, *816*(1), 31(1–11). https://doi.org/10.3847/0004-637x/816/1/31

Sansonetti, J. E., & Martin, W. C. (2005). Handbook of basic atomic spectroscopic data. *Journal of Physical and Chemical Reference Data*, *34*(4), 1559–2259. https://doi.org/10.1063/1.1800011

Schläppi, B., Litman, J. H., Ferreiro, J. J., Stapfer, D., & Signorell, R. (2015). A pulsed uniform Laval expansion coupled with single-photon ionization and mass spectrometric detection for the study of large molecular aggregates. *Physical Chemistry Chemical Physics*, *17*(39), 25761–25771. https://doi.org/10.1039/c5cp00061k

Scott, G. B. I., Freeman, C. G., & Mcewan, M. J. (1997). The interstellar synthesis of ammonia. *Monthly Notices of the Royal Astronomical Society*, *290*(4), 636–638. https://doi.org/10.1093/mnras/290.4.636

Sizun, M., Song, J.-B., & Gislason, E. A. (2002). Theoretical study of the reactions of Ar^+ + HX(v=0) and Ar + HX^+ (v) (X=H and D) at E = 0.1 eV using the trajectory surface hopping method. *The Journal of Chemical Physics*, *116*(7), 2888–2895. https://doi.org/10.1063/1.1434989

Smith, I. W. M., Herbst, E., & Chang, Q. (2004). Rapid neutral-neutral reactions at low temperatures: A new network and first results for TMC-1. *Monthly Notices of the Royal Astronomical Society*, *350*(1), 323–330. https://doi.org/10.1111/j.1365-2966.2004.07656.x

Smith, D., Adams, N. G., & Miller, T. M. (1978). A laboratory study of the reactions of N^+, N_2^+, N_3^+, N_4^+, O^+, O_2^+, and NO^+ ions with several molecules at 300 K. *The Journal of Chemical Physics*, *69*(1), 308–318. https://doi.org/10.1063/1.436354

Snow, T. P., & Witt, A. N. (1996). Interstellar depletions updated: where all the atoms went. *The Astrophysical Journal*, *468*(1), L65–L68. https://doi.org/10.1086/310225

Sunderlin, L. S., & Armentrout, P. B. (1994). Rotational temperature dependence of the reactions of N^+ and C^+ with H_2, HD, and D_2. *The Journal of Chemical Physics*, *100*(8), 5639–5645. https://doi.org/10.1063/1.467131

Sunderlin, L., & Armentrout, P. (1990). Temperature dependence of the reaction of O^+ with HD. *Chemical Physics Letters*, *167*(3), 188–192. https://doi.org/10.1016/0009-2614(90)85003-u

Tanarro, I., Herrero, V. J., Islyaikin, A. M., & Tafalla, D. (2007). Ion chemistry in cold plasmas of H_2 with CH_4 and N_2. *The Journal of Physical Chemistry A*, *111*(37), 9003–9012. https://doi.org/10.1021/jp073569w

Teloy, E., & Gerlich, D. (1974). Integral cross-sections for ion-molecule reactions. I. The guided beam technique. *Chemical Physics*, *4*(3), 417–427. https://doi.org/10.1016/0301-0104(74)85008-1

Tielens, A. G. G. M. (2005). The physics and chemistry of the interstellar medium (1st ed.). Cambridge: Cambridge University Press. https://doi.org/10.1017/CBO9780511819056

Turulski, J., & Niedzielski, J. (1994). The classical Langevin rate constant for ion/molecule capture: When, if at all, is it constant? *International Journal of Mass Spectrometry and Ion Processes*, 139, 155–162. https://doi.org/10.1016/0168-1176(94)90030-2

Tosi, P., Dmitriev, O., Bassi, D., Wick, O., & Gerlich, D. (1994). Experimental observation of the energy threshold in the ion-molecule reaction $N^+ + D_2 \rightarrow ND^+ + D$. *The Journal of Chemical Physics*, *100*(6), 4300–4307. https://doi.org/10.1063/1.466311

Tran, T. D., Rednyk, S., Kovalenko, A., Roučka, Š., Dohnal, P., Plašil, R., … Glosík, J. (2018). Formation of H_2O^+ and H_3O^+ cations in reactions of OH^+ and H_2O^+ with H_2: experimental studies of the reaction rate coefficients from T = 15 to 300 K. *The Astrophysical Journal*, *854*(1), 25(1–5). https://doi.org/10.3847/1538-4357/aaa0d8 (see attachment)

van der Tak, F. F. S., Nagy, Z., Ossenkopf, V., Makai, Z., Black, J. H., Faure, A., … Bergin, E. A. (2013). Spatially extended OH^+ emission from the Orion Bar and Ridge. *Astronomy & Astrophysics*, *560*, A95(1–10). https://doi.org/10.1051/0004-6361/201322164

Vastel, C., Mookerjea, B., Pety, J., & Gerin, M. (2016). Deuterium fractionation of a distant cold dark cloud along the line of sight of W51. *Astronomy & Astrophysics*, *597,* A45(1–6). https://doi.org/10.1051/0004-6361/201629289

Viggiano, A. A., Doren, J. M. V., Morris, R. A., Williamson, J. S., Mundis, P. L., Paulson, J. F., & Dateo, C. E. (1991). Rotational temperature dependence of the branching ratio for the reaction of O^+ with HD. *The Journal of Chemical Physics*, *95*(11), 8120–8123. https://doi.org/10.1063/1.461291

Weinberg, D. H. (2017). On the deuterium-to-hydrogen ratio of the Interstellar Medium. *The Astrophysical Journal*, 851(1), 25(1–8). https://doi.org/10.3847/1538-4357/aa96b2

Wang, X.-L., Gao, F., Gao, S.-B., Zhang, L.-L., Song, Y.-Z., & Meng, Q.-T. (2018). Novel potential energy surface-based quantum dynamics of ion–molecule reaction $O^+ + D_2 \rightarrow OD^+ + D$. *Chinese Physics B*, *27*(4), 043104(1–5). https://doi.org/10.1088/1674-1056/27/4/043104

Wiedmann, R. T., Tonkyn, R. G., White, M. G., Wang, K., & Mckoy, V. (1992). Rotationally resolved threshold photoelectron spectra of OH and OD. *The Journal of Chemical Physics*, *97*(2), 768–772. https://doi.org/10.1063/1.463179

Wyrowski, F., Menten, K. M., Güsten, R., & Belloche, A. (2010). First interstellar detection of OH^+. *Astronomy & Astrophysics*, 518, A26(1–5). https://doi.org/10.1051/0004-6361/201014364

Xu, W., Li, W., Lv, S., Zhai, H., Duan, Z., & Zhang, P. (2012). Coriolis coupling effects in $O^+(^4S) + H_2(X^1\Sigma_g^+) \rightarrow OH^+(X^3\Sigma^-) + H(^2S)$ reaction and its isotopic variants: exact time-dependent quantum scattering study. *The Journal of Physical Chemistry A*, *116*(45), 10882–10888. https://doi.org/10.1021/jp305612t

Zeippen, C. J. (1987). Improved radiative transition probabilities for O II forbidden lines. *Astronomy & Astrophysics*, 173, 410–414.

Zhu, Z., Li, L., Li, Q., & Teng, B. (2020). Dynamics studies of $O^+ + D_2$ reaction using the time-dependent wave packet method. *Molecular Physics*, *118*(4), 1619855(1–7). https://doi.org/10.1080/00268976.2019.1619855

Zymak, I., Hejduk, M., Mulin, D., Plašil, R., Glosík, J., & Gerlich, D. (2013). Low-temperature ion trap studies of $N^+(^3P_{ja}) + H_2(j) \rightarrow NH^+ + H$. *The Astrophysical Journal*, *768*(1), 86(1–8). https://doi.org/10.1088/0004-637x/768/1/86

List of Studied reactions

The list of studied reactions represents the reactions that I worked the most time on. These reactions were experimentally studied in our group and presented in the thesis:

Reaction	k_{thesis}	Chapter	Article
$O^+ + H_2 \rightarrow OH^+ + H$	k_{O+}^{H2}	5.1	(Kovalenko et al., 2018)
$N^+ + HD \rightarrow$	k_{N+}^{HD}	5.2	(Plašil et al., 2020. Send for publication)
$N^+ + HD \rightarrow NH^+ + D$	k_{N+}^{HDa}	5.2	(Plašil et al., 2020. Send for publication)
$N^+ + HD \rightarrow ND^+ + H$	k_{N+}^{HDb}	5.2	(Plašil et al., 2020. Send for publication)
$N^+ + D_2 \rightarrow ND^+ + D$	k_{N+}^{D2}	5.2	(Plašil et al., 2020. Send for publication)
$O^+ + HD \rightarrow$	k_{O+}^{HD}	5.3	(Kovalenko et al., 2020. Under rewie)
$O^+ + HD \rightarrow OH^+ + D$	k_{O+}^{HDa}	5.3	(Kovalenko et al., 2020. Under rewie)
$O^+ + HD \rightarrow OD^+ + H$	k_{O+}^{HDb}	5.3	(Kovalenko et al., 2021. Under rewie)
$O^+ + D_2 \rightarrow OD^+ + D$	k_{O+}^{D2}	5.3	(Kovalenko et al., 2021. Under rewie)

The list of reactions that were used for testing and calibration:

Reaction	Corresponding article
$Ar^+ + H_2 \rightarrow ArH^+ + H$	(Michaelsen et al., 2017)
$O^+(^4S) + N_2 \rightarrow NO^+ + N$	(Le Garrec et al., 2003)
$O^+(^2P, ^2D) + N_2 \rightarrow N_2^+ + O$	(Le Garrec et al., 2003)
$H^+ + CH_4 \rightarrow CH_3^+ + H_2$	(Le Garrec et al., 2003)
$H^+ + CH_4 \rightarrow CH_4^+ + H$	(Tanarro et al., 2007)

The list of reactions with the corresponding article of whose experimental studies I was also involved in:

Reaction	Corresponding article
$OH^+ + H_2 \rightarrow H_2O^+ + H$	(Tran et al., 2018)
$H_2O^+ + H_2 \rightarrow H_3O^+ + H$	(Tran et al., 2018)
$NH^+ + H_2 \rightarrow NH_2^+ + H$ $NH^+ + H_2 \rightarrow H_3^+ + N$	(Rednyk et al., 2019)
$NH_2^+ + H_2 \rightarrow NH_3^+ + H$	(Rednyk et al., 2019)
$NH_3^+ + H_2 \rightarrow NH_4^+ + H$	(Rednyk et al., 2019)
$NH^+ + H \rightarrow N^+ + H_2$	(Roučka et al., 2020. In preparation)
$OD^- + H_2 \rightarrow OH^- + HD$	(Roučka et al., 2018)
$OH^- + D_2 \rightarrow OD^- + HD$	(Roučka et al., 2018)
$O^- + H_2 \rightarrow H_2O + e^-$ $O^- + H_2 \rightarrow OH^- + H$	(Plašil et al., 2019)
$O^- + D_2 \rightarrow D_2O + e^-$ $O^- + D_2 \rightarrow OD^- + D$	(Plašil et al., 2019)

List of Figures

List of Tables

List of Acronyms

ISM	Interstellar Medium	6
CR	Cosmic Rays	10
FA	Flowing Afterglow apparatus	19
SIFT	Selected Ion Flow Tube apparatus	19
CRESU	Cinétique de Réaction en Ecoulement Supersonique Uniforme apparatus	20
RF	Radio Frequency	22
22PT	22-Pole ion Trap	28
SIS	Storage Ion Source	28
QMF	Quadrupole Mass Filter	28
QMS	Quadrupole Mass Spectrometer	28
MCP, MCPD	MicroChannel Plate Detector	28
QB	Quadrupole Bender	29
UHV	Ultra-High Vacuum	29
IG	Ionisation Gauge	29
SRG	Spinning Rotor Gauge	29
RG	Reactant Gas	29
DP	Diaphragm Pump	31
TP	Turbomolecular Pump	31
SP	Scroll Pump	31
TDP	Turbo Drag Pump	31
mTP	Magnetic-levitation Turbomolecular Pump	31
SIFDT	Selected Ion Flow-Drift Tube apparatus	61
TDE	Thermodynamic Equilibrium	62
PES	Potential Energy Surface	63
TDWP	Time-Dependent Wave Packet calculations	64
MB	Merged Beams apparatus/experiment	65
CB	Cross Beams apparatus/experiment	65

FS	Fine Structure	80
CRDS	Cavity Ring-Down Spectrometer	81

List of Publications

Publications in impacted journals

Rednyk, S., Roučka, Š., Kovalenko, A., Tran, T. D., Dohnal, P., Plašil, R., & Glosík, J. (2019). Reaction of NH^+, NH_2^+, and NH_3^+ ions with H_2 at low temperatures. The pathway to ammonia production in the interstellar medium. *Astronomy & Astrophysics*, *625*(A74), 1-8. https://doi.org/10.1051/0004-6361/201834149 (see attachment)

Kovalenko, A., Tran, T. D., Rednyk, S., Roučka, Š., Dohnal, P., Plašil, R., Gerlich, J., & Glosík, J. (2018). OH^+ formation in the low-temperature $O^+(^4S)$ + H_2 reaction. *The Astrophysical Journal*, *856*(2), 100(1-6). https://doi.org/10.3847/1538-4357/aab106 (see attachment)

Tran, T. D., Rednyk, S., Kovalenko, A., Roučka, Š., Dohnal, P., Plašil, R., Gerlich, J., & Glosík, J. (2018). Formation of H_2O^+ and H_3O^+ cations in reactions of OH^+ and H_2O^+ with H_2: experimental studies of the reaction rate coefficients from T = 15 to 300 K. *The Astrophysical Journal, 854*(1), 25(1-5). https://doi.org/10.3847/1538-4357/aaa0d8 (see attachment)

Roučka, Š., Rednyk, S., Kovalenko, A., Tran, T. D., Plašil, R., Kálosi, Á., Dohnal, P., Gerlich, D., & Glosík, J. (2018). Effect of rotational excitation of H_2 on isotopic exchange reaction with OD^- at low temperatures. *Astronomy & Astrophysics*, *615*(L6), 1-5. https://doi.org/10.1051/0004-6361/201833264 (see attachment)

Plašil, R., Tran, T. D., Roučka, Š., Jusko, P., Mulin, D., Zymak, I., Rednyk, S., Kovalenko, A., Dohnal, P., Glosík, J., Houfek, K., Táborský, J., & Čížek, M. (2017). Isotopic effects in the interaction of O^- with D_2 and H_2 at low temperatures. *Physical Review A*, *96*(6), 062703(1-8). https://doi.org/PhysRevA.96.062703

Dohnal, P., Kálosi, Á., Plašil, R., Roučka, Š., Kovalenko, A., Rednyk, S., Johnsen, R., & Glosík, J. (2016). Binary and ternary recombination of H_2D^+ and HD_2^+ ions with electrons at 80 K. *Physical Chemistry Chemical Physics*, *18*(34), 23549–23553. https://doi.org/10.1039/C6CP04152C

Shpetnyi, I., Kovalenko, A. S., Klimenkov, M., Protsenko, I. Yu., Chernov, S. V., Nepijko, S. A., Elmers, H. J., & Schönhense, G. (2015). Characterization and magnetic properties of nanoparticles based on FePt solid solution with an oxide shell. *Journal of Magnetism and Magnetic Materials*, *373*, 231–235. https://doi.org/10.1016/j.jmmm.2014.01.071

Publications in conference proceedings

Kovalenko, A., Tran, T. D., A., Roučka, Š., Rednyk, S., Plašil, R., & Glosík, J. (2019). Reaction of O^+ with D_2 in the rf 22-pole ion trap between 100 K and 270 K. In J. Šafránková, & J. Pavlů (Ed.), *WDS'19* (pp. 77–80). Prague: MATFYZPRESS.

Tran, T. D., Kovalenko, A., Rednyk, S., Roučka, Š., Plašil, R., & Glosík, J. (2019). Reaction of O^- with HD at Low Temperatures. In J. Šafránková, & J. Pavlů (Ed.), *WDS'19* (pp. 72–76). Prague: MATFYZPRESS.

Rednyk, S., Plašil, R., Kovalenko, A., Tran, T. D., Roučka, Š., Dohnal, P. & Glosík, J. (2019). Investigation of Doubly Charged Carbon Cations in 22-Pole Ion Trap. In J. Šafránková, & J. Pavlů (Ed.), *WDS'19* (pp. 72–76). Prague: MATFYZPRESS.

Tran, T. D., Kovalenko, A., Rednyk, S., Roučka, Š., Plašil, R., & Glosík, J. (2018). The reaction of O^+ with HD at low temperatures. In D. Vernhet (Ed.), *45th EPS Conference on Plasma Physics.* Europhysics Conference Abstracts. Vol. 42A. European Physical Society.

Tran, T. D., Rednyk, S., Kovalenko, A., Roučka, Š., Plašil, R., & Glosík , J. (2017). Number Density Calibration of H_2 by Reaction with Ar^+. In J. Šafránková, & J. Pavlů (Ed.), *WDS'17* (pp. 94–98). Prague: MATFYZPRESS.

Tran, T. D., Mulin, D., Roučka, Š., Rednyk, S., Kovalenko, A., Plašil, R., & Glosík, J. (2016). Reaction $OD^- + H_2 \rightarrow OH^- + HD$ at Low Temperatures. In J. Šafránková, & J. Pavlů (Ed.), *WDS'16* (pp. 126–131). Prague: MATFYZPRESS.

Kovalenko, A., Roučka, Š., Tran, T. D., Rednyk, S., Plašil, R., & Glosík, J. (2016). Reaction of NH_2^+ with H_2 in the rf Ion Trap Between 100 K and 300 K. In J. Šafránková, & J. Pavlů (Ed.), *WDS'16* (pp. 116–120). Prague: MATFYZPRESS.

Rednyk, S., Roučka, Š., Kovalenko, A., Tran, T. D., Plašil, R., & Glosík, J. (2016). Study of the $NH^+ + H_2$ Reaction Using 22-Pole Ion Trap at Low Temperatures. In J. Šafránková, & J. Pavlů (Ed.), *WDS'16* (pp. 121–125). Prague: MATFYZPRESS.

Kovalenko, A., Roučka, Š., Rednyk, S., Tran, T. D., Plašil, R., & Glosík, J. (2015). Source of Atomic Hydrogen for Ion Trap Experiments: Review and Basic Properties. In J. Šafránková, & J. Pavlů (Ed.), *WDS'15* (pp. 155–161). Prague: MATFYZPRESS.

Rednyk, S., Mulin, D., Roučka, Š., Tran, T. D., Kumar, S. S., Plašil, R., Kovalenko, A., & Glosík, J. (2015). Study of the $NH^+ + H \rightarrow N^+ + H_2$ Reaction Rate Coefficient Using 22-Pole Ion Trap. In J. Šafránková, & J. Pavlů (Ed.), *WDS'15* (pp. 162–167). Prague: MATFYZPRESS.

Attached publications

Article I: Reaction of NH^+, NH_2^+, and NH_3^+ ions with H_2 at low temperatures. The pathway to ammonia production in the interstellar medium.

Article II: Formation of H_2O^+ and H_3O^+ Cations in Reactions of OH^+ and H_2O^+ with H_2: Experimental Studies of the Reaction Rate Coefficients from T = 15 to 300 K.

Article III: OH^+ Formation in the Low-temperature $O^+(^4S)$ + H_2 Reaction.

Article IV: Effect of rotational excitation of H_2 on isotopic exchange reaction with OD^- at low temperatures.

Article V: The reaction of $O^+(^4S)$ ions with H_2, HD, and D_2 at low temperatures: Experimental study of the isotope effect.